UC Berkeley
UC Berkeley Electronic Theses and Dissertations

Title

Lower-cost Particulate Matter Sensors Augment Ground-based Observational Capacity: Insights from Highly Polluted, Data-sparse Environments in India

Permalink

https://escholarship.org/uc/item/1547c3wx

Author

Campmier, Mark Joseph

Publication Date

2024

Peer reviewed|Thesis/dissertation

eScholarship.org Powered by the California Digital Library
University of California

Lower-cost Particulate Matter Sensors Augment Ground-based Observational Capacity: Insights from Highly Polluted, Data-sparse Environments in India

By

Mark Campmier

A dissertation submitted in partial satisfaction of the

requirements for the degree of

Doctor of Philosophy

in

Engineering- Civil and Environmental Engineering

in the

Graduate Division

of the

University of California, Berkeley

Committee in charge:

Associate Professor Joshua S Apte, Chair
Professor Robert A Harley
Adjunct Professor Thomas W Kirchstetter
Assistant Professor Ajay Pillarisetti

Summer 2024

Lower-cost Particulate Matter Sensors Augment Ground-based Observational Capacity: Insights from Highly Polluted, Data-sparse Environments in India

Copyright 2024
by
Mark Campmier

Abstract

Lower-cost Particulate Matter Sensors Augment Ground-based Observational Capacity: Insights from Highly Polluted, Data-sparse Environments in India

by

Mark Campmier

Doctor of Philosophy in Engineering- Civil and Environmental Engineering

University of California, Berkeley

Associate Professor Joshua S Apte, Chair

Seasonally Optimized Calibrations Improve Low-cost Sensor Performance: Long-term Field Evaluation of PurpleAir Sensors in Urban and Rural India

Lower-cost air pollution sensors can fill critical air quality data gaps in India, which experiences very high fine particulate matter ($PM_{2.5}$) air pollution but has sparse regulatory air monitoring. Challenges for low-cost $PM_{2.5}$ sensors in India include high aerosol mass concentrations and pronounced regional and seasonal gradients in aerosol composition. Here, we report on a detailed, long-time performance evaluation of a popular sensor, the Purple Air PA-II, at multiple sites in India. We established 3 distinct sites in India across land-use categories and population density extremes (North India: Delhi [urban], Hamirpur [rural]; South India: Bangalore [urban]), where we collocated the PA-II with reference beta-attenuation monitors. We evaluated the performance of uncalibrated sensor data, and then developed, optimized, and evaluated calibration models using a comprehensive feature selection process focused on reproducibility in the Indian context. We assessed the seasonal and spatial transferability of sensor calibration schemes, which is especially important in India because of the paucity of reference instrumentation. Without calibration, the PA-II was moderately correlated with the reference signal (R^2: 0.55 - 0.74) but was inaccurate (NRMSE $\leq$ 40%). Relative to uncalibrated data, parsimonious annual calibration models improved PA performance at all sites (cross-validated NRMSE 20-30%, R^2: 0.82-0.95), and greatly reduced seasonal and diurnal biases. Because aerosol properties and meteorology vary regionally, the form of these long-term models differed among our sites, suggesting that local calibrations are desirable when possible. Using a moving-window calibration, we found that using seasonally-specific information improves performance relative to a static annual calibration model, while a short-term calibration model generally does not transfer reliably

to other seasons. Overall, we find that the PA-II can provide reliable $PM_{2.5}$ data with better than $\pm$ 25% precision and accuracy when paired with a rigorous calibration scheme that accounts for seasonality and local aerosol composition.

Mapping Air Pollution in Polluted Data-Sparse Environments: Resolving Spatial-Temporal $PM_{2.5}$ Trends with Lower-cost Sensors in North India

North India faces the world's highest air pollution health burden across the urban-rural divide. Ground-based monitoring is essential for validating models and conducting holistic exposure assessments, but the high costs of reference instruments have limited their adoption to megacities. Here, we demonstrate an analytical approach to scaling a lower-cost sensor (LCS) network in North India using the commercially available PurpleAir PA-II sensor package. Our key constraint was to balance data completeness with representativeness, given the dynamic nature of LCS performance both out-of-the-box and for long-term deployment. We developed and applied our models across 13 diverse land-use collocations in the Delhi National Capital Region, resulting in robust out-of-sample seasonal performance (mean bias $<$ 10%). Validating our framework in Lucknow, another megacity in the region, demonstrated a high correlation between aggregated community-hosted LCS nodes and reference networks (Pearson's r $\geq$ 0.9) and well-constrained annual $PM_{2.5}$ estimates ($\leq$ 10%). While our data pipeline was developed in North India, our statistical framework offers paths forward for scaling similar regional networks in polluted, sparsely monitored environments.

Air Pollution Management Urgently Needed in Non-urban North India

High emissions from a diverse source mixture and unfavorable meteorology have resulted in extreme fine particulate matter ($PM_{2.5}$) air pollution in the Indo-Gangetic Plain (IGP) of North India. Most studies and abatement strategies have focused on densely populated megacities, but the majority of the population in the region (60-70%) reside in non-urban settlements. Therefore, although non-urban air quality is understudied in the IGP, it is critical to understand the regional health burden of $PM_{2.5}$ and develop informed policy. We implemented a lower-cost $PM_{2.5}$ monitoring network of over 80 sites across more than 15 settlements using the popular PurpleAir sensor. Our network spanned megacities to regional background sites and represents the first ground-based observations of $PM_{2.5}$ in most settlements. We observed sustained poor ambient air quality across the region (annual average $PM_{2.5}$ concentration $\geq$ 60 μg m^{-3}), with weak spatial gradients from urban core sites to regional background sites. Leveraging the high temporal resolution afforded by lower-cost sensors, we observed that although annual and seasonal trends were strongly correlated, diurnal patterns diverged across settlement population density strata. Megacities featured smooth diurnal profiles, with peaks later in the evening and larger intra-settlement variability

- indicating the complex mixture of traffic, heavy industry, and other sources. Conversely, non-urban and small city sites featured earlier and higher magnitude diurnal peaks (1.5 -1.7 $\times$ daily minimum), with low intra-settlement variability, likely indicating a higher relative prevalence of biomass burning. Policymakers should ensure clean air programs do not solely focus on relatively well-studied megacities at the expense of the large non-urban population distributed across the IGP.

Contents

Contents i

List of Figures iii

List of Tables vi

1 Introduction 1
- 1.1 Background on Lower-cost Sensors . . . 2
- 1.2 Background on Air Pollution in India . . . 3
- 1.3 Research Objectives . . . 4
- 1.4 Research Overview . . . 4

2 Seasonally Optimized Calibrations Improve lower-cost Sensor Performance: Long-term Field Evaluation of PurpleAir Sensors in Urban and Rural India 6
- 2.1 Introduction . . . 7
- 2.2 Materials & Methods . . . 8
- 2.3 Results & Discussion . . . 17
- 2.4 Conclusions . . . 31

3 Mapping Air Pollution in Polluted Data-Sparse Environments: Resolving Spatial-Temporal $PM_{2.5}$ Trends with Low-cost Sensors in North India 33
- 3.1 Introduction . . . 33
- 3.2 Materials & Methods . . . 34
- 3.3 Results & Discussion . . . 39
- 3.4 Conclusions . . . 51

4 Air Pollution Management Urgently Needed in Non-urban North India 53
- 4.1 Introduction . . . 53
- 4.2 Materials & Methods . . . 54
- 4.3 Implications . . . 64

5 Conclusions 66

5.1 Summary of Major Findings 66
5.2 Limitations 66
5.3 Policy Implications 67
5.4 Recommendations for Future Applications and Study 68

A Supplementary Information: Seasonally Optimized Calibrations Improve Low-cost Sensor Performance: Long-term Field Evaluation of PurpleAir Sensors in Urban and Rural India 70
A.1 Supporting Equations 70
A.2 Supporting Tables 72
A.3 Supporting Figures 78

B Supplementary Information: Mapping Air Pollution in Polluted Data-Sparse Environments: Resolving Spatial-Temporal $PM_{2.5}$ Trends with Low-cost Sensors in North India 99
B.1 Supporting Tables 99
B.2 Supporting Figures 102

C Supplementary Information: Rural Air Pollution Management Urgently Needed in North India 113
C.1 Supporting Tables 113
C.2 Supporting Figures 120

Bibliography 126

List of Figures

2.1 Diurnal profiles of mean hourly seasonal BAM (reference) and uncorrected PA $PM_{2.5}$ signals for Delhi, Hamirpur, and Bengaluru, using the CF1 channel. . . . 18
2.2 Normalized residual distributions for the uncalibrated PurpleAir data (CF1) and the calibration models for each site. 23
2.3 Regression metrics for the raw data, one-parameter model, two-parameter model, three-parameter model, and theory-driven hygroscopic growth model for each $PM_{2.5}$ channel. 24
2.4 Scatter plots of the best-performing annual models for each site, and model residual distribuitions stratified by season, and hour of day. 26
2.5 Assessment of inter-seasonal transferability of seasonal models by NMBE. 28
2.6 Assessment of the site-wise transferability of annual models. 30

3.1 Time-series plot, and monthly diurnal plots of reference and PurpleAir data at the IIT Delhi collocation testbed. 41
3.2 Summary of Monte Carlo simulation examining the trade-offs in sensor precision versus sample size. 44
3.3 Map of Delhi collocation regulatory sites used in the sensor accuracy and calibration analysis, along with reference-LCS time-series plot, diurnal plot, and distribution box-plots. 46
3.4 Map of QuantAQ deployments, with seasonal PM_1 and $PM_{2.5}$ concentrations. . 47
3.5 The bias distributions for each calibration regime at each Delhi collocation site. 49
3.6 Map of community-hosted LCS sites in Lucknow, and monthly average $PM_{2.5}$ concentrations from LCS, regulatory sites, and satellite-derived products. 50

4.1 Map of the study region in the Indo-Gangetic Plain of North India. 57
4.2 Example layout of the SAMOSA network deployment in a model non-urban settlement, Mai. 59
4.3 Seasonal $PM_{2.5}$ distributions at each LCS measurement site for each settlement category. 61
4.4 Seasonal diurnal mass concentration for all LCS sites, stratified by settlement category. 62
4.5 Map and time-series plot of Jaunpur, Mai, and Varanasi during contrasting pollution events. 64

A.1 Scatter plots between PurpleAir ATM channel and CF1 channel, and PurpleAir ALT channel and CF1 channel. . . . 78
A.2 Map of collocation sites within India and within each settlement. . . . 79
A.3 Mean diurnal profiles of $PM_{2.5}$ by season averaged across all reference sites in Delhi. 80
A.4 Mean diurnal profiles of RH and temperature by season averaged at the Delhi collocation site. . . . 81
A.5 Mean diurnal profiles of RH and temperature by season averaged at the Hamirpur collocation site. . . . 82
A.6 Mean diurnal profiles of RH and temperature by season averaged at the Bengaluru collocation site. . . . 83
A.7 Mean diurnal profiles of $PM_{2.5}$ by season averaged across all reference sites in Bengaluru. . . . 84
A.8 Time series of Delhi PurpleAir and reference signal throughout the collocation period. . . . 85
A.9 Time series of Hamirpur PurpleAir and reference signal throughout the collocation period. . . . 86
A.10 Time series of Bengaluru PurpleAir and reference signal throughout the collocation period. . . . 87
A.11 Bland-Altman plots for PA at the Delhi collocation site. . . . 88
A.12 Bland-Altman plots for PA at the Hamirpur collocation site. . . . 89
A.13 Bland-Altman plots for PA at the Bengaluru collocation site. . . . 90
A.14 Intra-Plantower R^2 and NRMSE for the collocated PurpleAir units at all sites. . 91
A.15 Scatter plots of PurpleAir raw performance versus collocated reference signal. . 92
A.16 Adjusted Coefficient of Determination for data-driven models for all sites. . . . 93
A.17 Normalized Residual distributions for the raw PurpleAir data (CF1) and the calibration Models for each site. . . . 94
A.18 Assessment of inter-seasonal transferability of seasonal models by MBE. . . . 95
A.19 Assessment of inter-seasonal transferability of seasonal models by NRMSE. . . . 96
A.20 Model results from 4-week rolling ordinary least squares (ROLS) exercise stratified by month. . . . 97
A.21 Comparison of calibration model performance (NRMSE) in each month for annual and monthly models. . . . 98

B.1 Distributions of $PM_{2.5}$ and RH measured by LCS, and stratified by monsoon and post-monsoon. . . . 102
B.2 Seasonal diurnal trends for temperature, relative humidity, and inverse ventilation coefficient at the IIT Delhi collocation site. . . . 103
B.3 Seasonal wind roses at the IIT Delhi collocation site. . . . 104
B.4 Time-series and diurnal plots of IIT Delhi reference monitor, and two nearby regulatory monitors. . . . 105
B.5 Orthogonal Distance Regression derived slope and intercept deviance values for each collocated PA-II relative to the fleet performance. . . . 106

B.6 Time-series plots and scatter plots of the fleet mean, standard deviation, and coefficient of variation during collocation phase C1. 107
B.7 Block and random data missingness experiments for the distribution p_{50} in the C1 phase subset. 108
B.8 Median and inter-quartile range of PA-II intra-unit disagreement as a function of sensor age. 109
B.9 Inter-site mean bias error and normalized mean bias error between training a calibration regression on the site on the x-axis and applying to data on the y-axis. 110
B.10 Inter-season mean bias error and normalized mean bias error between training a calibration regression in the season on the x-axis and applying to data on the y-axis. 111
B.11 Scatter plots of aggregate hourly PA-II data at each collocation site versus the reference $PM_{2.5}$ at the site binned by site, and RH. 112

C.1 Maps of population density, and satellite-derived population in India, with population-normalized concentration distribution plot. 120
C.2 Time-series plot and map of monitored districts in the Indo-Gangetic Plains. . . 121
C.3 Map and population normalized plot of both monitored and unmonitored district 2022 annual average $PM_{2.5}$ from satellite-derived products. 122
C.4 Indo-Gangetic Plains states population normalized $PM_{2.5}$ concentration distributions. 123
C.5 Time series of the distribution of sensors in each of the settlements in the winter episodic analysis. 124
C.6 Time series of the distribution of sensors in each of the settlements in the monsoon episodic analysis. 125

List of Tables

2.1 Summary of campaign measurements. 12
2.2 Most relevant parameters selected through sequential feature selection for each PurpleAir $PM_{2.5}$ channel by site. 21

3.1 Data overview for SAMOSA Campaign collocation test bed at IIT Delhi. 42
3.2 Data overview for SAMOSA Campaign reference-LCS calibration collocations. . 45

A.1 Most relevant parameters selected through sequential feature selection for each $PM_{2.5}$ channel from Delhi collocation. 72
A.2 Most relevant parameters selected through sequential feature selection for each $PM_{2.5}$ channel from Hamirpur collocation. 73
A.3 Most relevant parameters selected through sequential feature selection for each $PM_{2.5}$ channel from Bengaluru collocation. 74
A.4 Fitted coefficients from the hygroscopic growth model for each site and data channel. 75
A.5 NRMSE comparison of best-performing CF1 models for each site. 76
A.6 Mean Bias Error comparison of best-performing CF1 models for each site. . . . 77

B.1 Seasonal calibration coefficients derived from pooling all calibration sites and performing a regression fit. 100
B.2 Site-wise calibration coefficients derived from pooling all seasons and performing an Ordinary-Least Squares regression fit. 101

C.1 10^{th}, 25^{th}, 50^{th}, 75^{th}, and 90^{th} percentiles of the 2022 annual $PM_{2.5}$ concentrations for monitored and unmonitored districts in the Indo-Gangetic Plains States using satellite-derived $PM_{2.5}$. 114
C.2 10^{th}, 25^{th}, 50^{th}, 75^{th}, and 90^{th} percentiles of the 2022 annual $PM_{2.5}$ concentrations for monitored and unmonitored districts in the Indo-Gangetic Plains States using satellite-derived $PM_{2.5}$, stratified by state. 115
C.3 Settlement descriptions including number of LCS sites, campaign mean calibrated LCS $PM_{2.5}$, number of hourly data points, and settlement population. Note that campaign timeline is not identical for all sites. 116

C.4 Non-urban settlement type site-wise data summary, including number of samples, campaign mean LCS $PM_{2.5}$, and site land-use. Note that campaign timeline is not identical for all sites. 117
C.5 City settlement type site-wise data summary, including number of samples, campaign mean LCS $PM_{2.5}$, and site land-use. Note that campaign timeline is not identical for all sites. 118
C.6 Megacity settlement type site-wise data summary, including number of samples, campaign mean LCS $PM_{2.5}$, and site land-use. Note that campaign timeline is not identical for all sites. 119

Acknowledgments

"One must wait until the evening. To see how splendid the day has been."

– Sophocles, *Oedipus Tyrannus*, as translated by Robert Caro, *The Power Broker*

I first and foremost thank my advisor, Professor **Joshua Apte**. Josh's consistent support for my work, and advocacy for my interests stretches across more than 6 years and 1,500 miles at both UC Berkeley, and UT Austin. I am proud of our work together, and look forward to the exciting research we continue to develop. I am also thankful to my Dissertation, Qualifying Exam, and Preliminary Exam Committee members: Professors **Rob Harley**, **Cesunica Ivey**, **Tom Kirchstetter**, and **Ajay Pillarisetti**. I am profoundly appreciative of your thoughtful feedback, dedication, and wisdom. At UC Berkeley, I am additionally thankful to Professors **Allen Goldstein**, and **Justin Remais**. At UT Austin I am grateful to Professors **Lea Hildebrandt Ruiz**, **Kerry Kinney**, **Pawel Misztal**, **Paola Passalacqua**, and **Charlie Werth**.

I am especially grateful to two of my colleagues at UC Berkeley for their persistent advocacy of my work, indefatigable effort despite enormous odds, and, ultimately, their guidance in charting my career path - Professor **Saumya Singh**, and **María Hernández**. Saumya persevered in organizing one of the most ambitious atmospheric chemistry observational networks in history despite severe operational challenges. María's scientific vision and organizational skills were the linchpin of the SAMOSA campaign. I am awed by their tenacity, and this dissertation is very much a celebration of their determination and intellectual contributions to the fields of atmospheric science and public health.

Throughout my doctoral studies, I have been supremely fortunate to work with many sublime colleagues in the Apte Group. At UC Berkeley, I am grateful for the scholarship, friendship, and compassion of **Haley Bryne**, **Libby H Koolik**, and **Chirag Manchanda**. At UT Austin, I was particularly blessed to be patiently mentored by the wonderful Professor **Shahzad Gani**, Dr. **Sarah Chambliss**, and Professor **Jonathan Gingrich**. Beyond the Apte Group, I am deeply indebted to the Kirchstetter Crew for their continuous support and kindness; thank you to Dr. **Chelsea Preble**, Dr. **Rebecca Sugrue**, and **James Butler**. I am also broadly grateful to the entire Airheads Community for their companionship, especially Dr. **Betty Molinier**, **Michael Milazzo**, and Dr. **Pietro Vannucci**. I additionally appreciate the experience working with Dr. **Sahil Bhandari**, Dr. **Kanan Patel**, Professor **Yutong Liang**, and Dr. **Deep Sengupta** toward peer-reviewed publications not included in this dissertation.

None of this work would have been possible without the collaboration of my colleagues in India. I thank my colleagues at IIT Delhi, especially Professor **Sagnik Dey**, and Dr. **Sofiya Rao**. I am grateful to the entire SAMOSA team, especially the operational support of **Karthik Ganesan**, **Tanushree Ganguly**, **Adeel Khan**, **Sairam Dhandapani**, and **Saurabh Mendiratta**. I am profoundly thankful to the teams who helped jump-start my

entire sensor research focus: Professor **Ravi Kant Pathak**, Dr. **Sreekanth Vakacherla**, **Adithi Upadhya**, **Pratyush Agrawal**, **Meenakshi Kushwaha**, **Harsh Raj Mishra**, **Nisar Baig**, **Ravindra Srivastava**, and **Shreya Mishra**.

Finally, I thank my parents and family for seeing me through graduate school. Every year of my doctoral studies brought about a "once in a lifetime" level event, with setbacks both personal and professional. But my parents, **Barry Campmier** and **Rita Campmier**, my brother and his wife, Drs. **David Campmier** and **Brianna Campmier**, and my cousin **James St. John** brought me through it. No one accomplishes a PhD alone, and I certainly rest on the steadfast support of my family. A PhD pays dividends that are not immediately materially available, but that did not ever diminish their encouragement. My family believed in my vision before I had accomplished anything, and their love throughout my studies sustained me.

Chapter 1

Introduction

Fine particulate matter air pollution ($PM_{2.5}$) is the leading environmental risk factor for ill health and death. While estimates vary based on the specific concentration-response function, most evidence converges on approximately 4.1 million deaths attributable to ambient (outdoor) $PM_{2.5}$ [92]. An additional 3.1 million deaths are attributable to household air pollution - primarily indoor $PM_{2.5}$ - with clear linkages to ambient air pollution [127, 13, 92]. The burden is not evenly distributed across the world [122, 4]. In the United States (US), Western Europe, and other wealthy post-industrial nations of the Global North (population $\sim$ 1.6 billion), clean air policies since 1970 have successfully abated $PM_{2.5}$ and its precursors [140, 137]. In the Global South (population $\sim$ 6.3 billion), comprised of countries in Latin America, Africa, and Asia formerly colonized by the Global North, air pollutant concentrations have decreased slowly or increased [54]. Consequently, 90% of ambient $PM_{2.5}$ attributable deaths occur in the Global South [92].

To quantify exposure, enforce regulation, and validate models, governments operate networks of ground-based reference-grade instruments [93, 24, 138]. The design of robust $PM_{2.5}$ measurement networks balances representativeness across multiple spatial (microscale[$<$ 3 km] to synoptic[$>$ 1000 km]) and temporal (sub-hourly to decadal) scales to offer a holistic characterization of particle-phase pollutant dynamics [43, 24, 128]. Although considerable research has been dedicated to optimizing the placement of continuous monitors, regulatory networks are constrained by practical considerations. PM instruments have steep capital expenses ($\geq$ 10,000 USD), requiring secure facilities, consistent power supplies, and climate control, thus limiting placement [17, 85]. Additional budgetary constraints come from operating expenses - including instrument maintenance and staff. While these costs can be difficult to summarize globally, they could far exceed capital costs as a specialized and highly educated workforce is required to collect, process, and interpret data.

Most countries have no publicly accessible regulatory monitoring [85, 4]. In the United States, where the regulatory network is relatively well developed, the network has been found to poorly constrain intra-regional exposure disparities [21, 90]. Consequently, researchers have sought to provide other observational estimates of ground-level $PM_{2.5}$. Satellite remote sensing derived $PM_{2.5}$ products have provided spatially complete maps ($0.01^\circ \times 0.01^\circ$)

at monthly or annual intervals [117, 35, 79, 33]. Mobile monitoring, or equipping mobile platforms such as research trucks with reference instruments, has similarly improved spatial resolution - especially detection of neighborhood-scale hotspots [6, 20, 5]. However, these supplementary techniques do not provide real-time publicly accessible measurements, rely on fixed-sites to validate data processing algorithms, and are expensive.

1.1 Background on Lower-cost Sensors

As early as 1926, researchers sought to develop cheap real-time alternatives to gravimetric methods by leveraging the optical properties of particles to infer mass concentration [45, 101]. In brief, these devices sample particles from ambient air either passively via convection or mechanically using a fan or pump. The instrument then measures the light scattered or absorbed from a source of known quality (wavelength, power, phase, etc.) by the sampled particles. Throughout the 20^{th} century, optical measurement techniques gradually miniaturized and became widely used in individual-scale PM exposure studies, especially in occupational settings [19, 73]. As laser technology advanced, manufacturing costs decreased, allowing for increasingly cheap miniaturized PM sensors to enter the market. These optical particle sensors, costing less than $\sim$500 USD, have been alternatively dubbed "air sensors," "low-cost sensors," "lower-cost sensors," or "lower-capital cost sensors." For simplicity, I refer to this class of instruments as "lower-cost sensors" or LCS.

Broadly, there are two classes of optical PM LCS: nephelometers and optical particle counters. Nephelometers infer PM mass concentrations by measuring the light scattered from an ensemble of particles, while optical particle counters measure single particle scattering intensity [51]. From these measurements, the particle volume can be calculated, and mass concentration estimated using a density assumption [29, 28]. Both methods are biased and therefore inaccurate relative to reference methods since particle scattering properties are strongly influenced by the underlying particle size distribution and refractive index. Since this constitutes an inverse problem, it can be difficult to predict the accuracy of an LCS for any arbitrary aerosol [16]. Accordingly, semi-empirical or empirical methods are employed to derive calibration relationships with reference instruments through collocation studies [144]. Most often, relative humidity (RH) has been found to play a key role in LCS bias, as hygroscopic particles uptake water vapor as aerosol liquid water, thus influencing both their refractive index and size distribution [51]. Typically, commercial LCS do not treat ambient air with the same tightly prescribed standards as reference instruments.

Despite these limitations, LCS have seen widespread adoption as a tool for enhancing $PM_{2.5}$ spatial-temporal observational resolution [78, 15, 2]. Specifically, the Plantower PMS series models have been readily incorporated in sensor packages by researchers, community groups, governments, and private enterprise. Unfortunately, Plantower's sparse documentation sowed confusion in the research community, leading many studies to hypothesize its instruments acted as nephelometers [95, 51, 56]. However, in-depth reverse engineering published in 2024 has demonstrated that although the Plantower output data is strongly

correlated with integrating nephelometers across several orders of magnitude, it is actually a low-efficiency optical particle counter [94, 91].

In the United States, the company PurpleAir has successfully scaled a crowd-sourced network of sensors primarily using the Plantower PMS5003. Their approach, which included offering a user-friendly website of nearby community-hosted sensors, saw rapid scaling in the aftermath of several large wildfire events in the Western US. For example, following the devastating 2018 Camp Fire, there were about 180 PurpleAir monitors in San Francisco County, compared to 1 multi-pollutant regulatory site [78]. Furthermore, the PurpleAir platform also allows users to apply various calibration correction factors derived by researchers through collocation studies. In the Global South, where the cost of monitoring remains a significant challenge in exposure assessment, LCS public data platforms could help communities, researchers, government bodies, and non-profit organizations combine their efforts to bridge the ground-based monitoring gap.

1.2 Background on Air Pollution in India

From the available evidence, India faces the highest $PM_{2.5}$ burden in the world, with an estimated 1 million attributable deaths per year or around 25% of the entire global mortality burden of $PM_{2.5}$ [97, 3]. While significant progress since 1990 has arguably decreased the health burden of household air pollution, the health burden of ambient $PM_{2.5}$ has increased [97]. Within India itself, neither population centers nor $PM_{2.5}$ are uniformly distributed, with both the highest mass concentrations and highest population density in the Indo-Gangetic Plain - the northern basin bordering the Himalayan Mountains [109]. Both cities and rural communities within the Indo-Gangetic Plain are among the most polluted on the planet, with an annual population-weighted average of 76 $\mu g/m^3$, more than 15 times the World Health Organization air quality guideline of 5 $\mu g/m^3$, and almost double the Indian National Ambient Air Quality standard of 40 $\mu g/m^3$ [109, 3].

The speciation and sources of PM in India are diverse, especially in the Indo-Gangetic Plain. There are seasonally dependent large contributions from black carbon [37], ammonium chloride [42, 60], as well as consistently high regional secondary organic aerosol from sources including traffic, biomass burning, and industrial processes [131]. Consequently, mass concentrations are large and spatially variable both within Delhi and the Indo-Gangetic Plain. Work on non-urban sources in the Indo-Gangetic Plain emphasizes the roles of agricultural sources, including stubble burning [100]. Across both urban and non-urban settlements, the "informal sector," or small-scale manufacturing such as bricks and concrete, contributes significant emissions difficult to capture in emissions inventories [131]. Non-anthropogenic dust storms are also common in the Indo-Gangetic Plain, especially in the summer months leading up to the monsoon [118]. While there are fewer studies examining the sources and dynamics outside of the Indo-Gangetic Plain, literature reports rising levels of annual ambient $PM_{2.5}$ due to biomass burning and increasing traffic emissions [124, 105, 49]. Given the high burden and complexity of $PM_{2.5}$ throughout India, there is significant incentive to in-

crease understanding of the spatial-temporal nature of air pollution, effectively communicate risk to the public, and inform mitigative measures.

Prior to 2014, the only continuous reference monitors in India were hosted at the US diplomatic missions. Since 2016, the Central Pollution Control Board, along with the state-level agencies have begun scaling monitoring throughout urban India [47, 17, 98]. There are about 40 operational multi-pollutant reference stations in Delhi, with more than 3 stations in most megacities in North India. However, given the distribution of the largely non-urban population and the transient nature of the informal sector, these stations are still tens to hundreds of kilometers away from most Indians [47]. Scaling the reference network to every district or administrative jurisdiction is impractical - LCS offer the opportunity to augment the resolving power of the network. However, at the start of my research in 2018, LCS networks were untested and mistrusted in India, given the larger dynamic range and complexity of aerosol in India.

1.3 Research Objectives

Research Questions

- Can lower-cost sensors provide high-resolution, low-bias data in India?
- How can a lower-cost sensor network be scaled in highly polluted data-sparse regions of India?
- What actionable information can a lower-cost sensor network provide to stakeholders in India?

Air pollution in India and LCS technology are dynamic and complex topics with significant implications for human health, atmospheric chemistry, and environmental policy. My research here focuses on informing the application of $PM_{2.5}$ LCS in unmonitored environments and constraining the compounding uncertainties arising from network deployments.

1.4 Research Overview

As a guiding principle, I sought to estimate highly resolved $PM_{2.5}$ exposure using observations and statistical modeling, along with fundamental principles of aerosol and atmospheric science. **Chapter 2** entails a "proof-of-concept," in which I evaluate LCS performance across India and develop calibration correction factors. I discuss the trade-offs at play with regards to collocation length and aerosol seasonality. **Chapter 3** introduces the SAMOSA campaign, an ambitious LCS network across the Indo-Gangetic Plain. I build on the initial collocation datasets from the previous chapter and evaluate the competing sources of uncertainty with a much larger sample size. On top of precision and calibration analyses, I also demonstrate the value of the SAMOSA network in Lucknow, a megacity in the Indo-Gangetic

Plain. **Chapter 4** rests upon the methods development in the previous chapters to provide an overarching perspective of air pollution in the Indo-Gangetic Plain. The SAMOSA network coverage of small cities and non-urban communities highlights the overlap in high mass concentrations throughout North India, as well as the unique challenges facing unmonitored communities.

Chapter 2

Seasonally Optimized Calibrations Improve lower-cost Sensor Performance: Long-term Field Evaluation of PurpleAir Sensors in Urban and Rural India

The text and research in this chapter was published in *Atmospheric Measurement Techniques*. The citation for the published article is as follows:

Mark Joseph Campmier et al. "Seasonally optimized calibrations improve low-cost sensor performance: long-term field evaluation of PurpleAir sensors in urban and rural India". English. In: *Atmospheric Measurement Techniques* 16.19 (Oct. 2023). Publisher: Copernicus GmbH, pp. 4357–4374. DOI: 10.5194/amt-16-4357-2023

2.1 Introduction

Exposure to fine particulate matter, or $PM_{2.5}$ (particles with aerodynamic diameter ≤ 2.5 µm), is a leading cause of adverse health outcomes, including premature death [74, 132]. India experiences high mass concentrations in both its population-dense megacities and its rural areas, resulting in the largest number of deaths (about 1 million annual deaths and about 1.5-year reduction in life expectancy) attributable to ambient $PM_{2.5}$ worldwide [4, 97]. In particular, New Delhi, the surrounding Delhi National Capital Region, and the broader Indo-Gangetic Plain of north India occasionally experience hourly concentrations exceeding 1000 µg m^{-3} [42], resulting in ill health effects even from short-term exposure [46, 69]. South India generally experiences lower $PM_{2.5}$ concentrations but still has population-weighted annual mass concentrations that exceed World Health Organization (WHO) recommendations by a large margin [3]. As relatively fewer polluted megacities in south India continue to rapidly grow, the challenge of ambient $PM_{2.5}$ will also increase [49, 107].

Given the high exposure burden and complexity of $PM_{2.5}$ throughout India, there is a need to increase understanding of the spatial-temporal patterns of air pollution. Traditional regulatory monitors are expensive to install and maintain, as they require specialized teams and consistent power to maintain networks [17]. As a result, there is a dearth of monitors in India [17, 85]. Although satellite remote sensing can fill in the spatial gap, it lacks high-quality temporal coverage and relies on ground-based monitoring for calibration algorithms [54], which can, as is the case in India, result in biased estimates of surface $PM_{2.5}$ [33].

Starting in around 2010, advancements in miniaturized electronics and laser technology have resulted in the growth of lower-cost ($\leq$ USD 500) $PM_{2.5}$ sensor technologies. These light-scattering monitors are popular within the research community and among citizen scientists. The company PurpleAir (PA) has been especially successful in developing (1) a USD 200–280 lower-cost sensor that utilizes a commercially available, light-scattering sensor developed by Plantower (PMS5003); and (2) a platform for individuals and organizations to share data from indoor and outdoor PurpleAir lower-cost sensors.

Light-scattering lower-cost sensors require extensive data quality control and careful selection of calibration models to offer measurements comparable to reference quality instruments [51, 52]. Optical sensors inaccurately estimate mass from aerosol scattering properties, since $PM_{2.5}$ is a mixture of particle sizes and chemical compositions, thus resulting in spatial-temporal variability in optical properties [51, 75, 145]. The roles of relative humidity, mass concentration range, sensor aging, and diverse source profiles have been extensively studied in laboratories and field conditions in the USA, Australia, and Europe. Lab studies report that the Plantower sensors do not adequately characterize fine particles above 0.8 µm [72], deteriorate under extreme mass concentrations [88, 129], and are vulnerable to overestimation at RH greater than 60% [61].

Field studies in low to moderate pollution environments show that PA units can be calibrated to reference instruments using simple empirical regression techniques with environmental variables [11, 82, 141]. Models are often specific to a season and location; however, Barkjohn, Gantt, and Clements [11] demonstrated that a continental USA calibration equa-

tion could be effectively deployed for daily data.

Recently there has been increased interest in understanding lower-cost sensor performance in the Global South to fill major monitoring gaps [10, 62, 83, 87, 105, 125, 141, 142]. In north India, Zheng et al. [141] deployed Plantower models in Kanpur, Uttar Pradesh, for 90-d and found that multilinear regression improved Plantower performance, albeit with significant error for hourly data. In south India, Puttaswamy et al. [105] calibrated Plantower units for 68-d in Chennai and found a multilinear regression approach that reduced uncertainty to within 15% and 18% for $PM_{2.5}$ and PM_{10}, respectively. lower-cost sensor studies in India report the importance of climate and emissions variability on aerosol characteristics and advise future deployments to test calibration algorithms across longer timelines [83, 105, 125, 141, 142].

In this study, we deployed and evaluated PurpleAir PA-II sensors in Delhi, Hamirpur, and Bengaluru by collocating with regulatory-grade instruments for 335-d, 154-d, and 312-d, respectively. We built hourly local calibration models using multilinear regression. With proper data quality constraints, a relatively simple calibration model can produce high-accuracy and low-bias data. Despite this success, model performance degrades when attempting to transfer a model trained in each environment to data collected in a dissimilar environment. We found a more pronounced reduction in performance when attempting to transfer a model trained in one season to another season, as aerosol characteristics can shift rapidly – even at the same site. Our work demonstrates that lower-cost sensors are a viable option for measuring spatial-temporal trends throughout India, but calibration models are vulnerable to the local and seasonal effects on aerosol properties.

2.2 Materials & Methods

Lower-cost sensors

The sensor used in this study was the PurpleAir PA-II. The PA-II is marketed as PurpleAir's outdoor aerosol monitor and is composed of a weatherproof plastic shell containing two Plantower PMS5003 sensors (labeled as A and B channels), an Adafruit model BME280 atmospheric sensor (temperature, RH, and pressure), and a wireless transmitter module to upload data via Wi-Fi. The PMS5003 reports the particulate matter (PM) mass concentrations (µg m^{-3}) of all particles with an aerodynamic diameter smaller than 1, 2.5, and 10 µm, as well as particle number concentrations (dL^{-1}) of all particles larger than 0.3, 0.5, 1.0, 2.5, 5, and 10 µm [143].

PurpleAir reports mass concentrations from PA-II models in three forms, which are referred to as CF1, ATM, and ALT. CF1 is the "uncorrected" data from the Plantower. The CF1 data have been demonstrated to strongly correlate with collocated integrating nephelometer data [95]. ATM or atmospheric-corrected data use a piecewise function to attempt to account for overestimation. Figure A.1 in the appendix illustrates this function across the full dynamic range for the data collected in Delhi. Between 0 and 20 μg m^{-3}, the

CF1 and ATM data are 1 : 1, between 20 and 100 µg m^{-3} the ATM to CF1 ratio transitions from 1 : 1 to approximately 0.66 : 1, and at greater than 100 µg m^{-3} the ATM to CF1 ratio is stable at 0.66 : 1. Although it is reasonable to hypothesize that the ATM data may better represent exposure ambient $PM_{2.5}$ than the CF1 data, there is no transparent reasoning in the user manual for this design choice [135, 143]. Finally, the ALT (alternative data reconstruction) data represent a reconstruction of the $PM_{2.5}$ data from the particle number data reported by the Plantower. Briefly, the ALT method adds all the particle counts from bins smaller than 2.5 µm and calculates the particle volume concentration, assuming spherical particles. The particle volume concentration is then multiplied by the unit density (1 g cm^{-3}) to estimate the $PM_{2.5}$ mass concentration. Wallace et al. [135, 136] used these data to develop calibration relationships, reporting the ALT data as being more transparent than using the CF1 or ATM data. However, the particle number data are known not to reflect the actual ambient size distribution, since the Plantower PMS5003 is not a particle sizing instrument but rather reflects a modeled size distribution using assumptions for relationships between size bins that are not always accurate for the atmospheric conditions [95, 51, 56, 72]. Figure A.1 shows that the ALT to CF1 ratio is approximately 0.15 : 1. Although the CF1 and ATM data have dominated most calibration efforts [83, 105, 11, 87, 81, 82], the usage of ALT data continues to propagate in peer-reviewed literature [134, 133]. Therefore we use CF1, ATM, and ALT in our study to work towards harmonizing a calibration approach for PA-II in India.

Regulatory-grade monitors

We compared our PurpleAir measurements against U.S. Environmental Protection Agency (EPA) Federal Equivalent Method (FEM)-certified continuous monitors. Our selected FEMs are Met One Instruments, Inc., BAM (beta attenuation mass monitor) models 1020 and 1022, which are widely used devices [53] that use the beta wave attenuation technique to determine particle mass based on a sample deposited on a filter tape. The FEM certification applies to 24 h averaged data, while the BAM models can provide measurements at hourly or higher time resolution. We used the 1-h block as our highest level of temporal resolution, similar to other lower-cost sensor calibration studies using beta attenuation reference monitors in the USA and India [63, 81, 125, 141].

At the Delhi site, we used the BAM 1020 model; data from this monitor are public and maintained by the U.S. Department of State's AirNow service [112]. The Hamirpur and Bengaluru sites utilized the BAM 1022 model managed in collaboration with field teams from the Indo-Gangetic Plains Centre for Air Research and Education and the Center for Study of Science, Technology, and Policy, who manually retrieved data at regular intervals. Staff at each site followed the manufacturer's recommended operation and maintenance, which resulted in downtime for each dataset.

Deployment sites

Three separate long-term measurement efforts were conducted to evaluate the PA-II performance under different meteorological and aerosol composition regimes. Each campaign was scheduled to last approximately 1 year, enabling a comparison of a range of mass loadings and the effect of season. We use the definition of four seasons from the Indian Meteorological Department (IMD), namely winter (January and February), pre-monsoon (March, April, and May), monsoon (June, July, August, and September), and post-monsoon (October, November, and December; [36]). A reference map of the collocation sites is presented in Fig. A.2.

U.S. Embassy, New Delhi, National Capital Territory of Delhi, India

The Indian National Capital Region, including the capital city of New Delhi (elevation of about 230 m), is the second-largest megacity in the world, with a metro-area population of around 28.5 million people. It has also been called the most polluted megacity in the world, experiencing annual average $PM_{2.5}$ concentrations exceeding 120 µg m^{-3} (Fig. A.3; Gani et al. [42]). The National Capital Region, along with the rest of north India experiences dynamic meteorology, with cold and wet winters, warmer and drier post-monsoons and pre-monsoons, and hot and wet monsoons (Fig. A.4).

Our measurement site was the U.S. Embassy (28.5975 °N, 77.1878 °E) in the Chanakyapuri neighborhood of central New Delhi. The embassy is located within the city's spacious diplomatic enclave, which has abundant green space, relatively low traffic flows, and minimal local industrial emissions. We collocated 2 PA-II units with the embassy BAM from July 2018–April 2020. During the course of our campaign, Delhi experienced extreme $PM_{2.5}$ concentrations during the post-monsoon agricultural burning seasons and characteristic winter inversion layers, with a relatively low-pollution monsoon season, consistent with expected seasonal trends [48].

Indo-Gangetic Plains Centre for Atmospheric Research and Education, Hamirpur, Uttar Pradesh, India

We established a rural $PM_{2.5}$ monitoring site in the Hamirpur district, located within north India, in India's most populous state of Uttar Pradesh (UP). Our monitoring site was established in partnership with the Indo-Gangetic Plains Centre for Atmospheric Research and Education. This remote, solar-powered rural monitoring site is situated on a rooftop (20 m above ground level) of a solitary building (25.9552 °N, 80.1522 °E) located about 800 m outside Ruri Para village in Hamirpur district, Uttar Pradesh. The immediate surroundings within 500 m of the site are a mixture of agricultural fields, ravines, and scrubland forests. The closest major town, Hamirpur (population about 35,000) is approximately 30 km away from the site, and the closest large city, Kanpur (population about 3 million) is 80 km away. Meteorological patterns are similar to Delhi (Fig. S5). We collocated three PA-II sensors with a BAM 1022 model on the Indo-Gangetic Plains Centre for Atmospheric Research and

Education rooftop beginning in January 2020. Here, we report on data for the year from January 2020 to January 2021.

Although campaign-median $PM_{2.5}$ concentrations at the site (Table 2.1) are high in the global context, this site's remote location outside of both cities and villages means that the concentrations do not reach the same peaks as in Delhi. However, there are still many local sources of aerosol air pollution in rural north India, such as biomass burning for cooking and heating [110]. The Hamirpur dataset is additionally differentiated from the Delhi dataset in that most of the data were collected during the first year of the COVID-19 pandemic, which was observed to change patterns of emissions throughout India [99, 120].

Table 2.1: Summary of campaign measurements (quality assured according to methods outlined in 2.4 and summarized in 3.1 - 3.3) including 10^{th} percentile (p_{10}), 25^{th} percentile (p_{25}), 50^{th} percentile (p_{50}), 75^{th} percentile (p_{75}), and 90^{th} percentile (p_{90}) for the campaign periods (Delhi: 2018 July – 2020 April, Hamirpur: 2020 January – 2021 January, Bangalore: 2019 June – 2020 August)

	Delhi	Hamirpur	Bangalore
BAM 1020/1022 $PM_{2.5}$ ($\mu g/m^3$)			
p_{10}	23.0	10.6	10.8
p_{25}	39.0	17.9	15.3
p_{50}	71.0	34.3	21.8
p_{75}	142.0	67.4	30.8
p_{90}	237.0	125.4	42.1
PA-II CF1 $PM_{2.5}$ ($\mu g/m^3$)			
p_{10}	31.0	18.1	12.7
p_{25}	52.2	31.3	18.1
p_{50}	117.0	63.4	31.0
p_{75}	243.0	124.3	52.9
p_{90}	375.0	218.0	74.5
PA-II ATM $PM_{2.5}$ ($\mu g/m^3$)			
p_{10}	30.4	18.1	12.7
p_{25}	43.0	30.2	18.1
p_{50}	83.8	47.0	30.0
p_{75}	180.0	82.7	42.4
p_{90}	285.0	146.7	51.3
PA-II RH (%)			
p_{10}	20.6	29.8	34.2
p_{25}	29.6	44.1	48.0
p_{50}	41.0	62.9	62.9
p_{75}	48.5	77.4	73.8
p_{90}	53.1	85.7	78.6
PA-II Temperature (°C)			
p_{10}	18.7	17.2	23.7
p_{25}	22.8	24.5	25.0
p_{50}	29.2	30.6	27.7
p_{75}	35.1	35.3	32.3
p_{90}	39.0	40.3	37.1

Center for Study of Science, Technology, and Policy, Bengaluru, Karnataka, India

Bengaluru, in south India, is the third-largest city in India, with a population of 8.4 million, and the capital of Karnataka. South India experiences different meteorological conditions and considerably lower air pollution burdens than north India [3, 36] (Figs. A.6, A.7). Although continuous $PM_{2.5}$ regulatory monitors are sparse in Bengaluru, the current network estimates a citywide annual average of 30 μg m^{-3}. While the annual average is low in comparison to Delhi and the Indian National Ambient Air Quality Standard of 40 μg m^{-3}, it exceeds the WHO annual guideline value of 5 μg m^{-3}, and hourly winter concentrations often exceed 50 μg m^{-3}. Consequently, Bengaluru has been designated for air quality improvement under the Indian National Clean Air Programme [40]. In Bengaluru, emissions are dominated by traffic and dust resuspension [49]. Compared to Delhi and Hamirpur, winters are milder, and the climate is more consistent year-round in Bengaluru (Fig. A.6). The winter and pre-monsoon seasons are distinguished from the monsoon and post-monsoon seasons primarily by RH and precipitation. Monsoon and post-monsoon are cloudy and rainy, with RH typically exceeding 70% all day and possibly remaining above 90 % before sunrise. Winter and pre-monsoon RH are more moderate, with hourly averages fluctuating between 40% and 80%.

Our collocation site was the Center for Study of Science, Technology, and Policy office in northern Bengaluru. We maintained a BAM 1022 model on the rooftop of a three-story office building (13.0485 °N, 77.5795 °E). Although the site is located near a highway (Outer Ring Road), the annual diurnal patterns matched the regional signature from the average of the regulatory monitors. Furthermore, the area surrounding the site is mostly office buildings, with some residential housing. There are no large industrial sites or obvious large point sources in the neighborhood, other than occasional small solid-waste fires. It is likely that the Bengaluru BAM is thus mostly influenced by urban background and regional aerosol conditions. We set up two PA-II sensors from June 2019–July 2020, during which Bengaluru experienced hourly spikes above 100 μg m^{-3} during the festival of Diwali and dynamic changes in traffic patterns due to the COVID-19 pandemic and lockdowns.

Quality assurance

PurpleAir PA-II $PM_{2.5}$

Many light-scattering $PM_{2.5}$ sensors, including the PA-II, can report unrealistic measurements, lack accuracy (especially at high mass loadings), and are only recommended for operation within a specific range. To minimize these effects, we removed unreasonably small and large points (outside the range of 5–500 µg m^{-3}), averaged each individual Plantower unit by the hour, averaged across all units for a given site, removed imprecise points, and calibrated the resulting clean dataset. We conducted quality assurance (QA) procedures separately for each sensor correction factor (CF1, ATM, and ALT).

We removed all raw $PM_{2.5}$ data points outside of the range 5–500 μg m^{-3} [68, 81, 143]. Analyses of PurpleAir data typically report the percent error between channels A and B for

a given unit to remove imprecise points, thus treating them as joint measurements and all other nodes as independent [11]. However, at our collocation sites, there was always more than one PA-II, so we treated all Plantower sensors as replicate measurements and averaged them together as a single data point. For instance, if we had three PA-IIs at a site, then we averaged the six values together – two from each unit – to estimate a single data point. We established 80 % completeness criteria (or 24 2-min data points) for each hourly average and at least two valid Plantower hourly averages for the resulting site PA data point. Imprecise data points were removed using the coefficient of variation (CV), the quotient of the standard deviation, and the mean of the collocated Plantower sensors for a given 2-min raw sample. CV values greater than 0.2 were removed, which is broadly consistent with approaches used by other studies [9, 29].

PurpleAir PA-II temperature and relative humidity

The Adafruit model BME280 is considered to be a reliable and accurate lower-cost environmental sensor [7]. There are occasional incidents of sensor miscommunication with the microprocessor, leading to unrealistic values, which we filtered out by restricting RH to 0%–100% and temperature to -10 to 50 °C. We computed the dew point temperature from the measured temperature and RH, following Malings et al. [82].

Met One BAM 1020 and BAM 1022

The BAM instrument flags low-quality data with a specific code to (1) potentially remove them from analyses and (2) diagnose underlying issues, which can include power loss and pump errors. The default concentration range of the BAM 1020 and BAM 1022 models is 3–1000 μg m^{-3}. Unlike the PA-II, the hourly limit of detection of the BAM 1022 and BAM 1020 is well constrained to 2.4 μg m^{-3} [81], which is considerably below the typical concentrations in our dataset. Like other linear regression studies using Met One BAM models and Plantower nephelometers, we utilized an ordinary least squares approach [11, 82, 87, 88, 135, 141].

Calibration regression

Since optical-based sensors are known to provide biased measurements of $PM_{2.5}$ measurements relative to reference-grade instruments, in large part due to hygroscopic growth, calibration procedures attempt to account for bias due to RH, index of refraction, and mischaracterizing the particle size distribution. One approach is to leverage the environmental data (RH, temperature, etc.) from lower-cost sensor nodes to develop the best-fitting model without imposing any a priori assumptions about aerosol growth or chemistry [11, 87, 82, 135, 141]. We label this approach as "data-driven." From decades of work with optical instruments, corrections have been developed by assigning non-linear growth terms as a function of RH and known $PM_{2.5}$ chemical characteristics [82, 19]. In our work, we label this approach

as "theory-driven", since it attempts to fuse the best-fitting function form from theory with the best-fitting regression coefficients. Although the theory-driven model should produce the most transferable models, since theory should apply in all environments, the underlying data processing of the Plantower – a truncated nephelometer proxy [95] – may result in a bias structure that is better explained by a linear RH correction than a non-linear correction for the dynamic range of RH under real-world conditions.

Data-driven model selection

To ensure that our work is easily reproducible within India, we relied only upon variables reported or calculable by the PA-II as independent variables, namely PM, RH, temperature, and dew point. For our PA-II $PM_{2.5}$ variable, we evaluated CF1, ATM, and ALT values. We evaluated all regression models using ordinary least squares, with the BAM $PM_{2.5}$ as the dependent variable and our candidate parameters as independent variables. To iterate across all possible arrangements of predictors – including additive terms, interaction terms, and polynomial terms up to the third order – we implemented sequential feature selection (SFS), using the Python package scikit-learn 0.24.2. SFS uses a "greedy" approach to converge on the best-performing model for a user-defined number of parameters [108, 38]. For example, if a user wanted a two-parameter model from a set of 10 features, then SFS would iteratively compare 90 models (i.e., the set of all possible two-parameter feature permutations), using a robust regression metric (such as the adjusted R^2 or Bayesian information criterion, BIC). In our approach, we first use SFS to define the best-performing n-parameter model, starting with all possible parameters ($n = 34$). We then compare the adjusted R^2 across best-performing n-parameter models to measure the impact of the model complexity. If increasing the parameters results in only marginal improvements ($\Delta R^2 \approx 0.01$), then it is unnecessary to use those additional features. The overall most robust model, therefore, reflects both the best possible selection of features and the feature parsimony.

Theory-driven model selection

From the κ-Köhler theory, we expect wet $PM_{2.5}$ scattering to increase exponentially with increasing RH, resulting in strongly non-linear dynamics. Therefore, we applied a calibration function relying on empirically fitted coefficients from the training data, with a non-linear RH term to capture the expected trends from the theory. Studies have attempted to apply a non-linear RH term for light scattering lower-cost sensors, with results similar to or less accurate than an additive term [19, 82, 129, 141]. Given the difference in emission sources, size distribution, mass loadings, and meteorology, we decided to include a non-linear RH term, using the following form in Eq. (2.1).

$$C = \frac{\alpha \times P}{1 + \beta \frac{\mathrm{RH}^2}{1-\mathrm{RH}}}, \tag{2.1}$$

where α and β represent the regression coefficients to be fitted via non-linear least squares, P is the PurpleAir signal (ATM, CF1, or ALT), RH is the unitless relative humidity scaled from 0 to 1, and C represents the corrected $PM_{2.5}$.

Cross-validation

To evaluate our calibration models, we sought to design an appropriate cross-validation scheme that would permit a balanced evaluation of model performance among all seasons. A simple test–train split would likely over-represent seasons with more measurements. We thus performed a stratified k-fold cross-validation, in which each fold contains equal representation from each of the four seasons; we evaluated each model by leaving one fold out in subsequent iterations.

Temporal sensitivity

As a point of contrast with the seasonally balanced calibration described above, we performed a data experiment to investigate the temporal stability of a hypothetical shorter-term calibration. This exercise was motivated by the common practice in many lower-cost sensor deployments that perform a short-term initial calibration before deploying sensors in the field and then, if the lower-cost sensors are available, perform another short post-study collocation. Previously, Levy Zamora et al. [76] identified diminishing returns in improvements to calibration regressions after about 4 weeks of collocation in Baltimore, USA, if that period encapsulated a representative range of $PM_{2.5}$ and RH conditions. Here we build on this work by seeking to identify which 4-week period is ideal at our sites in India, since annual median $PM_{2.5}$ concentrations at the Delhi and Hamirpur sites are about $10\times$ higher than Baltimore and reflect a different mixture of chemical composition and aerosol properties. To explore the potential bias from extrapolating a short-term calibration to a longer period, we fitted 4-week rolling ordinary least squares models with the features selected via SFS and compared the performance against all other 4-week periods during our yearlong data collection to understand the implications of short-term calibration for other studies.

Performance metrics

As a guiding principle, we selected those models which balanced parsimony with low error, low bias, and strong temporal consistency for presentation. We selected analytical methods and performance metrics to optimize these parameters and have designated these best-performing models as being "robust". Given the high concentrations and high variability within and between sites, we report the normalized root mean square error (NRMSE), allowing a comparison of model performance across sites and time periods [119]. Additionally, we used the coefficient of determination (R^2) to evaluate model accuracy [119]. For multivariate regression models, we used the adjusted R^2 metric to account for spurious correlations with increasing numbers of independent variables. To penalize the overfit and minimize the number of parameters, we used the Bayesian information criterion, a metric

for parsimonious feature selection, when selecting between models during the SFS process. Finally, we assessed the mean bias error (MBE) and normalized mean bias error (NMBE) to characterize the average direction of error [119].

2.3 Results & Discussion

Reference instrument data summary and quality assurance

BAM and PA measurement summary statistics are summarized in Table 2.1 for each site, with time series plots in Figs. A.8–A.10. Overall, BAM monitors used at each site provided consistent performance, despite the challenging deployment circumstances due to intermittent power loss; extreme weather, including heavy rains; and a relatively broad range of mass concentrations.

The U.S. State Department monitor in Delhi employs the U.S. EPA's data reduction process [112, 130], resulting in a loss of about 3 % for the data points, with a continuous gap from 10 February to 18 March 2019. For context, we compared this site's time series with 39 other sites in Delhi's regulatory network and found a R^2 of 0.86 and a mean difference from the regulatory network average of $-$ 8.4μg m^{-3}, likely resulting from this monitor's location in one of the city's cleanest neighborhoods. The diurnal plot for the Delhi BAM in Fig.A.1 reflects the roles of time-varying emissions and boundary layer dynamics with peaks during the morning traffic rush hour (07:00–10:00 LT) and extremes in the winter exceeding an average of 200 μg m^{-3} during the night and early morning. During the monsoon, we observed a relatively low daily dynamic range of 35–50 μg m^{-3}.

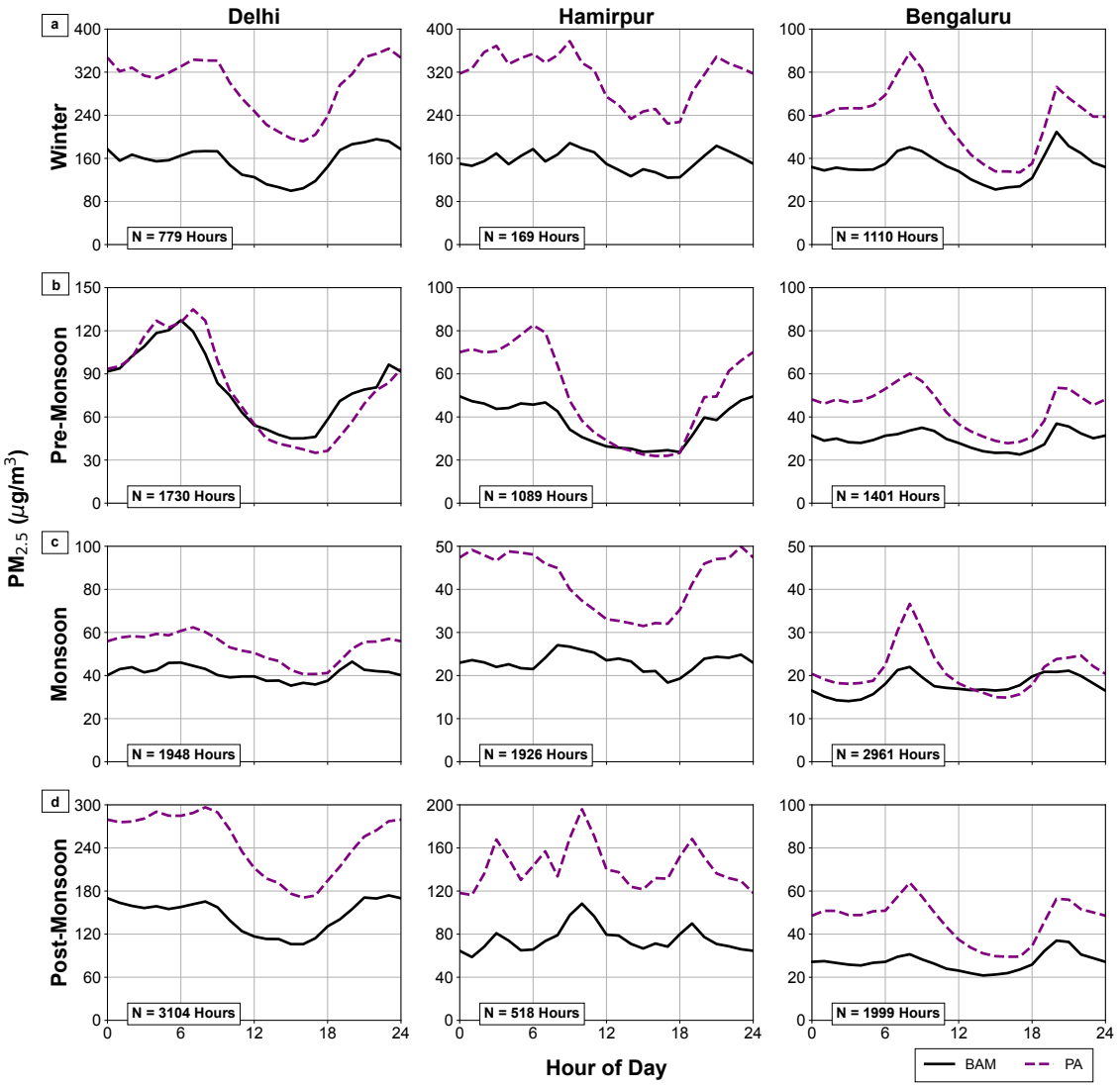


Figure 2.1: Diurnal profiles of mean hourly seasonal BAM (reference) and uncorrected PA $PM_{2.5}$ signals for Delhi, Hamirpur, and Bengaluru, using the CF1 channel. The number of valid hourly averages (quality assured according to methods outlined in Sect. 2.4 and summarized in Sect. 3.1–3.3) in each dataset is presented at the bottom left of each subplot. Winter (January and February), pre-monsoon (March, April, and May), monsoon (June, July, August, and September), and post-monsoon (October, November, and December) are shown. No single hour of the day represents more than about 7% of the total dataset shown in the bottom-left corner of each plot.

At both the site in Hamirpur and the site in Bengaluru, we used the manufacturer's specified data flags to perform quality assurance, resulting in 6 % and 11 % data loss for the Hamirpur site and Bengaluru site BAMs, respectively. Unlike Delhi, the Bengaluru

network is sparse ($n = 40$ in Delhi versus $n = 8$ in Bengaluru), with relatively low data completeness from the official monitors. Diurnal plots in Fig. 1 show a morning peak, with maximum values typically at 08:00–09:00 LT for the collocation site BAM. The closest regulatory monitor to the Hamirpur site is in Kanpur, more than 50 km away, which is too far for meaningful comparisons of local conditions. Figure 1 shows similar trends to the U.S. Embassy site in Delhi, with a morning peak between 07:00–09:00 LT in the morning, extreme mass concentrations throughout the winter, and a low dynamic range during the monsoon. There are no long continuous gaps from this monitor; however, power outages were more frequent in Hamirpur than the other two sites, since it is a rural site, leading to significant data loss – about 14 % of the total campaign hours, concentrated in the pre-monsoon period.

PA-II quality assurance

We evaluated the unit-to-unit precision of the PA-II sensors by comparing the individual channels of all co-located Plantower sensors at each site. Because each PA-II contains two Plantower sensors, there were always a minimum of four Plantower sensors operating at each monitoring site. The PA-II $PM_{2.5}$ channels were highly precise, with a strong correlation ($R^2 \geq 0.9$) both within nodes and between nodes across the mass concentration distribution, which is consistent with the existing literature [68, 75, 111]. Bland–Altman plots indicate high precision across all sites and units, with mean differences centered near 0 μg m^{-3} and most hourly points within ≤ 20 % (Figs. S11–S13). The between-Plantower R^2 range for the CF1 data across all collocated PA-II sensors was between 0.94–0.99 for the Delhi site, 0.92–0.99 for the Bengaluru site, and 0.95–0.99 for the Hamirpur site (Fig. S14). Disagreement was more pronounced at high concentrations (≥ 100 µg m^{-3}) at which R^2 ranges at each site dropped to 0.90–0.95, 0.83–0.88, and 0.92–0.94 for Delhi, Hamirpur, and Bengaluru, respectively. Similar intra-sensor correlations were found for the ATM and ALT data. Given the consistent between-sensor hourly precision across sites (NRMSE ≤ 10 %), we can confidently state we expect a random error of at most 10 %.

Applying the detection limit thresholds removed 1 % of the total Delhi dataset and < 1 % from the Hamirpur and Bengaluru datasets. The CV test removed about 15 % from each site. RH and temperature microcontroller errors were limited to about 4 % of the total data in Delhi and Hamirpur and < 1 % in Bengaluru.

After removing the filtered data points, accounting for power losses, and applying the completeness criteria for 1 h hourly averages, the site-averaged PA data resulted in an average coverage of 47 % ($n = 9260$ h), 63 % ($n = 5958$ h), 86 % ($n = 8567$ h) for Delhi, Hamirpur, and Bengaluru, respectively, across CFs. Finally, the reference dataset was synchronized with the PA dataset, and the combined dataset coverage is 38 % ($n = 7504$), 39 % ($n = 3744$), and 75 % ($n = 7473$) for Delhi, Hamirpur, and Bengaluru, respectively. The smaller number of data points available for the Delhi and Hamirpur sites principally arose because of relatively more downtime of the BAM instruments at these two locations.

PurpleAir data summary

Across sites, the PA-II captured diurnal and seasonal trends with similar results to the collocated BAMs, as evident in Figs. 2.1 and A.15. However, inconsistent biases among the season and location were also observed for all three $PM_{2.5}$ channels (CF1, ATM, and ALT), resulting in poor accuracy for the uncalibrated dataset. Although the poor accuracy is unsurprising, our findings highlight the importance of dynamic emissions and meteorology across the Indian subcontinent and field performance at extreme mass concentrations.

In Delhi, the PA data (CF1) correctly identified the winter and post-monsoon periods as being the most polluted seasons, with a strong diurnal range peaking at 08:00–09:00 LT (Fig. 2.1). The PA also characterized the Delhi monsoon well, with a low diurnal range and a daily average less than 60 μg m^{-3}. The uncalibrated lower-cost sensor overestimates concentrations during the extremely polluted and humid post-monsoon and winter. There is notably more accurate performance during the dry and hot pre-monsoon, albeit with a tendency to underestimate mass concentrations relative to the reference at least half of the hours of the day. The PA units at Hamirpur follow a similar trend. Although both the Delhi and Hamirpur sites feature relatively low bias in the pre-monsoon period, they underestimate mass concentrations in this season, perhaps due to the influence of wind-blown mineral dust, as observed elsewhere in field and lab evaluations [58, 72, 75, 111, 113]. While crustal material does not generally dominate $PM_{2.5}$ mass, during dust storms the lower tail of the coarse-mode aerosol can lead to substantially elevated $PM_{2.5}$ concentrations in India.

Since Bengaluru's meteorology exhibits comparatively low seasonality, and emissions are more strongly influenced by mobile sources rather than the more complex mixture in Delhi, lower-cost sensor performance is different than in Delhi and Hamirpur. During the day (09:00–19:00 LT), accuracy is biased by more than +25 % during the winter, pre-monsoon, and post-monsoon periods, with systemically lower bias, including underestimates in the less polluted monsoon season (Fig. 2.1). Accuracy is lower during higher mass loadings at night and during early morning hours, with strong overestimates across seasons peaking during the most polluted hour (07:00–08:00 LT).

Model selection

Data-driven model fitting

The SFS results are summarized in Table 2.2 (with extended results in Tables A.1–A.3 in the Supplement), where the four most relevant parameters are listed in order of decreasing importance for each CF and site. Across sites, R^2 stabilized at two parameters (about 0.8 for Delhi and about 0.9 for Hamirpur and Bengaluru). For all sites, sensor-estimated $PM_{2.5}$ was generally selected as being the single most relevant parameter for predicting concentrations measured by BAM, followed by a variation in the RH (i.e., RH^2 and RH^3). The form of the most robust Bengaluru model is different from the Delhi and Hamirpur sites, with an interaction term between temperature and ALT $PM_{2.5}$ (rather than CF1 $PM_{2.5}$) being selected as the most predictive $PM_{2.5}$ data stream. Furthermore, the Bengaluru dataset

Table 2.2: Most relevant parameters selected through sequential feature selection for each PurpleAir $PM_{2.5}$ channel by site CF1 (uncorrected PurpleAir $PM_{2.5}$), ATM (atmospheric-corrected PurpleAir $PM_{2.5}$), and ALT (alternative PurpleAir $PM_{2.5}$ – reconstructed from the modeled size distribution data). Parameters include relative humidity (RH), temperature (T), and dew point (D).

	CF1	ATM	ALT
Delhi	$PM_{2.5}$	$PM_{2.5}$	$PM_{2.5}$
	RH	RH^2	$RH^2 \times T$
	$PM_{2.5} \times RH$	$PM_{2.5} \times RH^2$	$PM_{2.5}^2 \times D$
Hamirpur	$PM_{2.5}$	$PM_{2.5}$	$PM_{2.5}$
	RH	RH	$PM_{2.5} \times RH \times T$
	RH^3	RH^2	$PM_{2.5}^2 \times D$
Bengaluru	$PM_{2.5} \times T$	$PM_{2.5}^2 \times T$	$PM_{2.5}$
	$PM_{2.5} \times T \times D$	$PM_{2.5}^3$	$PM_{2.5} \times RH^2$
	$PM_{2.5}^2 \times T$	$PM_{2.5}^2$	$PM_{2.5}^2 \times T$

ranked temperature and dew point as being more relevant than the Delhi and Hamirpur datasets. Constraining Bengaluru to the same top parameters as the Delhi and Hamirpur sites (CF1 $PM_{2.5}$ and RH) reveals only marginal differences (ΔNRMSE $\approx 2\%$) in the performance from the most robust model selected by SFS (ALT $PM_{2.5}$ and RH^3). As such, we choose to standardize our calibration across all sites, with only CF1 $PM_{2.5}$ and RH as relevant parameters.

Regression coefficients of the CF1 $PM_{2.5}$ data were positive values less than 1, indicating that the CF1 data generally overestimate but are positively correlated with reference monitors. RH term coefficients at the Delhi and Hamirpur sites are negative, indicating that increasing RH should negatively weigh the PA reading, consistent with the expected artifacts of hygroscopic growth in the atmosphere. The Bengaluru dataset similarly assigns RH terms a negative weight. Temperature and dew point terms only imparted marginal improvements to calibration models ($\Delta R^2 \approx 0.01$; see Fig. A.16), and it is not determinable if the models are deriving a spurious correlation or detecting underlying aerosol or instrument properties.

Theory-driven model fitting

Table A.4 summarizes the best-fitting model coefficients from the training dataset for each site and each CF. Across sites, the $PM_{2.5}$ regression coefficient (α) does not vary substantially; it is about 14 % for CF1. Hygroscopic growth regression coefficients (β) vary greatly from site to site for CF1, even within the same region; β_{CF1} for Delhi is double that for Hamirpur, which is perhaps due to a higher abundance of hygroscopic species [23, 42].

The lack of consistency in fit is reasonable, as the Plantower proprietary algorithm and underlying physical–optical design of nephelometers mean that the sensor does not explicitly

account for the underlying aerosol size distribution and composition. The resulting datasets are therefore somewhat divorced from the expected pattern, based on the κ-Köhler theory. The ALT dataset removes the proprietary ATM correction and assumptions of particle density present in the CF1 data, resulting in more consistent β intra-regional values, though with less consistent α values.

Model evaluation

For the Delhi and Hamirpur sites, both located in north India, two-parameter ATM and CF1 models yielded consistent improvements compared to one-parameter models, as summarized in Fig. 2.3 for Delhi and Hamirpur, respectively. The CF1 models were consistently more accurate than their ATM counterparts in Hamirpur, albeit by about 1 % NRMSE and less than 1 % R^2. Conversely, in Delhi, the ATM models systematically outperformed the CF1 models by about 1 % NRMSE and R^2. As evident in Fig. 2.1, Hamirpur experiences overall lower mass loadings than Delhi. Consequently, the absolute difference between the two signals due to the Plantower piecewise function (Fig. A.1) above about 20 μg m^{-3} is likely less important in Hamirpur than in Delhi, where mass loadings are consistently elevated.

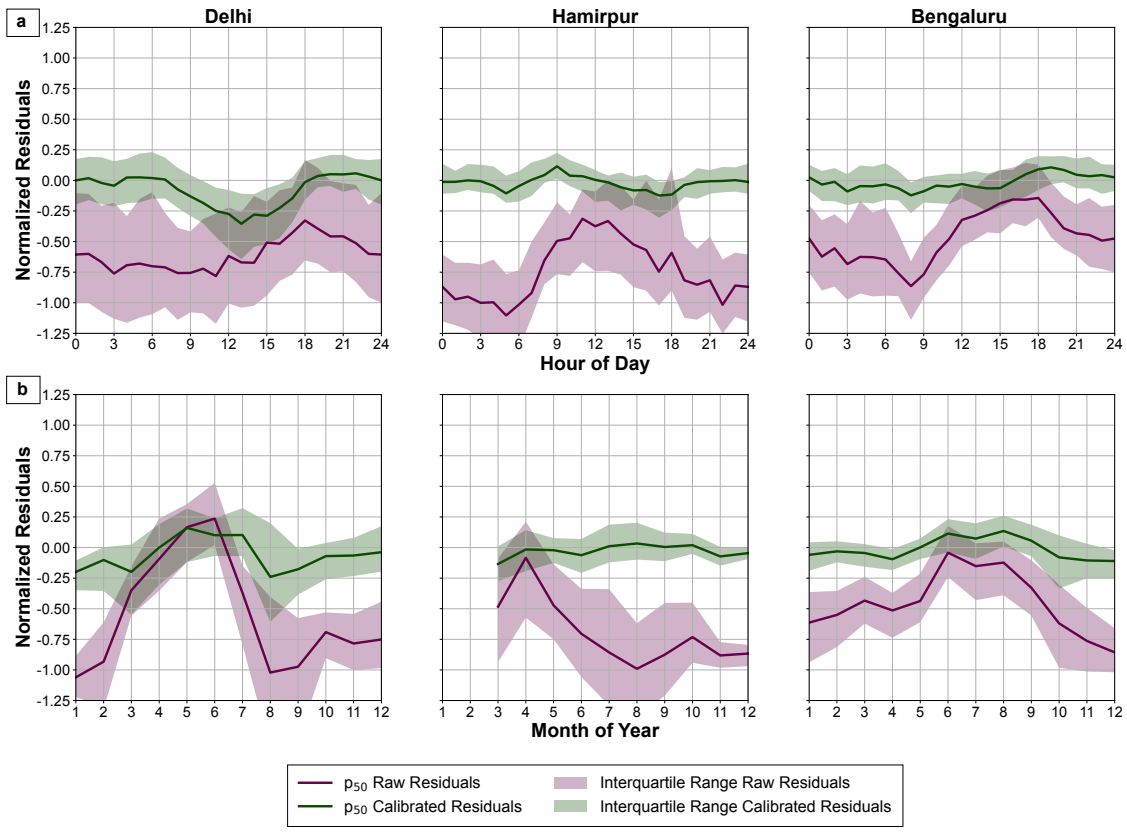


Figure 2.2: Normalized residual distributions for the uncalibrated PurpleAir data (CF1) and the calibration models for each site. Bold lines represent the median (p_{50}) of the distribution, while the shaded area represents the interquartile range (p_{75}–p_{25}). Panel **(a)** shows the diurnal distribution, while panel **(b)** shows the normalized residual distribution binned by month. Compared to the residual distribution for uncalibrated (raw) data, the calibration effectively eliminates most seasonal and diurnal biases.

The theory-driven hygroscopic growth correction consistently improved the performance from the uncalibrated baseline data across sites by 12% for ATM and 60% for CF1, on average (Fig. 2.3). In Delhi and Hamirpur, the theory-driven model performs within about 2% of the one-parameter models and outperforms the one-parameter ATM model in Hamirpur by 4.3%.

However, since the Plantower PMS5003 is a nephelometer, the signal should not necessarily follow the expected non-linear hygroscopic growth with increasing RH above 60%, as expected from a size-resolved measurement technique [28, 51]. As a result, the two-parameter CF1 models in Delhi and Hamirpur, with their additive RH terms, outperformed the theory-driven model by at least 3 %. In Bengaluru, the theory-driven model performance was comparable to the data-driven models (about 1% NRMSE; see Fig. 2.3). This contrast

in performance between the two methods in north India is likely a result of the less seasonally variable meteorology and source mixtures in Bengaluru, leading to less dynamic aerosol hygroscopicity.

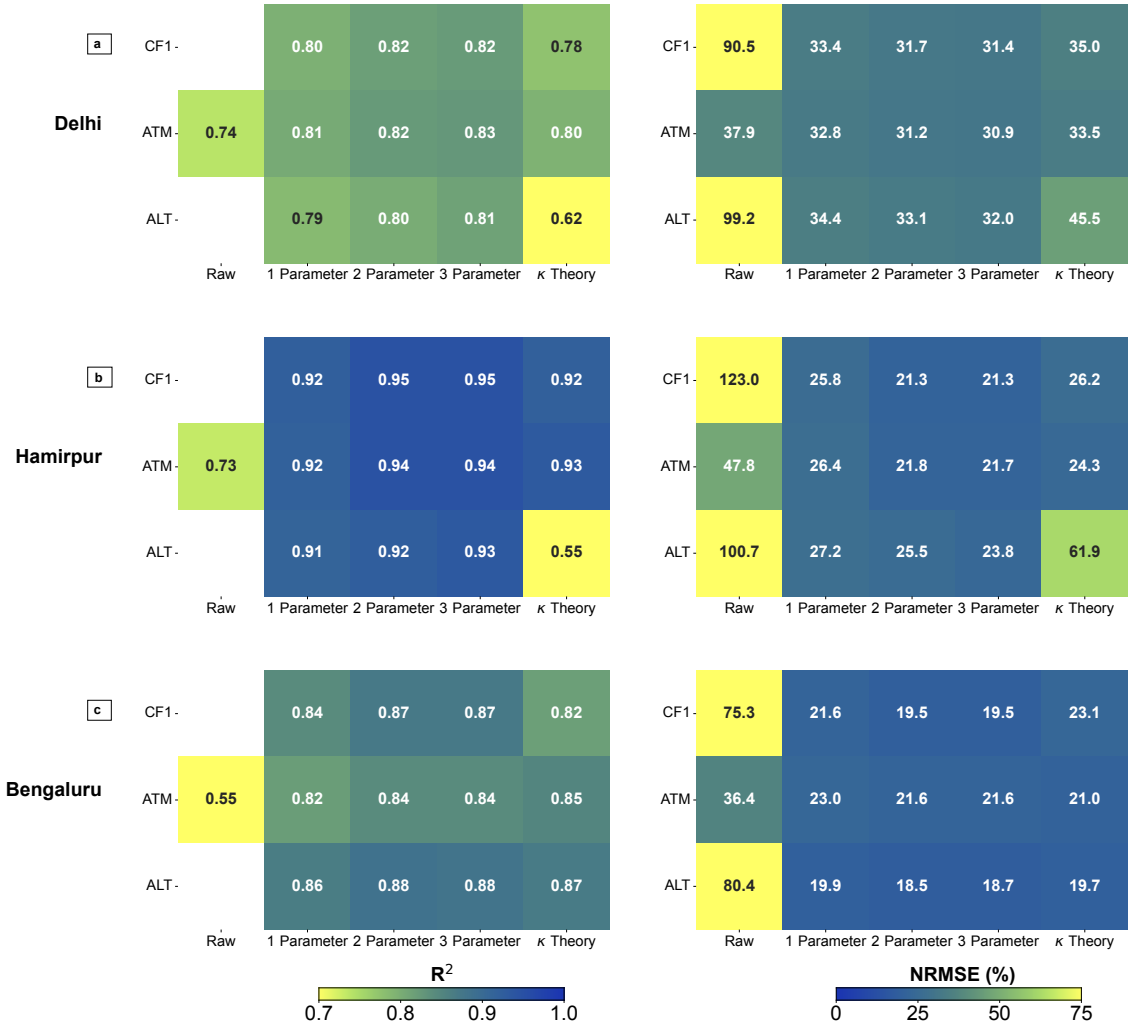


Figure 2.3: Regression metrics, R^2 (left) and NRMSE (right), for the raw data, one-parameter model, two-parameter model, three-parameter model, and theory-driven hygroscopic growth model for each $PM_{2.5}$ channel (CF1, ATM, and ALT) for each site (Delhi in panel **a**; Hamirpur in panel **b**; Bengaluru in panel **c**). The largest improvements are from the raw data to the one-parameter model, with only marginal improvements in the three-parameter and theory-driven models.

Since CF1 data produce models as accurate as or more accurate than ATM models, have been validated in studies around the world, and do not feature the same non-linear behavior as the ATM channel, we recommend using CF1 for calibration in Delhi and Hamirpur. In

Bengaluru, the ALT data may be useful and warrant further study in similar environments, including across south India. From our results, the CF1 data are suitable for deployment in Bengaluru and provide uniformity in calibration guidance. Additionally, the two-parameter model (with RH as additive terms to $PM_{2.5}$) follows previous studies [11, 87, 141] across continents and aerosol regimes. In Barkjohn, Gantt, and Clements [11], the large sample size of PA-II across the continental United States was used to derive a similar calibration regression. In Tables A.5–A.6, we compare the NRMSE and MBE for our best CF1 model forms from the SFS procedure (up to three parameters), theory-driven CF1 model, and Barkjohn, Gantt, and Clements [11] model output. We have found from our seasonally balanced test dataset that our models perform moderately better (ΔNRMSE of about 5 % across sites) than the EPA model, which is perhaps intuitive, given the differences in PM composition and concentrations in India relative to the USA. Furthermore, the MBEs of our site-specific models are close to 0 μg m^{-3}, while the Barkjohn, Gantt, and Clements [11] model systemically suppresses mass concentration estimates, with an MBE as high as 22 μg m^{-3} in Delhi, compared to an MBE of -0.7 μg m^{-3} when using the Delhi site-specific model or 3.25 μg m^{-3} when using the Hamirpur model on the Delhi test dataset. Overall, while the site-specific models we develop here clearly outperform the model of Barkjohn, Gantt, and Clements [11] for these three Indian sites, it is nonetheless striking that this USA-developed calibration still performs quite well at these three Indian sites. Given these findings, we selected the following multi-season correction equations (Eqs. 2.2–2.4) for Delhi, Hamirpur, and Bengaluru, respectively. Although relatively simple, our calibration models greatly improve the reliability of lower-cost sensor data across aerosol regimes. Figure 2.2 summarizes each model's bias in at each collocation site, with seasonally and diurnally segregated residuals. Across all sites, the monthly bias of the calibrated data is within $\pm$25 %, in contrast to the uncalibrated data. Figure 3 summarizes model accuracy, with NRMSE improvements from uncalibrated data ranging between 5 %–20 %. Figure A.17 additionally explores the residual structure and demonstrates the value of the selected model forms at reducing bias due to RH and mass loading factors. The calibrated residual distributions demonstrate marked improvements across the full range of mass concentrations (5–500 μg m^{-3}), unlike the raw residuals, which show increasing uncertainty at high mass concentrations. The selected calibration equations reduce the median bias to near 0 % across sites from a median bias as high as 150 %, using the uncalibrated data at RH $>$ 60 %. Figure 4 summarizes the performance of Eqs. (2.2)–(2.4), highlighting that although performance is robust in the aggregate, seasonal and diurnal shifts in aerosol properties can shift performance and uncertainty bounds, therefore motivating further investigation into the role of calibration sensitivity to temporal factors.

$$C = 0.546 \times \text{CF1} - 0.936 \times \text{RH} + 50.3 \text{ (Delhi)} \tag{2.2}$$

$$C = 0.496 \times \text{CF1} - 0.296 \times \text{RH} + 22.0 \text{ (Hamirpur)} \tag{2.3}$$

$$C = 0.515 \times \mathrm{CF1} - 0.139 \times \mathrm{RH} + 14.1 \text{ (Bengaluru)} \tag{2.4}$$

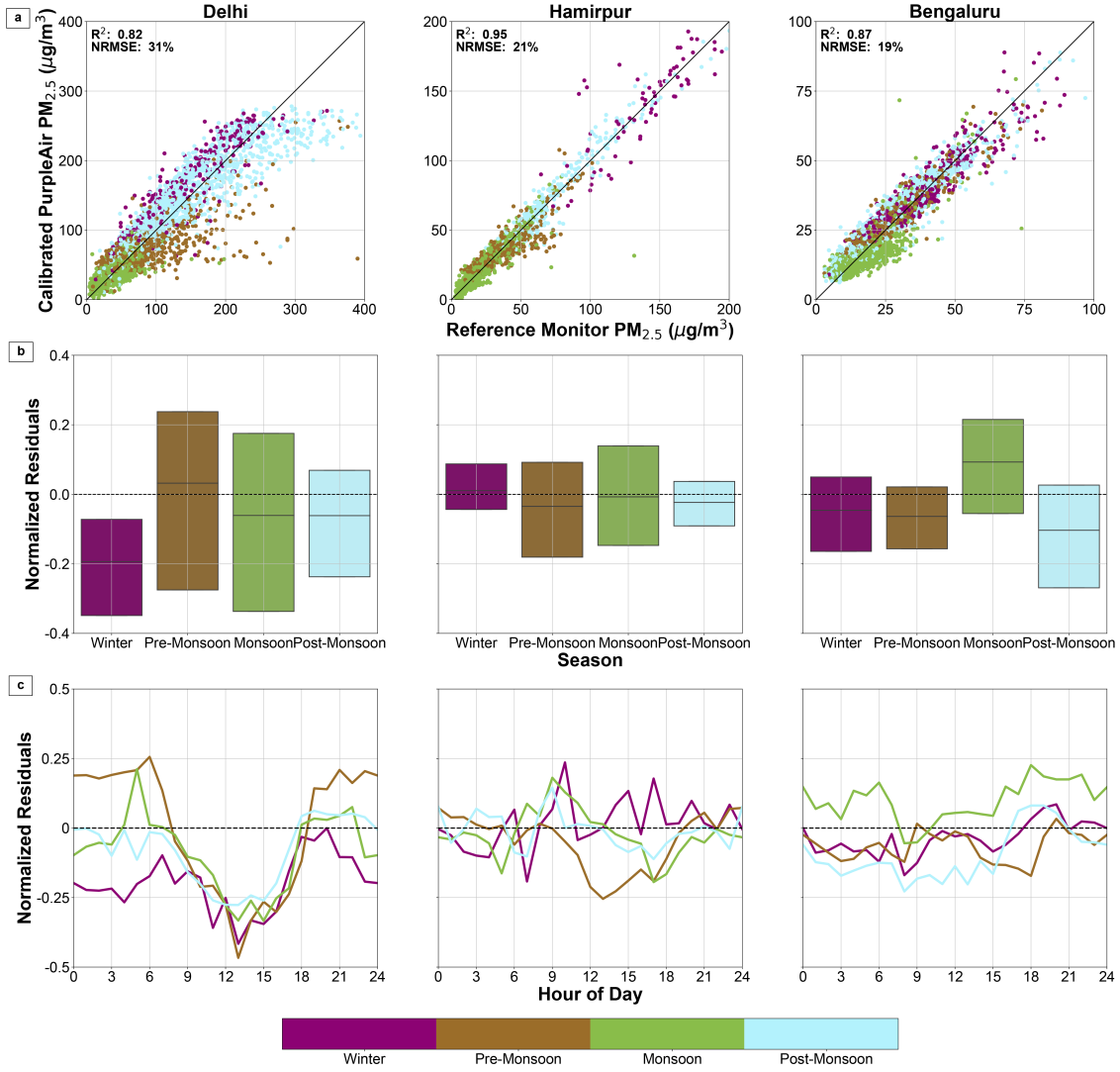


Figure 2.4: Scatter plots of the best-performing two-parameter annual models for each of the sites in panel **(a)**, with the corresponding normalized model residuals segregated by season in panel **(b)** and segregated by the time of day in panel **(c)**. In panel **(a)**, the solid line represents unity. In panels **(b)** and **(c)**, the dashed line represents the normalized residual value of zero. In comparison to Fig. 2a, the normalized diurnal residuals in panel **(c)** are presented over a restricted y axis, accentuating the residual structure.

Model evaluation

Temporal sensitivity

To identify the stability of the model and its parameters, we computed the 4-week rolling ordinary least squares (ROLSs) for each of our selected models and compared performance to all other 4-week moving ROLS models. Each model's NMBE across time is shown in Fig. 2.5, where the gray squares in the top panel indicate less than 50 % data completeness. Additionally, the bottom panel of Fig. 2.5 tracks the distribution of the diagonal of the matrices present in the top panel of the figure. Across sites, the choice of the calibration period greatly changes the performance of the regression throughout the rest of the dataset and influences the selection of regression coefficients. Figure A.18 additionally explores the absolute bias, demonstrating that the biases in Eqs. (2.2)–(2.4) are centered near zero. Figure A.19 illustrates the same analysis with NRMSE, showing that the monthly ROLS model performance is generally stronger than the annual model within the training month, but that it rapidly deteriorates.

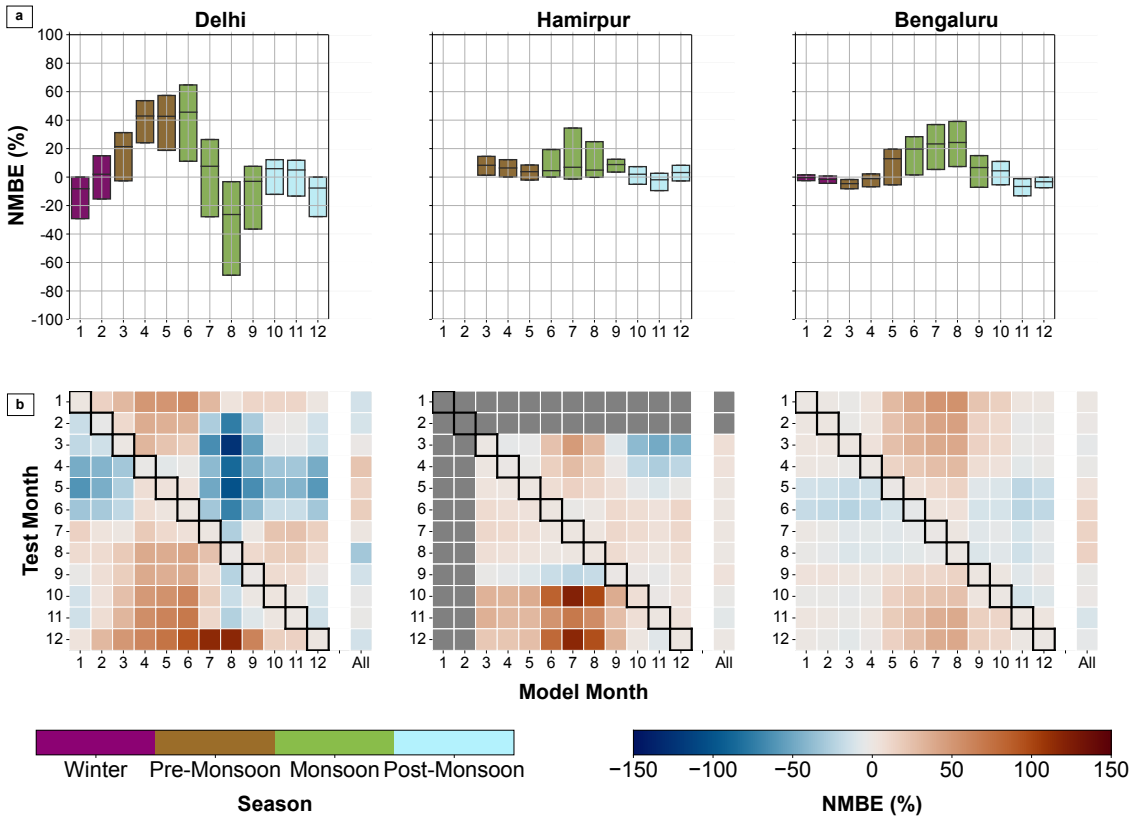


Figure 2.5: Assessment of inter-seasonal transferability of seasonal models. Panel **(a)** depicts box plots of the distribution of normalized mean bias error (NMBE) for a given model starting month of a 4-week ROLS model on all other windows. The bottom, solid line, and tops of the boxes represent the 25th, 50th, and 75th percentiles, respectively. Panel **(b)** presents the median NMBE of a 4-week ROLS model trained to start in the month (colored by season) on the x axis and evaluated on all other windows, as binned by the starting month on the y axis. Gray boxes represent months without sufficient data. Models trained in the pre-monsoon period underpredicted in other seasons, contrary to the typical pattern of overprediction – this pattern is consistent at Delhi and Hamirpur. As a point of comparison, we present the performance of our long-term calibration in individual months at each site in the column **(b)** labeled "All", which is consistent with our observation that 4-week models trained in a single month generally do not perform as well in other months.

In Delhi, model performance and coefficient selection exhibit a seasonal pattern, with post-monsoon and winter month models (January, February, March, September, October, November, and December) performing well and selecting similar regression coefficients even across years (Fig. A.20). When evaluating model performance on data within the same season, NRMSE is typically below 30 %, and R^2 is above 0.7. However, the post-monsoon and winter models perform poorly when evaluated on pre-monsoon data (March and April),

with NRMSE exceeding 100 % and R^2 falling below 0.1. For even the best performing pre-monsoon models, NRMSE rises above 50 % during the pre-monsoon period data and above 70 % for other seasons. Monsoon models (May, June, July, and August) also lack transferability to other seasons but perform well when evaluated on data from the same season (NRMSE < 30 %). Monsoon meteorological conditions contrast with other seasons – it is humid, windy, cloudy, hot, and frequently rains (Figs. A.4–A.6). These conditions result in lower emissions (i.e., less biomass burning for heating relative to winter) and act to suppress emissions (i.e., wet deposition), resulting in lower average seasonal mass concentrations in the monsoon period (Figs. A.3 and A.7). Consequently, models trained in the monsoon period translate poorly to other seasons.

The Hamirpur ROLS results are like those of Delhi but over a shorter period and with a more robust summer performance. The pre-monsoon models fit the largest magnitude $PM_{2.5}$ regression coefficient and fail to perform well (NRMSE > 50 %) both within the data for their own seasons and across the data of other seasons. All other windows perform well (NRMSE ≤ 25 %, $R^2 \geq 0.9$) within their training window and across all other non-pre-monsoon test windows. The regression coefficients stabilize ($\beta_{PM_{2.5}} \approx 0.5; \beta_{RH} \approx -25$), resulting in less seasonally variable model performance than in Delhi. Most likely, the less robust performance of the Delhi model across seasons relative to the performance of the Hamirpur model is due to the broader diversity of sources in Delhi, making it more difficult to constrain the uncertainty due to factors including hygroscopic growth and particle size distribution.

Bengaluru and Hamirpur results are similar in that both models are relatively stable and transferable across seasons. Bengaluru model performance degrades and features less season-to-season transferability in the monsoon season months (July and August) but features accurate performance (NRMSE < 20 %) for the other seasons. Regression coefficients in Bengaluru are relatively consistent, despite having more spread during the pre-monsoon period.

Although model results and calibration formulation differ across sites, the temporal sensitivity analysis reveals several key lessons. First, there is no "free lunch" or universal model. Rather, aerosol and meteorological regimes vary sharply by season, leading to underfit for annual models or overfit for seasonal models. Since annual models use data from across the distribution of aerosol compositions and size distributions, they generally perform within 5 % of monthly models (Fig. A.21). Outliers can be especially concerning at the physical limitations of nephelometers, such as during pre-monsoon dust storms or the extremely humid monsoon. Therefore, models trained within 1 single month-long period do not necessarily transfer well to the next month, even within the same season and model feature selection. Consequently, we recommend calibration procedures in India and other similar environments maintain a long-term collocation with at least one lower-cost and reference pair after the initial collocation period in the region of interest.

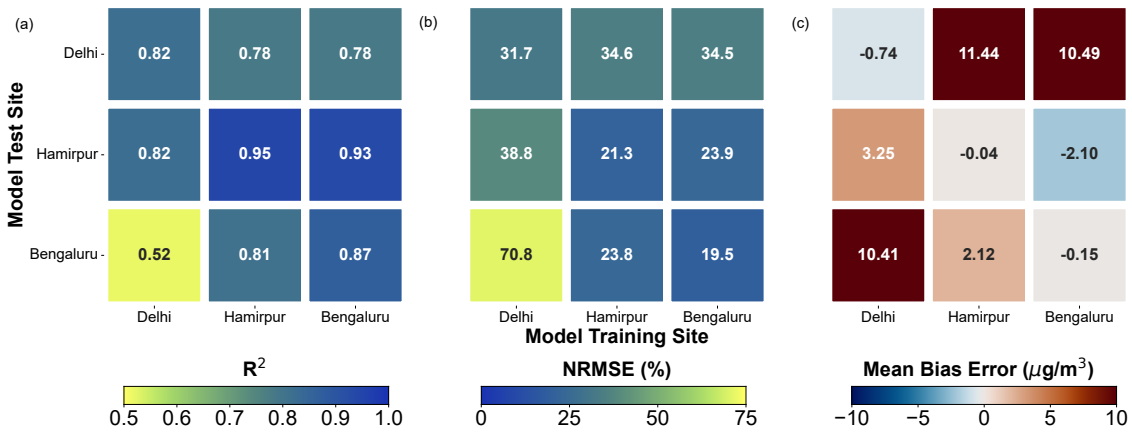


Figure 2.6: Assessment of the site-wise transferability of annual models. Performance evaluation metrics of Eqs. (2)–(4), with the training site on the x axis and the test site on the y axis. Metrics are the coefficient of determination (R^2) **(a)**, normalized root mean square error (NRMSE) **(b)**, and mean bias error (MBE) **(c)**. For each metric, the diagonal pattern of the best performance (from the upper left to the lower right) illustrates how calibration models perform best in the locations where they are trained. At each site, we compute the performance metrics by comparing the calibration model output to an independent test set that was held out from model training. This finding illustrates how regional differences in meteorology and aerosol composition can limit the transferability of calibration relationships. It is noteworthy that the calibration model trained in Delhi performed quite poorly in Bengaluru.

Spatial transferability

Due to proximity and similarities in climate and aerosol characteristics, and since data-driven models from Delhi and Hamirpur sites share the same parameters (CF1 and RH), we hypothesized that Delhi and Hamirpur models may be transferable. Figure 2.6 summarizes the relevant performance metrics with respect to spatial calibration transferability. The Hamirpur dataset performance weakened after applying the Delhi model (R^2 decreased to 0.82; NRMSE increased to 39 %) but still outperformed uncalibrated CF1 data. The Delhi dataset performance also weakened after applying the Hamirpur model (R^2 decreased to 0.78; NRMSE increased to 35 %), a relatively modest performance degradation. From this exercise, we understand that although $PM_{2.5}$ is highly variable in Delhi and Hamirpur, there may be enough of a "fingerprint" in aerosol characteristics from the background site so that a single calibration equation could provide an adequate performance improvement. However, a local calibration can provide performance improvements due to fine-scale $PM_{2.5}$ variability unique to urban environments, especially for a megacity like Delhi.

Applying the Delhi and Hamirpur models to the Bengaluru test dataset resulted in contrasting performance, with NRMSE values of 71 % and 24 % from the Delhi and Hamirpur

models, respectively. It is likely the largely regional aerosol from Hamirpur has enough overlap in the speciation and mass concentration range with the Bengaluru aerosol that the models are somewhat interchangeable. This hypothesis is additionally evidenced by the overlap in coefficients from the theory-driven hygroscopic growth equations. Clearly, the differences in the composition of the Delhi and Bengaluru aerosols prevent an exchange between the models at these two sites, but there is enough preserved from the regional contribution to allow some support from the Hamirpur model to the Delhi data.

Some calibration efforts have sought a unified continental model for lower-cost sensors by combining multiple reference and lower-cost sensor pairs into one regression model [11]. Other studies have focused on interpolating between calibration sites to avoid washing out local effects, typically in a dense sensor network [142]. Our results show that although there are overarching similarities in model parameter selection, urban and rural environments are heterogeneous to the point of potentially barring a unified model. Additionally, seasonal variability within India necessitates at least monthly updates to the model coefficients.

2.4 Conclusions

We collocated lower-cost sensors with reference grade $PM_{2.5}$ monitors in three environments in India, two urban (Delhi and Bengaluru) and one rural (Hamirpur), over the course of multiple seasons to characterize lower-cost sensor performance across shifting emissions and meteorological regimes and develop calibration models. Internally, PA-II units demonstrated strong consistency, with low intra-sensor bias and high correlation. Relative to reference instruments, uncalibrated sensor performance varied diurnally and seasonally, with shifts being strongly associated with extreme mass concentrations, RH, and coarse-mode particles. The lower-cost sensor signal generally overestimated mass concentrations relative to the reference instruments, which is a trend observed in the literature to be associated with hygroscopic growth [61, 82]. We identified periods of lower-cost sensor signal underestimation by a factor of 2–6$\times$ in the pre-monsoon period in Delhi and Hamirpur, when supramicron wind-blown dust particles are relatively abundant.

We demonstrated a relatively simple multilinear regression model, using only the lower-cost sensor $PM_{2.5}$ signal, and a lower-cost sensor RH could produce results that were well correlated ($R^2 \geq 0.8$) with the reference signal at each site. These site-specific models provide the basis for a computationally efficient, well-constrained (NRMSE $\leq 25\,\%$), and scalable calibration approach for lower-cost sensing in India, despite the non-stationary and diverse aerosol dynamics of the region. Furthermore, we showed that our models can be transferred from site to site and still improve performance above the uncalibrated baseline, although a site-specific model generally has superior performance.

Our work also highlights a key caveat to lower-cost sensor deployments and calibration in India, especially regarding long-term deployment. Models trained at a site with data from only one season may perform more accurately within that season than a seasonally balanced model but are unreliable at other times of the year. Based on our analysis, we

hypothesize that it is better to use a model developed at a background site such as Hamirpur to correct data from an urban environment such as Delhi, since the composition of PM in Hamirpur represents a good subset of the variability in Delhi. On the other hand, since there are PM species only found in some urban environments in India, using models from these industrial microenvironments will less likely to produce accurate results outside of the training location. Our results showed that seasonality is especially important, given the contrast in meteorology and mass concentrations between the pre-monsoon and monsoon seasons. Although a multilinear regression approach produces well-constrained results, these models are not transferrable among seasons. Therefore, we advise future deployments to continuously operate a collocation site with at least one reference and lower-cost sensor pair to evaluate calibration drift. Accounting for the temporal and spatial dynamics of aerosol characteristics will allow for the rapid scaling of lower-cost sensors for communities in India to communities in need of transparent and accurate data.

Chapter 3

Mapping Air Pollution in Polluted Data-Sparse Environments: Resolving Spatial-Temporal $PM_{2.5}$ Trends with Low-cost Sensors in North India

3.1 Introduction

Ambient $PM_{2.5}$ air pollution (aerosol less than 2.5 microns in aerodynamic diameter) is the top environmental risk factor for ill health and death [122, 54, 132, 4]. The global burden of air pollution is not evenly distributed – high-income countries generally experience low to moderate ambient $PM_{2.5}$ exposure, while low- and middle-income countries experience sustained high $PM_{2.5}$ burdens throughout the year [54, 137, 4]. Since 1990, conditions have worsened in India, resulting in a widening disparity in $PM_{2.5}$ exposure [22, 77]. About 1 million premature deaths attributable to $PM_{2.5}$ exposure, nearly 25% of the worldwide mortality burden, occur in India, with substantial regional heterogeneity [97, 30].

Satellite remote sensing has contributed to understanding the sources of $PM_{2.5}$ and related health outcomes in India by providing spatially complete maps, typically at monthly or annual intervals [117, 33]. However, remote sensing data sets do not directly measure $PM_{2.5}$ but rely on ground-based observations to inform and tune model parameters [117, 65, 33, 96]. India lacks the comprehensive ground-based infrastructure to monitor extreme air pollution dynamics and inform interventions, in part due to the high costs of traditional fixed-site reference monitoring[47, 17, 85, 98]. As of 2024, nearly all publicly available reference monitoring is in mega-cities, despite observations of extreme concentrations across land-use categories, broadly impacting the highly distributed non-urban population [109]. Commercially-available, miniaturized lower-cost sensors (LCS), sold for under ∼500 USD, can complement reference networks at scale for diverse applications, greatly increasing the spatial-temporal resolution of monitoring [80, 106, 26, 102, 78, 27].

LCS for $PM_{2.5}$ measurement relies on inference from optical scattering and thus requires careful quality assurance and calibration procedures [144, 44, 51]. In India, these challenges are magnified by the range of mass concentrations, heterogeneity in aerosol properties, and meteorological dynamics [34, 83, 126, 71, 111]. Despite these challenges, in-situ performance assessments have demonstrated that calibrated popular $PM_{2.5}$ LCS are of moderate to high accuracy ($R^2 \geq 0.7$; NRMSE $\leq 30\%$) [59, 103, 18, 126, 125, 62]. Most $PM_{2.5}$ LCS network studies in India have focused on sensor calibration within strictly regulated sites in urban environments [80, 105, 125, 104, 142]. Scaling an urban-rural regional network of just hundreds of LCS would result in many nodes tens of kilometers from the nearest LCS and potentially hundreds of kilometers from the nearest reference monitor [17]. While calibration remains a crucial concern, hosting sensors in disparate lower-resourced communities results in less control over routine in-field continuity procedures (e.g., continuous power, sensor replacement, and precision checks).

Recent urban center-to-background and urban-to-rural deployments have reported LCS capacity to map spatial-temporal $PM_{2.5}$ gradients in India [80, 105, 104, 142]. Prakash et al. and Zheng et al. both investigated pilot networks in Delhi and observed that LCS sites were strongly collinear with adjacent reference sensors. Madhwal et al. deployed 71 sensors in the Lucknow metro area over six months. They observed the seasonality and relative magnitude (LCS-LCS comparison) of urban-rural hotspots and reported on differences in rural versus urban-core seasonal observations in a qualitative manner using a categorical scale (i.e., "No Risk" versus "Hotspot").

Across three years (2021-2024), we tested over 500 PurpleAir PA-II, a popular LCS package, at a central test-bed in Delhi. To address calibration accuracy and test our understanding of spatial-temporal differences within a settlement, we further distributed PA-II at 11 regulatory sites in Delhi, collocated with reference-grade air pollution instruments. Finally, we distributed sensors in a community-hosted network throughout North India, including mega-cities with existing infrastructure and settlements of varying population densities with no ground-based monitoring. Our work demonstrates that although LCS networks are vulnerable to dynamic and significant bias, applying empirically based metrics to control for uncertainty along the complete data pipeline results in accurately quantified $PM_{2.5}$ spatial-temporal trends.

3.2 Materials & Methods

Sensors

Like most $PM_{2.5}$ LCS on the market, the sensors used for this study rely on optical techniques to infer ambient particle mass concentrations without the rigorous constraints necessary for regulatory certification [95, 143]. Regulatory grade instruments have stringent RH standards to ensure particle mass is not biased by aerosol liquid water, which varies as a function of particle size, species, and meteorology [53]. Furthermore, aerosol optical properties, including

scattering and absorption, vary with speciation and size, strongly biasing LCS [28, 61]. As a result, all optical LCS methods are inaccurate and require rigorous quality assurance and calibration to account for bias [144, 51, 123].

PurpleAir PA-II

The PA-II is a sensor package rather than a sensor model itself. It contains (2) Plantower model PMS5003 PM sensors (labeled "A" and "B" arbitrarily) and (1) Adafruit BME280 temperature, relative humidity (RH), and pressure sensor. All data is reported through PurpleAir's online platform, either privately or publicly, through their crowd-sourced maps. Previous work has suggested the Plantower models function as a reciprocal nephelometer based on its high correlation with integrating nephelometers [95]. However, in-depth reverse engineering has revealed that the PMS5003 and similar Plantower models are, instead, low-efficiency optical particle counters, which can serve as nephelometer proxies [94, 56]. As a result of this design, there are physical limitations on the size of particles the PMS5003 can reliably characterize. Specifically, the PMS5003 fails to characterize supramicron particles (aerodynamic diameter > 1 micron) well, resulting in poor estimates of $PM_{2.5}$ and PM_{10} when these coarser aerosols dominate mass distribution [94, 91, 72]. Although other Plantower models, such as the PMS6003, are sometimes marketed as resistant to this pain point since they feature fewer sharp angles along the optical chamber, this fundamental constraint is not addressed [94, 91, 51]. PurpleAir reports the PMS5003 $PM_{2.5}$ in three ways - denoted CF1, ATM, and ALT [18]. From global field evaluations, including in India, the CF1 data was the most suitable for calibration models due to its uniformly linear response compared to other optical instruments [18, 87, 11]. We will refer to CF1 as the uncalibrated signal or PurpleAir $PM_{2.5}$ (P) to avoid confusion.

QuantAQ MODULAIR-PM

Our study also featured limited deployments of the QunatAQ model MODULAIR-PM sensor package. Although the MODULAIR-PM has a much lower cost than a reference-grade sensor, the package is nearly ten times the price of the PA-II, and thus, it was not scalable for our deployment. The MODULAIR-PM features a Plantower nephelometer-like sensor and the Alphasense OPC-N3, a lower-cost optical particle counter. By leveraging the scattering information from the Plantower and the OPC-N3, QuantAQ provides proprietary PM_1, $PM_{2.5}$, and PM_{10} data and the raw particle size distribution data from the OPC-N3 [50]. While evaluation reports show that the size data from the OPC-N3 is inaccurate relative to reference instruments, it typically assigns the modes of the ambient size distribution correctly and, therefore, can robustly estimate $PM_{2.5}$ over a broader range of size distributions than Plantower models [106, 66, 67]. The size information, in tandem with the Plantower sensor, is valuable for exploring the underlying sensitivity of the nephelometer-like signal to changes in the particle size distribution.

Study Areas

Collocation Test Bed – Indian Institute of Technology, Delhi

We collocated all PA-II in batches to ensure all instruments met our quality assurance guidelines concerning precision and linearity quality assurance standards. As a secondary objective, the IITD site served as a validation site for our calibration framework by hosting a BAM-1022 reference instrument. Our chosen collocation site was at the Indian Institute of Technology, Delhi (IITD) in the South Delhi campus on the rooftop of the Block VI building (28.5471°N, 77.1905°E, ∼12 m above ground level). The campus has been used in many studies of ambient air pollutant trends in North India due to its capacity to support research equipment and the relative lack of local sources (nearest arterial road ∼100 m) [14, 100, 8, 41]. Our LCS batch collocations occurred over two years, from 2021 August to 2023 August, with valid reference data from 2021 August to January 2022.

Regulatory Agency Collocations

The Central Pollution Control Board (CPCB), Delhi Pollution Control Council (DPCC), and Uttar Pradesh Pollution Control Board (UPPCB) operate multi-pollutant ($PM_{2.5}$, PM_{10}, CO, NO_2, SO_2, O_3) FEM sites to assess compliance with the Indian National Ambient Air Quality Standards in urban North India (e.g. Delhi, and Lucknow). Most regulatory sites were commissioned to reflect regional exposure unbiased by local sources. However, a few sites were explicitly located to understand the impacts of near-road conditions or dense industrial zones. The CPCB ingests data from all the state-level agencies and provides 1-hr resolved quality-controlled data freely to the public via a web platform.

Our study collaborated with the DPCC to collocate at nine Delhi National Capital Region regulatory sites to validate our calibration framework across land-use categories and local source profiles during 2023 March – 2023 August. This collocation period is a critical transition from the highly polluted and humid winter to the moderately polluted and dry pre-monsoon, finishing during the moderately polluted and humid monsoon season. Given the variability in reference sites and aerosol characteristics, our DPCC collocation is a robust test case for our calibration framework.

Community Host LCS Sites

Previous analyses of the PurpleAir network have ingested the entire network and implemented a few quality assurance rules to automate analysis rather than knowing how each citizen scientist contributing to the network has sited their sensor [31, 78, 15]. For studies in the San Francisco Bay Area, for example, there are sufficient duplicate sensors within a 1 km area, and a biased signal due to a poorly sited sensor could not meaningfully skew the distribution [78]. In our study, we used a uniform approach to siting our network. In each settlement, we optimized host selection to ensure we represented the major land-use categories of that settlement. For example, in Lucknow, a major city of over 4 million people

in the metro area, our sites covered the factory district, the major intra-city arterial road, greenspace, and several residential neighborhoods.

We instructed all hosts to place the sensors between the top of the ground floor (∼3 m) and the mid-level of the second floor (∼7.5 m). We ensured all sensors were placed outdoors from a balcony or attached to a pole outside the house or apartment. The outdoor location was also specified to be away from adjacent local sources, such as kitchens, parking spaces, and tobacco smoking areas. When persistent errors were detected at the site, we would offer a replacement sensor. In a small number of cases, the hosts could not support the campaign for the entirety of the study period, so we started new sites within about $1 - 5$ km of the original site.

Based on our location selection criteria and siting guidelines, we have ameliorated the bias inherent in leveraging community-supported sampling for ambient $PM_{2.5}$. We still expect a positive bias or overestimation by the non-collocated LCS sites relative to their nearest reference site since they are purposefully designed to avoid exaggerating the impact of any source. As a result, regulatory bodies in India typically choose parks or large university campuses to house their sites, resulting in lower measurements of $PM_{2.5}$ than a factory district or dense apartment complex. However, since $PM_{2.5}$ varies on larger spatial scales (> 1 km) than other pollutants, such as NO [64], we expect our community LCS sites to be strongly co-linear with reference sites.

Quantifying Representativeness

Interpretation of LCS networks is challenging because many competing sources of bias contribute to the overall uncertainty in comparing measurements [44]. Consequently, even calibrated LCS networks may lack representativeness since spatial-temporal sample distributions may not characterize the "true" population distribution well. To systemically approach this problem, we break down network bias into four categories for investigation: (1) sensor precision, (2) temporal representativeness, (3) sensor accuracy, and (4) spatial representativeness. Although we apply different methods to develop benchmarks within each category, we broadly use the same structure in designing data experiments to isolate and quantify bias. First, we design a "target" distribution, constituting a distribution of known quality and representativeness. Then, using the target distribution as a seed, we can repeatedly and iteratively modify it in a Monte Carlo (MC) fashion to generate empirical estimates of the influence of a given source of bias. The results are bootstrapped uncertainty intervals along the axis of interest at each percentile, generated by calculating 95% confidence intervals for each MC distribution percentile.

Temporal Representativeness

Here, temporal representativeness is constrained to sources of bias introduced by data gaps or aggregation. Data gaps are a natural result of community deployments due to power loss, participant behavior, or sensor replacement. Furthermore, gaps may also result from

intentional removal due to sensor performance, often a function of mass loading, resulting in biased sensor output. Previous work has used similar methods to demonstrate that annual or seasonal air pollution medians can be approximated with a few samples via mobile monitoring [90, 89]. Those analyses demonstrated the empirical certainty derived from MC procedures, which, while helpful, is unique to the chemistry, concentration range, and observation principle. Therefore, while our work here may offer some generalizability to other LCS deployments, MC processes empirically converge on the deterministic influences of the experiment only as a function of the input probability distribution [1].

Precision

Quality assurance (QA) procedures for LCS differ by pollutant, application, and measurement technology. Consequently, many proposed standards and methodologies exist even for the same sensor model. For example, since the PA-II includes replicate Plantower nephelometer-like monitors, it is common practice to compute the "disagreement" between the "A" and "B" Plantower sensors [32], as shown in Eq.3.1, as a proxy for sensor noise.

$$Disagreement = \frac{2 \times |A - B|}{A + B} \times 100\% \tag{3.1}$$

Accuracy

Previous work in disparate aerosol regimes has exhaustively demonstrated that the Plantower sensor's uncalibrated signal can demonstrate strong co-linearity with reference signals (Pearson's r $\geq$ 0.9) but with strong bias and low accuracy [18, 70, 111]. Previous work in North India [18, 141] has demonstrated that Plantower instruments can be effectively calibrated with a relatively simple two-parameter linear regression model of the form:

$$C = \beta_P \times P + \beta_{RH} \times RH + \beta_0 \tag{3.2}$$

Where C represents the corrected signal, P represents the $PM_{2.5}$ data from the PMS5003, RH means the relative humidity from a collocated sensor (as is the case with the PA-II), and the terms represent the regression coefficients fit by collocating the LCS with a FEM.

In Campmier et al., a greedy approach was employed to converge on model parameters and coefficient values, remarkably similar to the continental US models developed and deployed by the US-EPA [12, 11]. However, both models are vulnerable to shifts in the particle size distribution [18, 58, 12]. Particle size distributions tend to exhibit seasonal autocorrelation [42], which, along with RH, is likely the deterministic force behind the seasonality of calibration coefficient selection. Since the MODULAIR-PM package offers more accurate size resolved information, we first explore the seasonality of these trends.

Then we utilize a domain adaptation approach inspired by transfer learning to allow for seasons to "share" information when building calibration relationships across sites or seasons. The domain adaptation technique we use is "Nearest Neighbors Weighting," (NNW)

a simple approach optimized for large datasets (> 10,000 data points). Like all domain adaptation approaches, NNW attempts to account for differences in the training distribution and prediction distribution. In brief, NWW calculates the distance (Minkowski is typical) between training data points used to build the model, and data points used for prediction. By weighting points in the training dataset more representative of the prediction dataset, NWW builds a more flexible better fit for the prediction dataset. Similar approaches have been deployed in LCS calibration throughout the world [139, 86]. To illustrate the intuition behind this approach figure B.1 shows the overlap in LCS data distributions between measurements taken in the monsoon and post-monsoon.

Spatial Representativeness

The datasets we use to assess bias represent idealized datasets: temporal completeness to understand temporal representativeness, high precision batches to understand noise, and multiple long-term PA-reference collocations to assess calibration accuracy. To evaluate network spatial representativeness out-of-sample, we explore the correlation structure in multi-seasonal trends in our LCS network within a mega-city with regulatory instruments in Uttar Pradesh: Lucknow. None of our community-hosted LCS measurement sites are collocated with reference sites in this city. From this dataset and bias analysis, we step-wise implement different data reduction techniques, and observe the impact on estimates of $PM_{2.5}$ relative to the reference network. We expect our sites to systemically over-estimate due to siting within communities rather than at idealized reference locations. This evaluation will guide our analysis of settlements in the network outside of the regulatory network, and provide bounds to the expected influence of site-wise spatial bias.

3.3 Results & Discussion

Our measurement campaign reported hourly $PM_{2.5}$ estimates and performance analytics for the PurpleAir PA-II in Delhi, and Lucknow, India. We present collocation results from our central test-bed at the Indian Institute of Technology, Delhi (IITD) to evaluate PA-II precision under the challenging measurement conditions in Delhi. Next we evaluate calibration procedures at nine collocation sites with varying land-use properties. Finally, we combine our QA procedures developed at the IITD collocation site, with our calibration procedures to understand the spatial representativeness of our community host LCS network.

For our deployments in North India, we define seasons based on the Indian Meteorological Department guidelines: Winter (January, February), Pre-Monsoon (March, April, May), Monsoon (June, July, August, September), and Post-Monsoon (October, November, December). Appendix figures B.2-3 summarize the relevant meteorological drivers of air pollution trends and LCS performance. Winters are cool and humid and characterized by shallow inversion layers, exacerbating extreme air pollution [42, 48]. Pre-monsoons are the least humid season, with increasing temperatures and stronger winds, resulting in an influx of

dust from the west of India. Monsoons are hot, humid, rainy, and feature a reversal of wind direction (from prevailing westerlies to easterlies), resulting in the least polluted conditions. The Post-Monsoon is a critical transition period from moderate to extreme pollution with seasonal biomass burning in the Northwest agricultural regions of India impacting air quality throughout the region as winds shift back to prevailing westerlies [100].

Sensor Precision and Temporal Representativeness

Test-bed Data Overview

Measurements from the main collocation site at IITD are summarized in Table 3.1. Reference and aggregated PA time-series are shown in Fig. 3.1. During collocation phase C1 (8 August 2021 – 10 January 2022), our reference instrument, the BAM-1022, reported valid data for about 73% of the period, or 2709 hours of data. After acquiring a new BAM-1022 in 2023, we introduced the reference instrument during mid-phase C7 (4 March 2023 – 2 May 2023), reporting for about 33% of the period or 1237 hours of data. Losses occurred due to power outages, quality flags from the manufacturer's specifications, and maintenance periods. The IITD reference site demonstrated high accuracy to two nearby regulatory sites (Sri Aurobindo Marg [SAM]; Sirifort [SFT]), reflecting the expected strong spatial auto-correlation of $PM_{2.5}$ ($R^2_{SAM-IITD} = 0.91$; $R^2_{SFT-IITD} = 0.95$). Fig. B.4 demonstrates that the IITD reference signal time series and diurnal patterns match expected trends based on the nearest regulatory sites during C1. Therefore, we are confident that the IITD reference signal can be a robust validation data source.

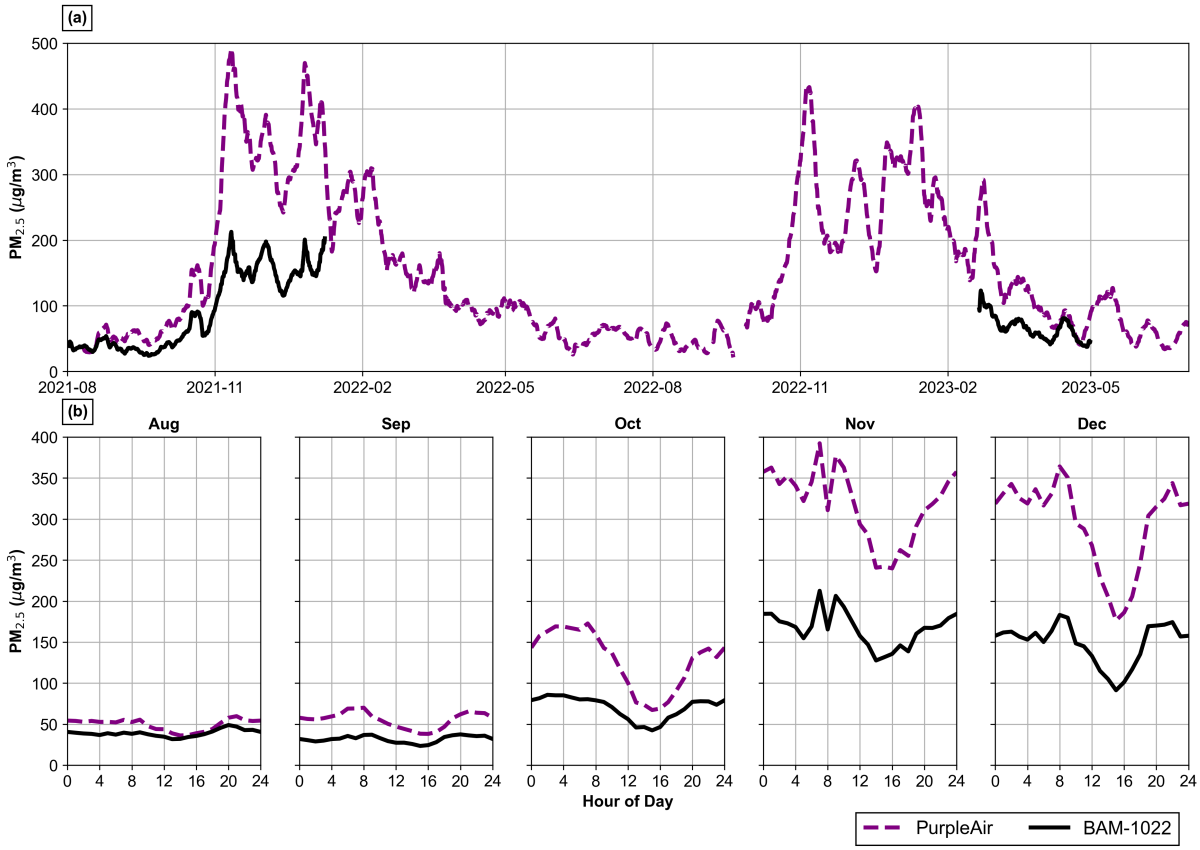


Figure 3.1: Panel **(a)** shows the aggregated PurpleAir signal at the IITD test-bed (more details in table 3.1) juxtaposed with a reference instrument signal (BAM-1022). Throughout most of the collocation phases, the PurpleAir tracked well with the reference signal (Pearson's $r \geq 0.9$). Panel **(b)** shows the monthly diurnal profiles for the PurpleAir LCS and reference instrument at IITD for the year 2022. Bias is strongly dependent on the month, with increasing bias during the highly polluted, cool, and humid November and December.

The PA and BAM demonstrated strong co-linearity during each month of data overlap ($r_{BAM-PA} \geq 0.90$) but highly variable bias from month to month ($NMBE_{BAM-PA}$: 1% – 25%). Both signals observe a sharp increase in $PM_{2.5}$ mass concentrations from October to November, marking the onset of extreme aerosol mass concentrations associated with increased biomass burning and unfavorable meteorology [100, 48]. Similarly, on the diurnal scale, both sensors identified sharp morning (07:00 – 09:00) and evening (19:00 – 21:00) peaks associated with increased emissions from traffic and residential energy use.

Collocation Phase	C1	C2	C3	C4	C5	C6	C7	C8	C9
Start	2021-08-09	2022-03-22	2022-04-21	2022-06-04	2022-07-08	2022-10-15	2023-03-04	2023-05-08	2023-07-18
End	2022-01-10	2022-04-19	2022-05-30	2022-07-07	2022-08-16	2022-11-07	2023-05-02	2023-07-10	2023-09-01
Total Sensors	164	29	38	39	47	40	136	136	106
Sensors Reporting	163	29	35	38	25	25	102	80	71
Precise Sensors	148	28	28	34	23	23	99	69	63
Total Valid Hours	3642	663	936	680	937	538	1394	1513	3788
Fleet CV Median	0.07	0.05	0.05	0.05	0.08	0.04	0.21	0.31	0.24
Fleet CV IQR	0.06	0.01	0.01	0.02	0.06	0.01	0.17	0.26	0.23
Fleet Median	140.1	83.4	72.9	46.5	44.7	265.2	82.7	51.8	102.3
Fleet IQR	274.9	81.4	66.9	47.0	31.0	203.0	80.9	50.5	247.0

Table 3.1: Data overview for SAMOSA Campaign collocation test bed at the Indian Institute of Technology. Data spans 9 distinct collocation periods from 2021 August through 2023 September. Here "Precise Sensors" refers to sensors with ${R^2}_{A-B} \geq 0.9$. Sensor performance is highly variable between collocation phases.

Batch-wise Variability

We evaluated over 500 PA-II sensor packages over two years, summarized in Table 3.1 as collocation periods C1 - C9. Before deployment, we required collocation sensors to report valid data at the collocation test-bed for at least one week, within the expected dynamic range (5 - 500 $\mu g/m^3$) and with high intra-unit precision (${R^2}_{A-B} \geq 0.9$). Due to documented and persistent Plantower manufacturing errors [115] and operational challenges, we found a step change in performance starting in phase C3, culminating in a failure rate of about 50% during phases C5 - C7 (July 2022 - May 2023). Table 3.1 further details this phenomenon, with the noticeable increase in batch CV, even when accounting for outliers in the inter-quartile range (IQR). To account for the within-batch variability and calculate the slope and intercept deviance of an individual Plantower to the batch, we used an Orthogonal Distance Regression [129, 123]. Figure B.5 illustrates the slope and intercept distributions from this analysis and demonstrates that the performance deviation is unacceptable [55] (0.9 $>$ intercept $>$ 1.1; -2 $>$ slope $>$ 2) for many sensors in these phases.

Data Gaps and Precision Simulations

To perform data experiments, we used a sub-sample of the C1 collocation phase from 16 November 2021 to 17 March 2022, when 3 – 5 PA-II units (6 – 10 Plantower signals) continuously reported data for 2881 hours. We aggregated all reporting sensors at each hourly time-step, resulting in a mean PA signal for the entirety of the sampling period. To ensure no single sensor's outliers or noise influenced the signal, we strictly required all aggregated data points to meet a CV threshold of 0.10, the standard used by the US-EPA for duplicate signals [29]. As shown in Figure B.6, the period is notable for its extreme mass concentrations reported by the PA-II, with hourly averages reaching as high as 400 $\mu g/m^3$ between 22 December and 29 December, and its high variability (Table 1). Therefore, we expect this data to be representative of a well-performing Plantower at a field-deployed site measuring

highly variable aerosol characteristics.

Figure B.7 summarizes the results of the time series distribution of random and block removal of data points from 1 – 99% data completeness. The confidence interval around the median of the distribution approximates the inverse square root function expected from the Central Limit Theorem, with symmetrical bounds converging on the true median of the sample. With approximately 50% of the sample, the true median can be estimated within a 95% confidence interval of ± 5% for a total width of 10%. Thus, if a given distribution on a monthly or multi-week scale follows a random missingness pattern and reports at least 50% of the sample, the distribution median can be estimated with high confidence. Left tail distributional extremes (e.g., 90^{th} percentiles) should higher data completeness.

Random removal simulations may well describe intermittent power or internet losses or the removal of a handful of spurious points. However, it is also expected to either introduce a new site partway through a sampling period of interest (e.g., halfway through a month) or remove all points following a catastrophic failure. In Figure B.7, we summarize the results of removing a random block of increasing size across the entirety of the distribution. Block data or systemic removal deviates significantly from a smooth inverse square root trend expected from the Central Limit Theorem [39]. Based on the results of our simulation, to accurately represent the distribution, the dataset should not have continuous missing data gaps of more than 20% of hourly data points within the total time series. Furthermore, block removal results in an unsymmetrical confidence interval around the median, so if a given time series features missing blocks, the median should be conservatively assumed as an overestimate of the true distribution.

To investigate the impact of the intra-unit disagreement on the bias, we again leveraged the C-1 dataset. We use the C-1 complete PA time series as the target distribution and build the MC experiment by modeling disagreement as a normal distribution centered at 0 and increasing the standard deviation from 0 to 99. To ensure the representativeness of our simulation, we observed the disagreement distribution across all deployed sensors as a function of age in Fig. B.8. We furthermore iterated over removal thresholds similarly to observe the trade-offs between disagreement and sample size. The results of the simulation are presented in Fig. 3.2. Overall, the 95% confidence interval width increases more rapidly with increasing removal threshold (i.e., decreasing sample size) than with disagreement, motivating a more permissive disagreement threshold. From Fig. B.8 we observe that the disagreement spread is about 13%, meaning setting a threshold of about 40% retains the maximum sample size while avoiding outliers.

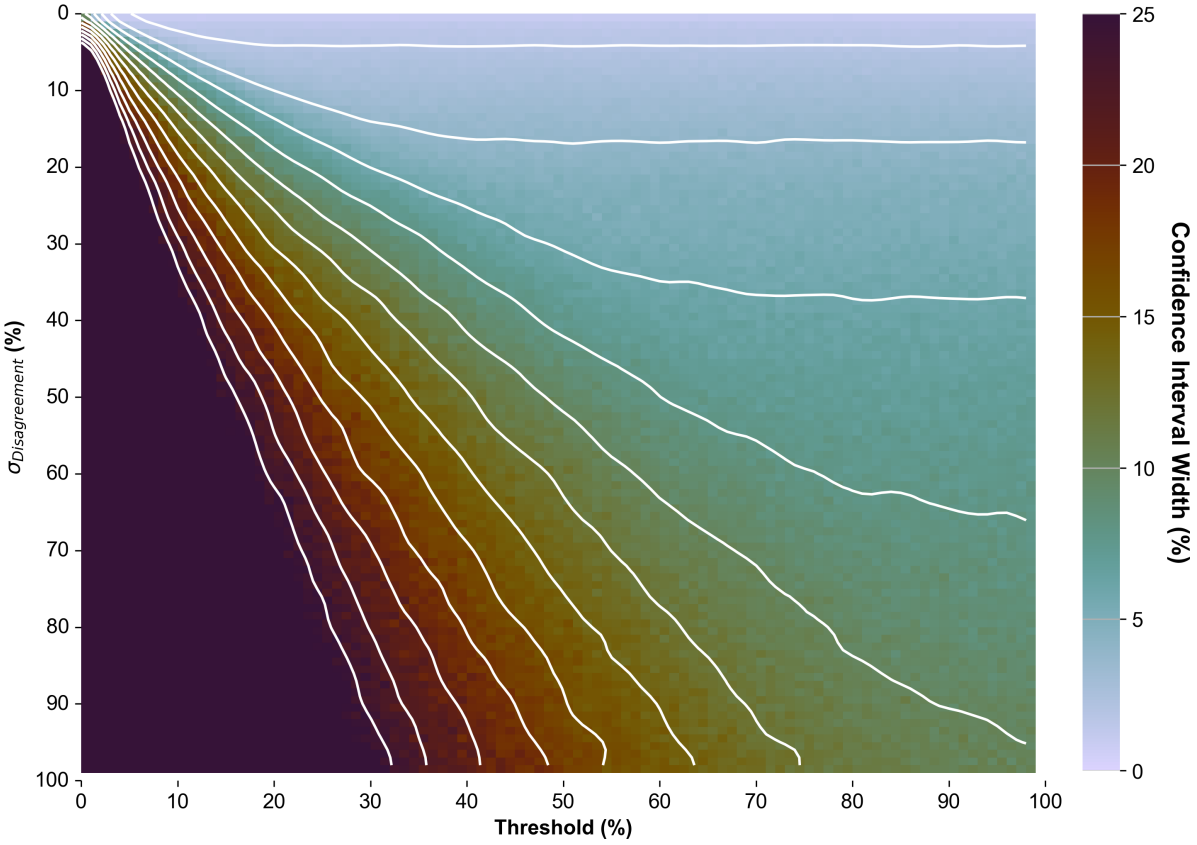


Figure 3.2: Summary of Monte Carlo simulation examining the trade-offs in sensor precision versus sample size. On the x-axis, "Threshold" represents the cutoff for considering a PurpleAir data point valid. On the y-axis, the standard deviation of Disagreement (see equation 3.1) represents the simulated spread in intra-unit precision. Each cell represents the width of the 95% confidence interval from 1000 simulations, with contour guidelines. Sensor uncertainty increases more rapidly as a function of decreasing sample size (i.e., higher threshold) than disagreement.

Accuracy and Calibration

Sensor Accuracy

We used the regulatory collocation dataset described in Table 3.2 and mapped in Figure 3.3 to investigate the role of calibration model selection on bias. The target distribution is the test or evaluation datasets withheld from the training dataset for cross-validation purposes. The uncalibrated PA-II bias at collocation sites follows expected trends, with relatively mixed bias site-wise, systemic overestimation as a function of RH, and distinct seasonality.

	Total Valid Hours	Fleet CV Median	Fleet CV IQR	r_{BAM-PA}	$NMBE_{BAM-PA}$ (%)
IITD	1514	0.24	0.17	0.54	-66.00
R K Puram	2333	0.03	0.04	0.92	-53.00
Najafgarh	3759	0.04	0.04	0.97	-84.00
Vivek Vihar	3761	0.02	0.02	0.78	-74.00
Patparganj	3782	0.06	0.10	0.78	-57.00
Wazirpur	4343	0.03	0.04	0.90	-44.00
Mandir Marg	4374	0.03	0.05	0.89	-67.00
Punjabi Bagh	4893	0.06	0.08	0.95	-15.00
Sri Aurobindo Marg	4995	0.04	0.25	0.94	-49.00

Table 3.2: Data overview for SAMOSA Campaign reference-LCS calibration collocations. Other than IITD, all sites were part of a regulatory agency collaboration (2023 February - 2023 October).

A naive approach to calibration, simply fitting new coefficients using Ordinary Least Squares based on season or site (Figures B.9-10; Table B.1-2), revealed calibration models with similar aerosol regimes share bias direction. Both the Post-Monsoon and Winter are characterized by high mass concentrations and high humidity and, therefore, report positive bias or overestimation when fit with a model trained in the drier, less polluted Pre-Monsoon [8, 42]. Similarly, the Punjabi Bagh and R K Puram sites only reported data during the Pre-Monsoon and early Monsoon seasons and are strongly biased when models trained at sites with broader seasonal coverage are applied. Therefore, in building a calibration model to propagate throughout the network, including sites far from reference monitors, it is critical to account for the underlying distribution in training the model and the deployment dataset [83, 51].

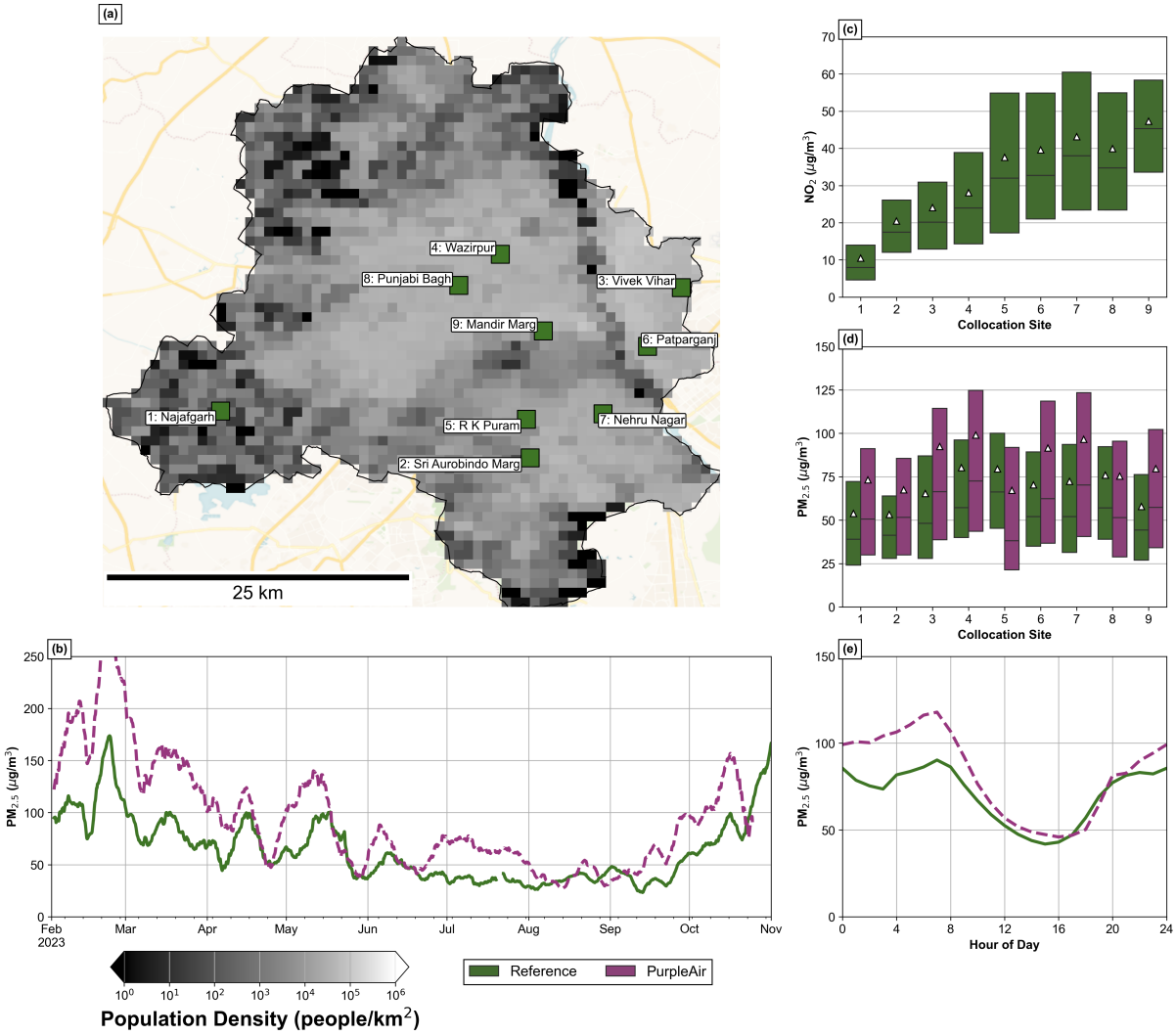


Figure 3.3: Panel **(a)** shows a map of collocation regulatory sites used in the sensor accuracy and calibration analysis juxtaposed with the population density of the Delhi National Capital Territory. Panel **(b)** shows the time series of aggregated PurpleAir LCS and reference data for the collocation campaign period. Panel **(c)** shows box plots of NO_2 as measured with reference instruments at the reference collocation sites (note: the Indian National Ambient Air Quality Standards measure NO_2 as a mass concentration rather than a mixing ratio. Panel **(d)** depicts the distribution of collocated PurpleAir data and reference data for each collocation site. Panel **(e)** shows the mean diurnal trends for both instrument types for the duration of the time series. Each site represents unique land-use, with starkly variable population density and NO_2 concentrations (a marker for primary combustion). However, $PM_{2.5}$ average concentrations are highly correlated, with much less variability, suggesting an expected strong secondary component. Differences in PurpleAir-reference bias is partially explained by different deployment timelines as described in Table 3.2.

Sensitivity to Particle Size Distribution

To inform our data structure, we use the PM_1 and $PM_{2.5}$ data from the MODULAIR sensor packages. Seasonal patterns are shown in Figure 3.4, with two sites each in Urban Delhi (IITD, and R K Puram reference sites), Urban Eastern Uttar Pradesh (Varanasi, and Jaunpur), and Rural Uttar Pradesh (Mai, and Hamirpur). Since we only deployed six MODULAIR-PM in total, these trends are more helpful in identifying regional phenomena rather than generalizing aerosol characteristics within a given settlement.

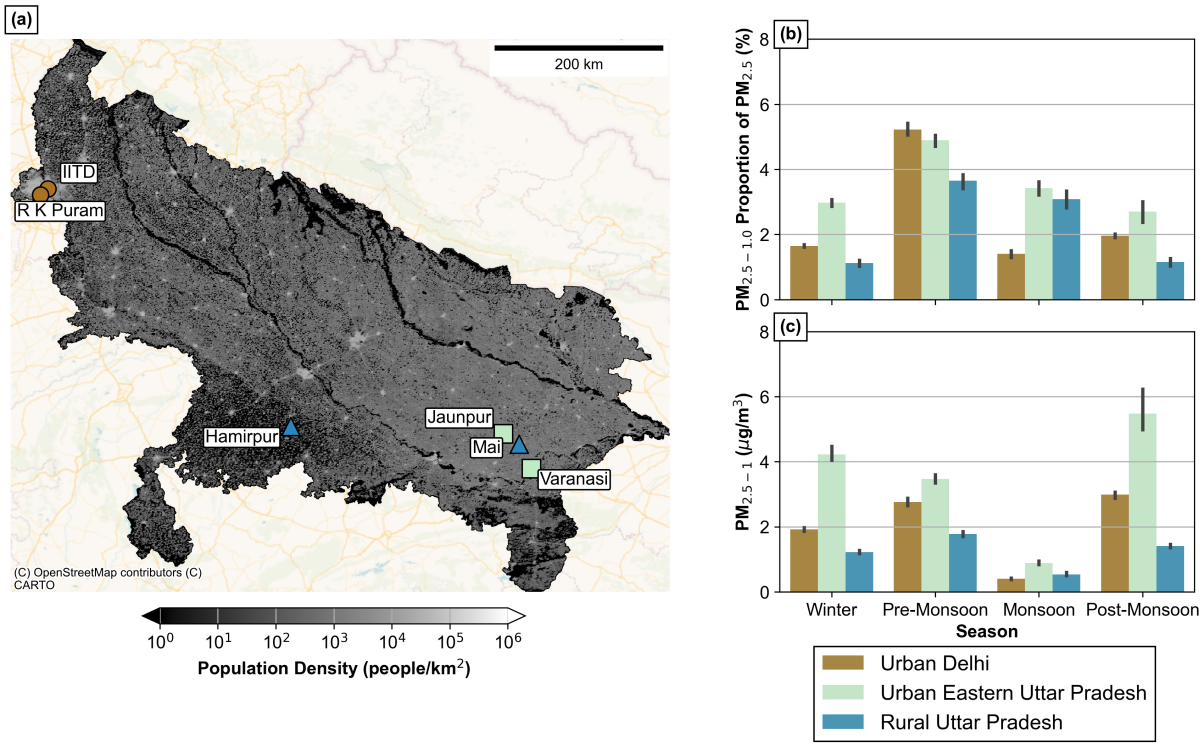


Figure 3.4: Panel **(a)** shows a map of QuantAQ deployment sites with three categories (Urban Delhi: [IITD, RK Puram], Urban Eastern Uttar Pradesh: [Jaunpur, Varanasi], and Rural Uttar Pradesh: [Hamirpur, and Mai]) with population density. Panels **(b)** and **c** show the seasonality of the supramicron component of $PM_{2.5}$ in both relative (**b**) absolute (**c**) terms with 95% confidence intervals. The pre-monsoon measurements, known for regional dust storms, shows a stronger supramicron component relative to the absolute concentration. This means PurpleAir data from this season may not transfer well to other seasons. See Table B.1.

We found that the PM_1 fraction of $PM_{2.5}$ dominated all sites, with low intra-seasonal variability across settlements. In the post-monsoon, relative concentrations of $PM_{2.5-1}$ increased, coinciding with the dry and windy conditions associated with regional dust storms.

Therefore, it is unsurprising that model coefficients change throughout the region, with LCS underestimating mass concentrations by a factor of 2 – 6 at all collocation sites (Figure B.11). While the median PM_1 and $PM_{2.5}$ distributions in the monsoon closely resemble winter and pre-monsoon conditions, there is high variability – particularly at urban sites. This likely occurs because the monsoon season is not uniformly wet but rather bands of rainy days interspersed with dry days, particularly in the early monsoon before the formation of strong low-pressure systems [64]. Therefore, it is unsurprising that although $PM_{2.5-1}$ concentrations in the pre-monsoon are about double the monsoon, they share PA-II calibration information (Figure B.10; Table B.1).

Collocation Site Evaluation

Across all seasons, urban settlements featured higher relative and absolute concentrations of supramicron particles, concurring with results finding more robust linearity in LCS performance in rural settlements compared to urban settlements and more calibration variability within cities than between cities. Thus, the model bias reported by the Delhi regulatory collocation dataset reflects a robust test of the proposed model procedures. We compare the bias in (1) uncalibrated PA-II, (2) Campmier et al. calibration ("Literature Calibration"), (3) a new model following eq 2 using NWW ("Domain Adaptation"), and (4) a site-season hierarchical model. We fit all models stratified by season to ensure even annual representativeness following the findings of Campmier et al. Scenario 4 is impractical for a scaled network as it lacks generalizability, but it serves as a helpful guideline for the theoretical performance ceiling of our models.

Figure 3.5 summarizes the findings of each model's biases. The literature calibration model performs surprisingly well, given the limitations of its training data, with near 0 mean bias at many sites. Its seasonal performance was limited to within 35 % NRMSE, comparable to the within sample NRMSE previously reported. Therefore, it is likely that although using a literature model "off-the-shelf" will sufficiently de-bias the LCS for citizen science use, additional techniques can help to additionally reduce bias and offer conservative $PM_{2.5}$.

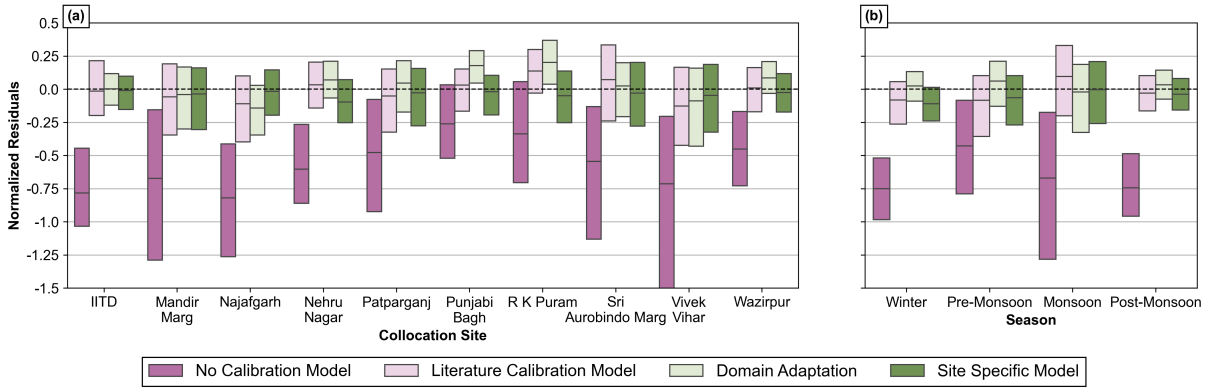


Figure 3.5: The bias distributions for each calibration regime: no calibration or "raw" PurpleAir data, literature or Campmier et al. calibration, domain adaptation or nearest neighbors weighing calibration, and a site specific model. The site specific model serves as a best-case scenario that is not feasible for deployment. Panel **(a)** shows the site-wise summary, with domain adaptation mostly matching or exceeding literature model performance. Panel **(b)** shows the seasonal breakdown, with domain adaptation more clearly outperforming the literature model.

Spatial Representativeness Evaluation

Post-collocation community-hosted LCS sites and reference sites for Lucknow are mapped in Fig. 3.6. Our spatial coverage approximates the reference network and offers additional coverage. Although our campaign continued throughout the course of 2021 - 2023, and extended beyond the urban environment, we use data from Lucknow from 2021 September - 2022 September to demonstrate the robustness of our approach in assessing community exposure. This time period reflects a return to pre-COVID lockdown activity patterns and emissions sources, with urban sources in the state of Uttar Pradesh including complex mixtures of traffic, biomass burning, industrial sources, and regional secondary formation and transport. Although all cities in North India are population-dense and polluted, Lucknow, the state capital, is especially burdened with extensive heavy industry districts (steel, batteries, detergents, chlorine products, etc.).

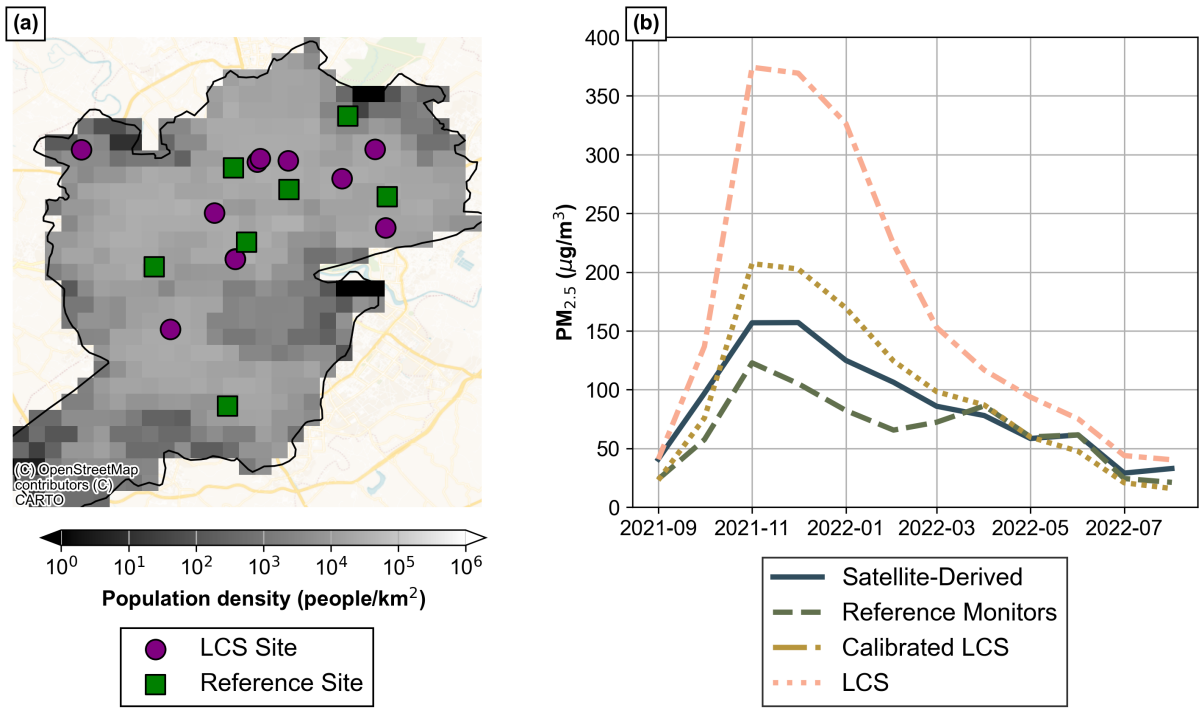


Figure 3.6: Panel **(a)** shows a map of PurpleAir community-hosted LCS sites from the SAMOSA campaign and reference monitors maintained by the Uttar Pradesh Pollution Control Board. Panel **(b)** shows the monthly average values from 2021 September through 2022 September for satellite-derived $PM_{2.5}$ (entire settlement averaged), the reference network, calibrated LCS, and uncalibrated LCS. Although methods deviate on settlement mean values, all track the seasonality of air pollution in North India similarly.

The uncalibrated LCS overestimates the settlement average compared to the reference network and satellite-derived values [117] by as much as 150%. However, calibration reduces these estimates to within 10% of the reference network average in the monsoon and pre-monsoon months. While the calibrated LCS signal does observe higher values than the reference and satellite in the pre-monsoon and winter months (November, December, and January), it is not necessarily true that this residual is solely due to calibration error. The satellite product estimates much higher values than the reference network for those months as well. Since the reference network is intentionally placed at secured facilities designed to represent regional rather than local exposure, the calibrated LCS values may be more representative of community-scale exposure. These community sources could include biomass burning for heating, a common source of local PM in the Indo-Gangetic Plain.

3.4 Conclusions

Lower-cost sensors offer the capacity for sensing in under-measured and low-resourced communities. In scaled LCS networks in the United States and Western Europe, interpretation is relatively straightforward: power is consistent, reference monitors are available in both urban and rural communities, LCS deployments are dense, and the mass concentration dynamic range is low. Conversely, in India, where LCS are urgently needed to complement ground-based observational infrastructure, LCS network interpretation is complex: both LCS and reference sites feature prolonged and intermittent gaps, sensor degradation is quicker and less studied in situ, and complex aerosol mixtures lead to dynamic calibration relationships with reference monitors.

Our study examined the influence of each parameter, first with an idealized toy dataset at the IITD collocation test bed, next at controlled collocation environments, and finally in community-hosted LCS networks throughout North India. We found significant sensor performance aberrations from new sensors out-of-the-box, emphasizing the need for collocation testing and caution when using crowd-sourced data. Analysis of sample size found that provided sensors reported data throughout at least 80% of the measurement period, the central tendency could be recovered with negligible bias with as little as 50% of the dataset. The PA-II's usage of a replicate sensor offers real-time insight into sensor degradation. Provided the mean disagreement is near 0%, including measurements with disagreement as high as 40%, the distribution can offer a low bias estimate of the central tendency. Adopting a more stringent precision requirement, while beneficial in constraining estimates of the distributional tails, often attenuates the sample size too much, resulting in an unrepresentative distribution.

Within Delhi, we found comparing calibrating LCS with both literature models and domain adaptation methods effectively reduced bias compared to reference monitors to near 0%, and improved accuracy better than uncalibrated methods (NMAE $\approx$ 25%; $R^2 \approx 0.78$). Scaling our deployment to other cities, we found by constraining our disagreement threshold to 30%; we were able to maximize our sample size, both in terms of spatial and temporal representativeness, while reducing the effect of outliers. In Lucknow, our network demonstrated high correlation to the reference network and satellite-derived estimates during the monsoon and pre-monsoon months. However, higher estimates from the LCS network in the winter months are difficult to disentangle from multiple competing factors, including calibration changes, sensor placement, and local sources.

Overall, we quantified and minimized bias due to sample size, and precision. Calibration uncertainty and siting bias remain difficult to quantify for any arbitrary location; however, our calibration approach effectively removes bias due to RH and considers seasonality. Therefore, we are confident that our network, when a settlement has multiple temporally representative sites active, can estimate both annual and seasonal means with bootstrapped confidence intervals. Future analysis of our network in non-urban locations will likely face less uncertainty due to calibration and siting factors since there are fewer heterogeneous source mixtures. Therefore, we are confident our framework for assessing and quantifying

sources of bias will enable robust exposure estimates in previously unmonitored communities throughout North India.

Chapter 4

Air Pollution Management Urgently Needed in Non-urban North India

4.1 Introduction

Ambient fine particulate matter air pollution ($PM_{2.5}$) is the largest environmental risk factor for premature mortality worldwide, motivating significant international, national, and sub-national abatement interventions [97, 25, 30]. Recent trends constrained through chemical transport modeling, remote sensing, and ground-based observational networks have observed improved air quality across all pollutants in North America, Europe, and East Asia over three decades (1990 - 2020) [57, 54, 137]. In contrast, advances in observational capacity have demonstrated that South Asia (Afghanistan, Pakistan, India, Nepal, Bhutan, Sri Lanka, and Bangladesh) has faced substantial and sustained air quality degradation over the same time period [33, 54]. In India alone, $PM_{2.5}$ attributable mortality exceeds 1 million premature deaths each year, reducing life expectancy by about 2.2 years [97, 4].

Within India, there is high spatial-temporal heterogeneity, with the population-dense (population about 400 million) Indo-Gangetic Plain (IGP) in North India experiencing one of the highest air pollution burdens in the world (Fig. C.1) [32, 109, 3]. From the existing sparse urban regulatory network and research stations, annual averages in megacities (metro-area population $\geq$ 1 million) all above 40 $\mu g/m^3$ (the Indian National Ambient Air Quality Standard for $PM_{2.5}$; Fig. C.2), winter seasonal averages exceed 100 $\mu g/m^3$, and peak pollution day hourly concentrations exceed 1000 $\mu g/m^3$ [42]. Although the Indian population is rapidly urbanizing, the majority of the population in the IGP resides in non-urban settlements [109]. From census data and satellite measures of urbanicity, studies estimate approximately 60 - 70% of the IGP population live in "non-urban" areas.

There are relatively few studies focusing on understanding $PM_{2.5}$ dynamics outside megacities in the IGP. Existing evidence exploiting remote sensing or chemical transport models relies on emissions inventories and the largely urban regulatory monitoring network. Given the high contribution of the "informal manufacturing" sector (e.g., brick kilns), global emis-

sions inventories poorly constrain annual $PM_{2.5}$ estimates (normalized mean bias error $\geq$ 50%). Additionally, although energy policy has focused on transitioning residential fuel from biomass to less polluting fuels, market conditions have resulted in mixed usage [116]. Local emissions inventories derived specifically for the IGP estimate $PM_{2.5}$ emissions in peri-urban or non-urban settlements may be higher than urban emissions (Fig. C.3-4; Tables C.1-2) [131].

To effectively scale ground-based observational capacity across the IGP, we developed the SAMOSA network (Sensor-based Air Measurement Observatory for South Asia), a regional network exploiting novel lower-cost sensor (LCS) technology to provide unprecedented spatial-temporal monitoring in the IGP. Our LCS choice, the popular PurpleAir PA-II, is ideally suited to this application, as it has a wealth of validation and application studies in many global contexts. Previous work from our study has effectively demonstrated, with proper data treatment, LCS can overcome its limitations (e.g., precision, accuracy, linearity, etc.) to provide robust high-resolution estimates of $PM_{2.5}$ across a wide range of environmental conditions, and $PM_{2.5}$ concentrations[18]. Previous work has demonstrated the value of dense urban deployments, particularly in the relatively well-studied Delhi National Capital Region [80, 104, 142]. The novelty of our strategy relied primarily on many sparse deployments to focus on intra-regional variability rather than intra-urban variability.

We deployed over 80 $PM_{2.5}$ LCS in 15 settlements from September 2021 to July 2023. Settlements were stratified into three categories: megacity ($\geq$ 1 million), small city ($\geq$ 250 thousand), and non-urban ($<$ 250 thousand) based on population data and land use. Fig. 4.1 shows the geographic distribution of these settlements throughout the Indo-Gangetic Plain and the settlement category. While the majority of our settlements are non-urban, we deployed more sites (typically 1 sensor per site) in urban environments, anticipating more spatial heterogeneity in those settlements, resulting in 43 non-urban sites, and 40 urban sites (city and mega-city combined; Tables C.3-5).

4.2 Materials & Methods

Sensor Quality Assurance

Quality assurance procedures were implemented to remove the influence of spurious data and ensure internal consistency within a PurpleAir package. The details of our data reduction pipeline are described elsewhere (see [18], and **Chapter 3**). In brief, we followed well-established global LCS data quality guidelines, with additional sensitivity analysis to account for sustained high concentrations. Our approach optimizes data retention with precision.

Sensor Calibration Model Implementation

$PM_{2.5}$ LCS accuracy strongly depends on the ambient aerosol's particle size distribution and refractive index. Consequently, uncorrected data can be strongly and dynamically biased,

with both underestimation and overestimation present in multi-seasonal datasets, depending on the aerosol regime. Previously, we found the seasonal-specific models best-constrained bias and improved accuracy relative to out-of-sample collocation data across representative land-use categories [18]. Therefore, we implemented a correction leveraging multi-seasonal multi-site collocations. We constrained normalized bias to near 0% and normalized mean absolute error to about 20% on an hourly basis.

Temporal Representativeness

Due to our QA procedures, the LCS time series includes both short-term sporadic and long-term sustained gaps. As a result, we performed rigorous data experimentation to ensure our incomplete time-series distributions were representative, a common problem in air pollution observational systems (e.g., satellite remote sensing, mobile monitoring, short-term fixed sites). Our metric for temporal representativeness required coverage on 80% of days within a monthly or seasonal sampling period, with at least 12 hourly samples or 50% coverage constituting a complete day.

Site Selection

Previous work has demonstrated the value of citizen science or unplanned LCS networks for opportunistic analysis [11, 78, 31]. However, even LCS entails a cost barrier to most citizens, resulting in inequitable spatial distributions of PurpleAir sensors, with wealthy communities benefiting from redundancy more than poorer communities. Consequently, these networks can fail to characterize the "true" underlying distribution within a settlement despite the high apparent density of sensors. Therefore, our network design was optimized around three characteristics: (1) regional variability, (2) settlement type, and (3) intra-settlement variability.

We leveraged community networks to build mutually beneficial partnerships, resulting in at least 3 sites within a given settlement. More heterogeneous settlements, such as the megacity Lucknow, featured more sites to capture expected land-use gradients. We applied uniform siting requirements regarding sensor placement within hosts' homes to ensure the hyperlocal impacts of host activity, such as cooking, minimally impacted $PM_{2.5}$ sites. Site-wise details and siting procedures can be found in Chapter 3 and the appendix.

Spatial Representativeness

Our quality assurance, calibration, and siting procedures all serve to ameliorate spatial bias in our network analysis. Furthermore, $PM_{2.5}$ in aggregate exhibits typically modest spatial gradients on the scale of 1-10 km from the source due to the large contribution of regional secondary formation processes. Existing work in North India has demonstrated despite high concentrations of primary PM, the relative contribution of secondary species dominates the accumulation mode. The supplement reports the relatively modest spatial

gradients within all settlements. Similarly, when aggregating across settlement types, we report the spread in removing a single settlement of that type. Our previous work has shown our pipeline to constrain long-term median estimates of $PM_{2.5}$ to within 10% of the well-developed regulatory network in Lucknow.

Results and Discussion

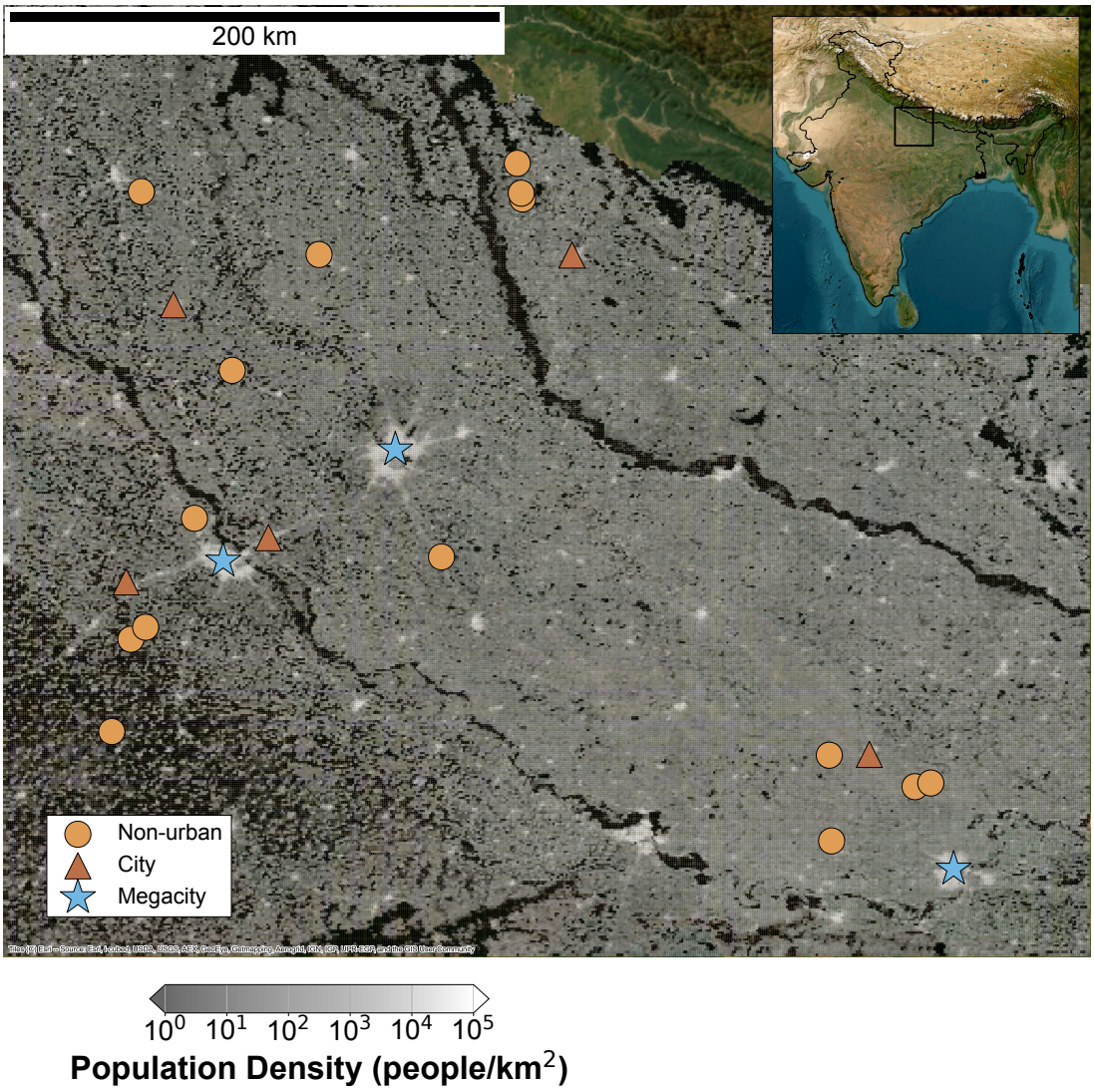


Figure 4.1: Map of the study region in the Indo-Gangetic Plain of North India, shaded by population density, and with markers for the three main settlement categories used in this study: megacity, city, and non-urban.

Non-Urban $PM_{2.5}$ Dynamics in an Example Settlement

Fig. 4.2a shows the spatial distribution of sensors, campaign time series, and seasonal diurnal profiles of LCS sites in Mai, Jaunpur District, Uttar Pradesh. This settlement is

representative of most non-urban communities in the region, about 10 km from the nearest city, Jaunpur, and about 70 km from the nearest regulatory measurement sites in Varanasi. With a population of about 5,000 people, the majority of the settlement is contained within a 1-km^2 area - or about 1 pixel of the most finely resolved AOD-derived satellite remote sensing dataset. Our network of 4 sensors represents typical non-urban dwellings aligned in a transect from south (Mai-1) to north (Mai-4), distinguished by proximity to the nearest highway (MDR-151E) in the south and the Gomti River in the north. Other import land-use features include brick kilns and other informal manufacturing sector biomass combustion sources ubiquitous in India [131].

Throughout 2022, we observed modest site-to-site variability in Mai, with high inter-site correlation (Fig. 4.2b). Although some quality assurance and calibration procedures have been found to attenuate spatial-temporal trends from LCS, this trend occurred across implementations. The most intra-settlement variability was observed in the winter months (January and February) when monthly average concentrations are also the highest ($\geq$ 100 μg/m^3). Spatial-diurnal variability was like-wise low across the settlement, unsurprising in the non-urban environment given the low spatial heterogeneity relative to cities (Fig. 2c).

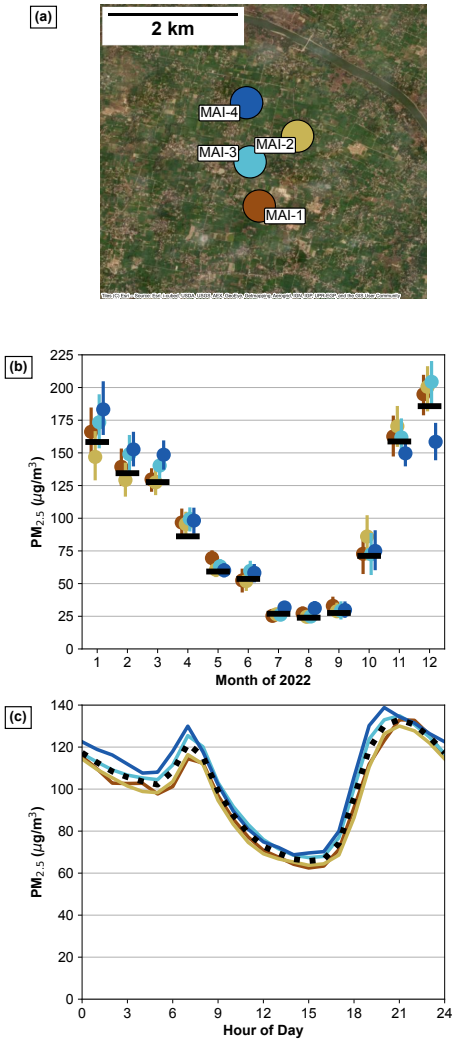


Figure 4.2: Example layout of the SAMOSA network deployment in a model non-urban settlement, Mai. Panel **(a)** shows the placement of the sensors throughout the settlement with our community hosts. Panel **(b)** shows the mean monthly values for the year 2022, with bootstrapped 95% confidence intervals stratified by day. Settlement mean values are depicted with a black dash. Monthly $PM_{2.5}$ values exhibit clear seasonality. Panel **(c)** shows the annual mean diurnal profiles of the sensors in Mai, with settlement mean displayed in black. Morning and evening peaks are clear in Mai.

Seasonal Trends

Typically, city-centered observational studies emphasize the importance of air pollutant gradients from the densely populated urban core to the sparsely populated outskirts. Our find-

ings highlight the pitfalls of applying such an approach to air pollution intervention in North India. The median non-urban site in our network was nearly as polluted as the median city or mega-city site across all seasons. Figure 3 shows the seasonal distribution (Winter: January, February; Pre-Monsoon: March, April, May; Monsoon: June, July, August, September; Post-Monsoon: October, November, December) of all sites within a settlement category. Each season corresponds with differing source profiles, for example the Post-Monsoon features crop residue burning episodes and residential heating emissions, while the hot and dry pre-monsoon is characterized by regional dust storms [100, 118]. Wintertime concentrations are exacerbated by shallow inversion layers, while aerosol deposition is augmented during the monsoon rain.

Our network followed expected trends from both remote sensing and the existing reference network in North India. Year 2022 reflects a return to business-as-usual after COVID related shutdowns and consequential shifts in emissions sources. As previously shown, mega-city sites were strongly correlated with nearby reference monitors (Pearson's $r \geq 0.9$; normalized mean difference $\approx 10\%$) and seasonal satellite estimates (normalized mean difference $\leq 15\%$). Seasonal average $PM_{2.5}$ concentrations exceed 125 $\mu g/m^3$ at most sites in the winter and post-monsoon, with the lowest concentrations observed in the monsoon (median site-average of about 32 $\mu g/m^3$). There is no obvious seasonal gradient from urban sites to non-urban sites, with all settlement type median site averages constrained to within 5%. From our network, there is no safe settlement class; all experience similarly high levels of air pollution.

Within a given settlement category, sites demonstrate intra-seasonal variability. Unsurprisingly the monsoon season features the least site-wise variability, while all other seasons see large differences between the least and most polluted sites (non-monsoon IQR ≈ 75 $\mu g/m^3$). Furthermore, the ordering of settlement-wise average mass concentrations is similar across seasons - non-urban sites are both the least polluted (Hamirpur), and the most-polluted (Kerakat). While sites closer to the Himalayas in north, and further from Delhi in the west tend to be less polluted, we observe settlements nearby each other can often contrast. For example, the non-urban site Mai's wintertime average is 15% lower than the nearby more populous non-urban site Kerakat. From these aggregated results can conclude that our network is faithfully capturing both regional and local trends similar to other observational methods. However, our network can resolve additional insights into $PM_{2.5}$ trends with its higher spatial-temporal resolution.

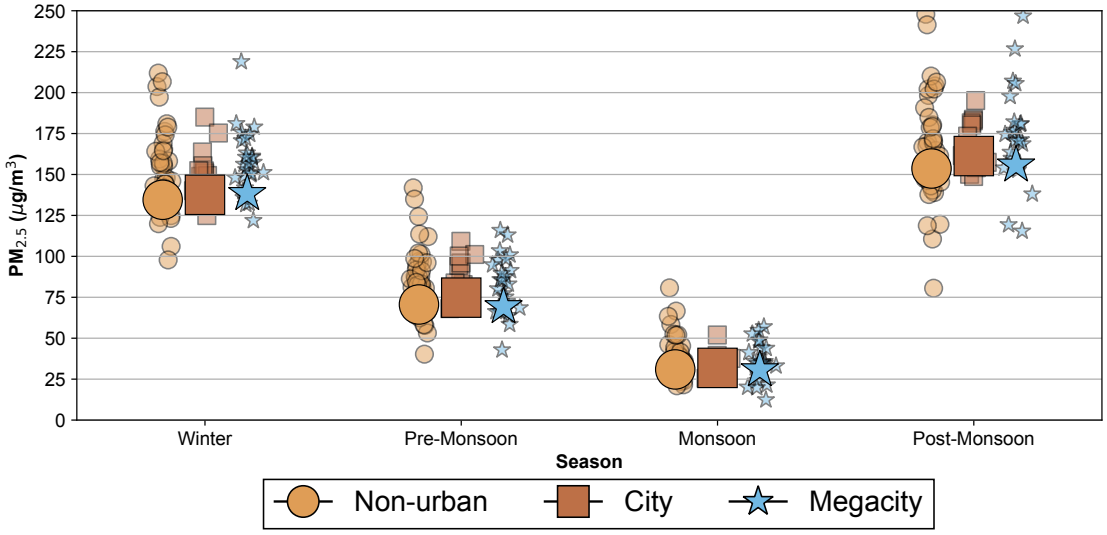


Figure 4.3: Seasonal $PM_{2.5}$ distributions at each LCS measurement site for each settlement category (megacity, city, non-urban). Small semi-transparent symbols represent the individual site means, while the large bold symbols represent the "median-of-means." Winter and post-monsoon seasons see the highest levels of exposure, with minimum mass concentration levels in the monsoon. Seasonal medians are nearly identical across settlement categories, but non-urban sites experience a larger spread.

Diurnal Profiles

Diurnal variability of $PM_{2.5}$ arises from the interactions between atmospheric ventilation, emissions, and secondary formation. Global studies have found that the spatial variability of normalized diurnal profiles is dominated by differences in terrain and mixing layer height. This suggests differences in diurnal patterns within the same region arise from local sources [84]. Furthermore, recent epidemiological evidence has found robust relationships between acute sub-daily $PM_{2.5}$ exposure and health impacts. Therefore, even if the annual or seasonal $PM_{2.5}$ spatial gradients are small or negligible, more finely temporally resolved differences may inform health impacts from different source mixtures, requiring tailored interventions.

Fig. 4.4 shows the diurnal profiles stratified by season and by settlement category. In the winter, pre-monsoon, and post-monsoon seasons, the magnitude and phase of the diurnal profiles vary by settlement category. Non-urban sites feature sharper morning (06:00-09:00 LT) and evening (18:00-21:00 LT) peaks, often $1.5 - 2\times$ higher than the daily midday trough (12:00-14:00 LT). By contrast, the mega-city site peaks are much less sharp. The monsoon season features the least variability, as well as the lowest mass concentrations (seasonal averages $\sim$ 30 $\mu g/m^3$) as a result of increased ventilation and rainfall, as well as lower emissions from the informal manufacturing sector. Even with these ameliorating factors,

mega-city profiles are less dynamic than non-urban profiles.

The diurnal cycles shown in Figure 4.4 offer additional evidence to suggest primary sources vary across settlement classifications. While primary emissions from biomass burning can be prevalent in North Indian mega-cities, mega-cities also feature a broader diversity of sources due as economic hubs. Consequently, mega-city diurnal profiles tend to be flatter relative to non-urban profiles. In contrast, the smaller cities monitored in our study more closely reflected the diurnal patterns found in non-urban settlements, reflecting their place in the energy transition. As smaller cities grow and rapidly develop, emissions will increase across sectors as energy demand increases. However, the transition has not been even, as poorer households retain biomass burning practices for heating, cooking, and waste management. Therefore smaller unmonitored cities in North India may be among the most polluted in the world. For example, our network in Jaunpur in eastern Uttar Pradesh was found to have a 2022 winter average $PM_{2.5}$ concentration of about 130 $\mu g/m^3$, (within 13% of remote sensing estimates), comparable to the reference network in the Delhi urban-core (138 $\mu g/m^3$; within 3% of remote sensing estimates).

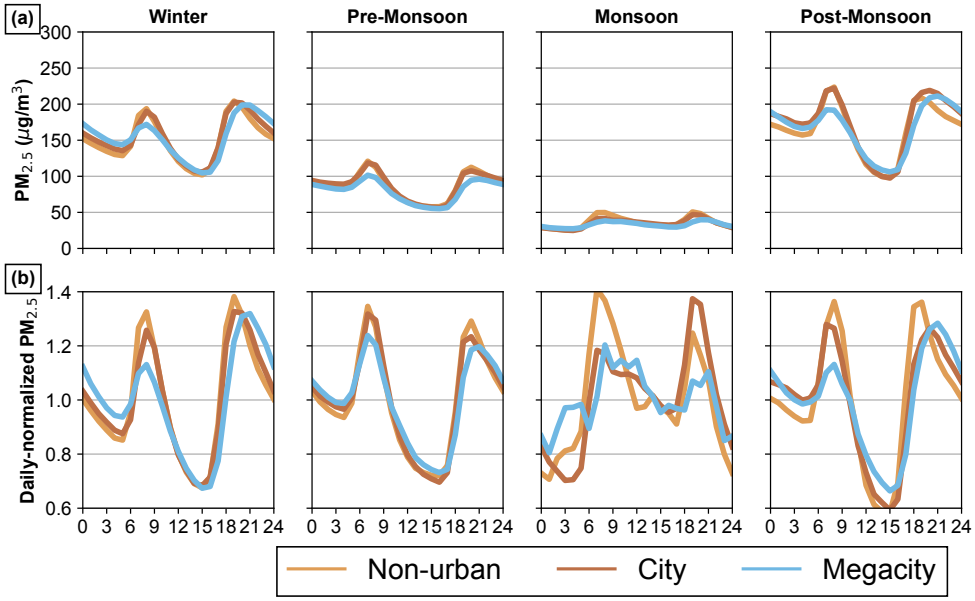


Figure 4.4: Panel **(a)** depicts the seasonal diurnal mass concentration for all LCS sites reporting more than 18 hours within a day. Although settlement categories share similar seasonal average concentration, zooming into hour-of-day trends resolves key differences between settlement types. Panel **(b)** shows the daily-mean normalized version of panel **(a)**. Normalizing diurnal trends more clearly distinguishes the differences between megacity and non-urban morning and evening peaks.

Episodic Regional Gradient Trends

Both satellite remote sensing products and our work indicate $PM_{2.5}$ air pollution in North India is a regional challenge, rather than restricted to a small number of localized hotspots. However, with the temporal resolution offered by LCS, we show that regional spatial gradients are a dynamic, rather than fixed process. Furthermore, we observe that while seasonal averages are similar between settlement types, spatial-temporal gradients emerge in morning and evening peaks resolved by our LCS network. To further illustrate the transient nature of spatial-temporal extremes in North India, we highlight two contrasting episodes emblematic of the regional management challenge. Figure 4.5 shows a transect of three settlements: Mai (non-urban), Jaunpur (city), and Varanasi (mega-city), showing low spatial heterogeneity (< 10 $\mu g/m^3$ maximum difference) within each settlement as well as between settlements during two episodes. The first time period takes place toward the end of the winter high pollution regime (13 - 20 February 2022), while the second period takes place during the pre-monsoon transition to moderate pollution regime.

Both periods are characterized by relative spatial homogeneity within the settlements (Fig. C.5-6). All sites in Mai and Jaunpur exhibit high correlation (Pearson's $r \geq 0.9$), with moderately high inter-site correlation in Varanasi (Pearson's $r \geq 0.7$). The winter episodes shows a clear spatial gradient from Jaunpur to Mai to Varanasi. Daily peaks accentuate this contrast, with Jaunpur and Mai morning peaks 25-80 % higher than Varanasi. Daily trough values in the winter show a reversal of this trend, with Varanasi noon time values at least 5 % higher than Mai midday mass concentrations on most days. Jaunpur exhibits both patterns, with strong morning and evening peaks, as well as midday values elevated above Varanasi.

In the pre-monsoon episode, the ordering changes to match an intuitive population density-based gradient: Varanasi, Jaunpur, and Mai with period mean $PM_{2.5}$ concentrations of 79 $\mu g/m^3$, 78 $\mu g/m^3$, and 71 $\mu g/m^3$ respectively. On top of reduced emissions from residential biomass burning for heating, the dominant wind direction in the period changes from Northwest to Southeast, resulting less transport from the extremely polluted Northwest Delhi corridor. The large differences in daily maximum values are not observed in this period, with spikes experienced in tandem across the majority of the time series. In the pre-monsoon episode, Mai becomes least exposed site, while in the winter Varanasi is the least exposed, demonstrating air pollution spatial extremes in North India are strongly linked to meteorology, and weakly correlated with population density. In both periods, Jaunpur is nearly as polluted or more polluted than the next most polluted settlement, reinforcing our finding demonstrating the predicament small cities face in North India.

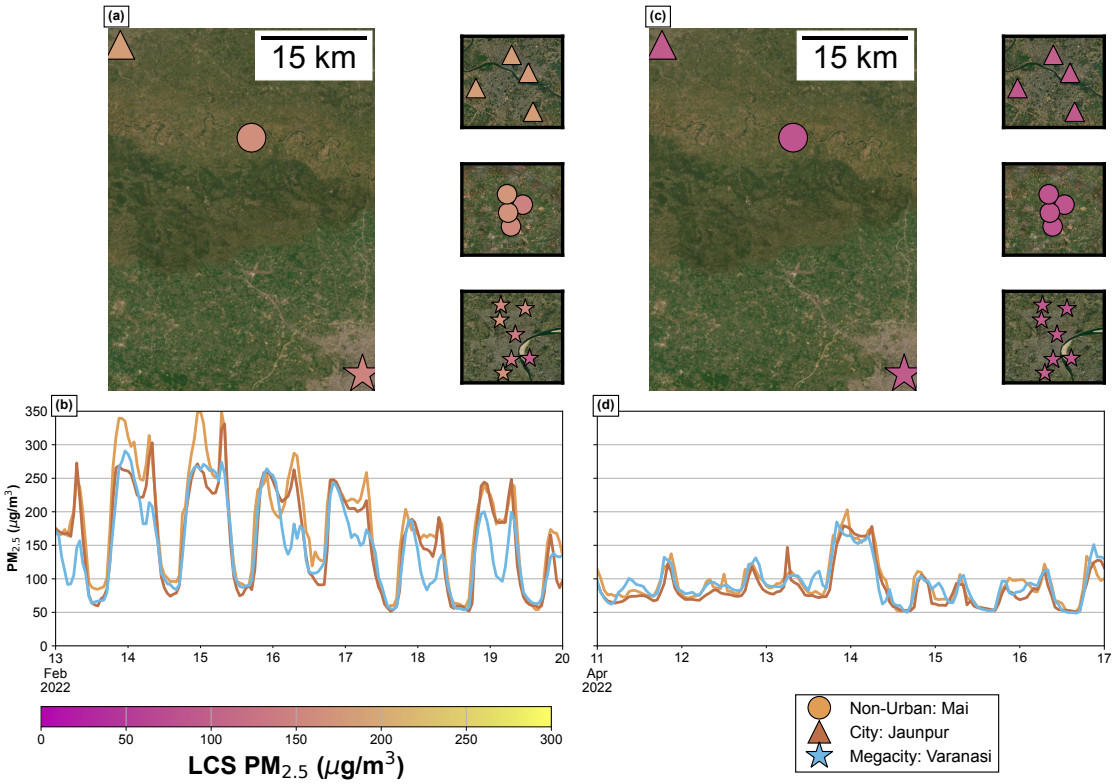


Figure 4.5: Panel **(a)** shows a map and map insets of Jaunpur [city], Mai [village], and Varanasi [megacity] during a peak wintertime pollution episode [13-20 February 2022]. Averaging to the entire period results in low intra-settlement and inter-settlement variability. In panel **(b)**, we observe that morning and evening peaks in the city, and non-urban sites are typically much higher than the megacity - by as much as 67%. This demonstrates the influence of primary sources not prevalent in megacities. Panel **(c)** shows the same settlements averaged to a pre-monsoon period with lower pollution levels [11-17 April 2022]. Similarly averaging to the entire period results in low intra-settlement and inter-settlement variability. In contrast panel **(d)** shows none of the same diurnal gradients observed in the winter episode, indicating the waning influence of sources less prevalent outside of megacities.

4.3 Implications

Emissions inventories, chemical transport modeling, satellite remote sensing, empirical models, and reanalysis products have previously demonstrated that extreme mass concentrations are a regional impact rather than strictly megacity problem in India [121, 33, 109, 131]. Our study is the first to use a regional ground-based observational network across multiple non-urban and urban sites to measure multi-seasonal $PM_{2.5}$ trends across North

India and, in most settlements, represent the first ground-based air pollution measurements. The SAMOSA network correlates well with the findings of other methods and serves as a compliment by offering unprecedented resolution into hourly community-level air pollution exposure.

There are several key caveats to our analysis. The design of Plantwower LCS packages can only infer $PM_{2.5}$ mass concentrations through particle counts in a narrow size range (0.5 - 0.7 μm), even with quality assurance and robust calibration procedures. Consequently, spatial-temporal gradients of nucleation mode primary combustion particles ($d_p < 0.1$ μm) nor supra-micron windblown dust (1 μm $< d_p <$ 2.5 μm) are characterized by this study. Therefore, we limit our conclusions to commenting on accumulation mode particles in aggregate, which is the typical size range of regionally characteristic aerosol. While our network design strove to represent the heterogeneity within settlements to develop realistic metrics, practical considerations meant we could only measure at 3 – 7 community-hosted sites within a settlement. Furthermore, we optimized for known land-use profiles (e.g., NDVI, road proximity, industrial zoning, etc.) in the site selection process; however, the informal manufacturing sector in India plays a key role in PM emissions and formation. Therefore, there are likely intra-urban hotspots not well characterized by our study.

Although our LCS network has drawbacks, the resolution and stratification of our network allow us to offer key insights. Smaller cities such as Jaunpur, while much less industrially developed than larger cities in the region such as Kanpur, suffer from extreme air pollution, making them the most polluted in the world. Smaller cities in India exist at a development transition point with features of mega-cities (e.g., traffic) and non-urban settlements (e.g., prevalent residential biomass burning) and should be prioritized for regulatory network monitoring expansion.

The status quo of relying on coarsely resolved remote sensing products does not constrain the system dynamics well, yet expanding regulatory monitoring to every non-urban settlement or district in India is not feasible. Therefore, future monitoring networks should focus on a hybrid approach, anchoring LCS deployments in well-resourced settlements and radiating out from that anchor. Given the unpredictable nature yet out-sized impact of the informal manufacturing sector, LCS can serve as a key indicator of progress in transitioning these industries to cleaner fuels. Additionally, since LCS data can be streamed in real-time, they offer more agency to communities wishing to carry out their own exposure assessments. Centralized support from regulatory and research organizations to ensure data is properly communicated with respect to quality assurance and calibration will be key to maintaining transparency on the interpretation of the data.

Chapter 5

Conclusions

5.1 Summary of Major Findings

This dissertation evaluates the efficacy and scalability of a lower-cost sensor package, PurpleAir, for monitoring $PM_{2.5}$ in India. Overall, while PurpleAir sensors show promise to plug the data gap, calibration is crucial for accurate data. Uncalibrated sensors provide strong correlation with reference monitors, and accuracy improves significantly (to within about 30% NRMSE) with calibration. Calibration must consider the seasonal variability of aerosol regimes and sensor siting. Scaling to create dense networks with these sensors makes them a valuable tool for improving spatial-temporal resolution of $PM_{2.5}$ trends. The SAMOSA network deployed these sensors in both megacities and non-urban areas, demonstrating hazardous levels of $PM_{2.5}$ across settlement categories. The novelty of the network lies in its ability to distinguish diurnal trends and quantify short-term (< 1 week) gradients across the Indo-Gangetic Plain. LCS network deployments, while requiring careful siting, quality assurance, and calibration procedures, can work to inform policy decisions aimed at improving air quality throughout India.

5.2 Limitations

This work is limited by the sensor technology used both in the LCS package and reference calibration. As detailed in each chapter, the PurpleAir sensors are sensitive to only a narrow range of particle diameters (0.3-0.7 μm). When making regional comparisons, this approach is largely valid, as accumulation mode particle mass concentration gradients are resolvable at this scale ($\sim$ 10 km). However, missing nucleation and coarse mode particles decreases the capacity to discern intra-urban variability, particularly due to vehicle traffic - a key emitter of ultrafine particles via combustion and coarse mode particles via resuspended road dust. The reference instrument used in this work, the MetOne BAM-1022/1020, is certified to measure the mass concentration of the full $PM_{2.5}$ size range. However, to comply with US-EPA federal requirements, the instrument treats humid air with a heating element to

maintain hourly mean RH between 30-40%. While this works to avoid bias due to aerosol liquid water, semi-volatile losses can be meaningful - especially in Delhi where particulate chloride is prevalent in the cool humid winter. Training PurpleAir on exclusively BAM-style instruments may carry the risk of overcorrection. Therefore, strategically collocating LCS with additional technologies such as filter-based monitors in environments with high semi-volatile emissions could balance compensatory bias corrections with deployment costs.

The other major limitation of this work is sensor placement and siting. Throughout this work, I detail the measurement sites and the standards we implemented to mitigate anomalous readings. However, due to the impracticality of regularly checking each site over hundreds of kilometers, as well as the COVID-19 pandemic shutdowns, LCS were often left unattended for weeks. Although we offered guidelines to sensor hosts regarding avoiding bias due to proximity to household sources, it was not possible to strictly evaluate the siting bias of each data point. Furthermore, while I had access to sub-hourly data points to diagnose BAM malfunctions at the sites managed by the measurement campaigns (IIT Delhi and CSTEP [Bengaluru]), sites offered by regulatory agencies only provided hourly data through centralized clearing houses. Although some data points could be eliminated due to obvious error (e.g., not following expected diurnal trends), it is not possible to know the calibration quality of opportunistic reference collocations.

5.3 Policy Implications

At present, lower-cost $PM_{2.5}$ sensor technology should not and can not replace reference-grade instrumentation for regulatory monitoring or attainment classification. However, this work demonstrates there are obvious advantages to dense LCS deployments despite the trade-offs. As reported in **Chapter 2**, the uncalibrated PurpleAir data has a Pearson's r of 0.9 with the reference instrument. At a baseline, even uncalibrated LCS can be useful in providing categorical or qualitative real-time information on air quality in India. Practically, uncalibrated data could be useful in optimizing indoor air filtration, where fan speed or filter specifications require only the trend in mass concentration. Furthermore, after even a simple two-parameter annual calibration, LCS data improved to R^2 of 0.7-0.9, with mean bias near 0%. Consequently, LCS can offer actionable information in micro-environments where reference monitors would be impractical to place. For example, a sufficiently dense network could be used to surveil fugitive emissions from the informal sector in a designated "low-emissions zone."

Chapter 3 and **Chapter 4** offer further policy-relevant investigations. Outside of megacities, the only observational data sources are satellite-derived products. Although useful, satellite products are not real-time and have been criticized as inequitable, as they prioritize the national interests of the few nations able to afford them. LCS offer a practical framework for democratizing access to air pollution data. Additionally, LCS can act as an educational resource by showing the impact of local activity and paths forward for actions to protect human health. For instance, during inversion events, LCS could show the rapid

increase in mass concentration throughout the region and reinforce the need for reduction of non-essential activity.

5.4 Recommendations for Future Applications and Study

The reality of lower-cost sensing technology represents nearly 100 years of engineering research and development. While Plantower and similar optical particle counter models have demonstrated their potential for actionable information, lower-cost sensor technology has continued to evolve and grow. It is inevitable that new models will achieve commercial viability, so the lessons learned here and in similar bodies of research should be refined to avoid unnecessary lines of investigation. Furthermore, although PurpleAir is currently positioned as a linchpin in international $PM_{2.5}$ data accessibility, there is omnipresent economic precarity in all social impact ventures. As of 2024, PurpleAir offers free downloads to sensor owners, and volume-based pricing on scrapping the entire network (with a self-described "generous" free limit). Therefore, here I outline future applications agnostic to individual sensor models or data platforms, but rather consistent with fundamental atmospheric science and environmental engineering.

In planning network measurement campaigns, particularly in regions with sparse reference coverage, all sensors must take part in a *pre-deployment* collocation phase. As seen in **Chapter 3**, previous findings on sensor precision are not guarantees of future outcomes. Although recent work has focused on demystifying common LCS, manufacturers neither provide quality assurance nor performance certification for large sensor batches in the same fashion as reference or laboratory-grade equipment. Collocation thus offers benchmarks for expected sensor performance and degradation. Furthermore, network deployments should consider a hierarchical approach in which differing LCS sensor technologies can complement each other's abilities to resolve aerosol mass concentration. For example, deploying a hybrid network of high-efficiency optical particle counters (e.g., AlphaSense OPC-N3) along with low-efficiency optical particle counters (e.g., Plantower PMS series) will inform network managers of when coarse mode particles are influencing the bias of the lower efficiency sensors.

With regard to interfacing with government bodies and community stakeholders, researchers should clearly state the trade-offs with each sensing technology and their implications for data interpretation. Although uncalibrated data can overestimate reference-grade $PM_{2.5}$ mass concentrations by as much as $2\times$, 200 versus 100 $\mu g/m^3$ both represent extremely poor air quality and demand remedy. On the other hand, Plantower-style sensors alone are not well positioned for source apportionment studies. Community groups often seek to quantify the impact of local sources, especially traffic and point sources (e.g., concrete manufacturing plants), and thus researchers should explain these shortcomings in plain language. With an emphasis on community autonomy and data transparency, researchers

can ensure government bodies do not feel "ambushed" nor communities exploited for the benefit of researchers.

Finally, researchers should leverage the organizing power of international groups such as the International Global Atmospheric Chemistry project, or World Health Organization to work toward interoperable networks. For example, throughout North India simultaneous to the SAMOSA deployment, several other networks were deployed with similar technology. As each network varied its siting and calibration approaches, there is potential to synergize these networks into a super-network "network of networks," particularly in highly burdened countries like India. Although current incentive structures often encourage competition rather than cooperation in these matters, the PurpleAir platform has shown how individual community members, government agencies, and researchers can cooperate to produce new insights not feasible without the cooperation of all groups. It is for the direct benefit of those disproportionately burdened by extreme air pollution that researchers surrender some control over the capital used to design and develop these networks. Air monitoring, while useful, should never represent an encumbrance to action.

Appendix A

Supplementary Information: Seasonally Optimized Calibrations Improve Low-cost Sensor Performance: Long-term Field Evaluation of PurpleAir Sensors in Urban and Rural India

A.1 Supporting Equations

Derivation of Theory-Driven Model Form

The correction equations used in Laulainen [73] and Chakrabarti et al. [19] take the form:

$$\mathrm{CF} = 1 + 0.25 \times \frac{\mathrm{RH}^2}{1 - \mathrm{RH}} \tag{A.1}$$

$$\mathrm{C_{corrected}} = \frac{\mathrm{C_{raw}}}{\mathrm{CF}} \tag{A.2}$$

Where RH represents the fractional RH, expressed on scale of 0 – 1, CF represents the hygroscopic correction factor, C_{raw} represents the light scattering instrument PM mass concentration, and $\mathrm{C}_{corrected}$ represents the PM mass concentration corrected for hygroscopic growth. Combining the two equations yields:

$$\mathrm{C_{corrected}} = \frac{\mathrm{C_{raw}}}{1 + 0.25 \times \frac{\mathrm{RH}^2}{1-\mathrm{RH}}} \tag{A.3}$$

From Laulainen [73], the selection of 0.25 in the denominator of (3) was found to vary with chemical composition, and in fact suggests a value of 0.328 at a site dominated by ammonium sulfate. As speciation across India is known to be strongly variable dependent based on seasonal and diurnal factors, we instead allowed for a best-fit approach described in the text to select the best fitting factor yielding the following:

$$\mathrm{C_{corrected}} = \frac{\mathrm{C_{raw}}}{1 + \beta \times \frac{\mathrm{RH}^2}{1-\mathrm{RH}}} \tag{A.4}$$

Furthermore, given that (A.1) was derived for use with integrating nephelometers, we chose to include an additional term (α) in the numerator to account for the differences in instrumentation. Therefore, we arrived at:

$$\mathrm{C_{corrected}} = \frac{\alpha \times \mathrm{C_{raw}}}{1 + \beta \times \frac{\mathrm{RH}^2}{1-\mathrm{RH}}} \tag{A.5}$$

Finally, we replaced C_{raw} with P to represent any $\mathrm{PM}_{2.5}$ mass concentration signal (CF1, ATM or ALT) from the PurpleAir, and simplified notation of $\mathrm{C}_{corrected}$ to C.

$$\mathrm{C} = \frac{\alpha \times \mathrm{P}}{1 + \beta \times \frac{\mathrm{RH}^2}{1-\mathrm{RH}}} \tag{A.6}$$

A.2 Supporting Tables

Table A.1: Most relevant parameters selected through sequential feature selection (SFS) for each $PM_{2.5}$ channel (CF1, ATM, ALT) from Delhi collocation. Parameters: relative humidity (RH), temperature (T), and dew point (D). As expected, the $PM_{2.5}$ was selected as the most relevant, followed by RH features.

Ranking	CF1	ATM	ALT
1	$PM_{2.5}$	$PM_{2.5}$	$PM_{2.5}$
2	RH	RH^2	$RH^2 \times T$
3	$PM_{2.5} \times RH$	$PM_{2.5} \times RH^2$	${PM_{2.5}}^2 \times RH$
4	$PM_{2.5} \times RH^2$	${PM_{2.5}}^2 \times D$	${PM_{2.5}}^2 \times D$
5	RH^2	${PM_{2.5}}^2$	${PM_{2.5}}^2$
6	${PM_{2.5}}^2 \times D$	${PM_{2.5}}^3$	${PM_{2.5}}^3$
7	${PM_{2.5}}^2$	${PM_{2.5}}^2 \times RH$	$PM_{2.5} \times RH \times T$
8	${PM_{2.5}}^3$	RH	$PM_{2.5} \times RH$
9	${PM_{2.5}}^2 \times T$	$PM_{2.5} \times RH$	D
10	${PM_{2.5}}^2 \times RH$	${PM_{2.5}}^2 \times T$	D^3
11	RH^3	RH^3	RH
12	$PM_{2.5} \times RH \times T$	$PM_{2.5} \times RH \times D$	$PM_{2.5} \times RH^2$
13	$PM_{2.5} \times T$	$PM_{2.5} \times RH \times T$	$PM_{2.5} \times RH \times D$
14	$PM_{2.5} \times D^2$	$PM_{2.5} \times D$	D^2
15	$PM_{2.5} \times T^2$	$PM_{2.5} \times D^2$	$PM_{2.5} \times D^2$
16	$PM_{2.5} \times T \times D$	T^3	$PM_{2.5} \times D$
17	T^3	$PM_{2.5} \times T$	$PM_{2.5} \times T$
18	$PM_{2.5} \times D$	$T^2 \times D$	T
19	$T^2 \times D$	D	${PM_{2.5}}^2 \times T$
20	D	$RH^2 \times D$	RH^3
21	$RH^2 \times D$	T	RH^2
22	$T \times D$	$RH \times T \times D$	$PM_{2.5} \times T^2$
23	T^2	$T \times D$	$PM_{2.5} \times T \times D$
24	$RH \times D^2$	$RH \times T^2$	$RH^2 \times D$
25	T	D^2	T^3
26	D^2	T^2	$T \times D^2$
27	D^3	$PM_{2.5} \times T^2$	$RH \times T$
28	$PM_{2.5} \times RH \times D$	$PM_{2.5} \times T \times D$	$RH \times D^2$
29	$RH \times T \times D$	$RH \times T$	$RH \times T^2$
30	$RH \times T^2$	$T \times D^2$	$T \times D$
31	$RH^2 \times T$	$RH^2 \times T$	$RH \times D$
32	$RH \times D$	$RH \times D$	$RH \times T \times D$
33	$T \times D^2$	$RH \times D^2$	T^2
34	$RH \times T$	D^3	$T^2 \times D$

Table A.2: Most relevant parameters selected through sequential feature selection (SFS) for each $PM_{2.5}$ channel (CF1, ATM, ALT) from Hamirpur collocation. Parameters: relative humidity (RH), temperature (T), and dew point (D). As expected, $PM_{2.5}$ was selected as the most relevant, followed by RH features.

Ranking	CF1	ATM	ALT
1	$PM_{2.5}$	$PM_{2.5}$	$PM_{2.5}$
2	RH	RH	$PM_{2.5} \times RH \times T$
3	RH^3	RH^2	${PM_{2.5}}^2 \times D$
4	RH^2	RH^3	${PM_{2.5}}^2 \times T$
5	${PM_{2.5}}^2 \times T$	${PM_{2.5}}^2 \times T$	$T^2 \times D$
6	$PM_{2.5} \times D$	T^3	$T \times D$
7	$RH^2 \times T$	$T^2 \times D$	T^3
8	$PM_{2.5} \times D^2$	$T \times D^2$	D^3
9	$RH^2 \times D$	D^3	$T \times D^2$
10	$RH \times D^2$	T^2	$RH \times T^2$
11	T^3	$PM_{2.5} \times D^2$	D
12	D^3	$RH \times D^2$	$RH^2 \times D$
13	$T^2 \times D$	D^2	RH^3
14	$RH \times T$	T	T^2
15	$T \times D^2$	$PM_{2.5} \times D$	D^2
16	$RH \times D$	D	$RH \times T$
17	D	$T \times D$	$RH \times D$
18	$RH \times T \times D$	$PM_{2.5} \times T^2$	$RH \times D^2$
19	T^2	${PM_{2.5}}^2 \times RH$	T
20	T	$RH \times T$	$RH \times T \times D$
21	$RH \times T^2$	$RH \times D$	RH
22	D^2	$RH^2 \times D$	RH^2
23	$T \times D$	$RH^2 \times T$	$RH^2 \times T$
24	$PM_{2.5} \times T^2$	$RH \times T \times D$	$PM_{2.5} \times RH \times D$
25	${PM_{2.5}}^2 \times RH$	$RH \times T^2$	$PM_{2.5} \times D^2$
26	$PM_{2.5} \times T$	$PM_{2.5} \times T$	$PM_{2.5} \times D$
27	$PM_{2.5} \times RH^2$	$PM_{2.5} \times RH^2$	$PM_{2.5} \times T \times D$
28	$PM_{2.5} \times RH$	$PM_{2.5} \times RH$	$PM_{2.5} \times T^2$
29	$PM_{2.5} \times T \times D$	$PM_{2.5} \times T \times D$	$PM_{2.5} \times RH$
30	$PM_{2.5}RH \times D$	$PM_{2.5} \times RH \times D$	$PM_{2.5} \times T$
31	$PM_{2.5} \times RH \times T$	$PM_{2.5} \times RH \times T$	$PM_{2.5} \times RH^2$
32	${PM_{2.5}}^2$	${PM_{2.5}}^2$	${PM_{2.5}}^2$
33	${PM_{2.5}}^2 \times D$	${PM_{2.5}}^2 \times D$	${PM_{2.5}}^3$
34	${PM_{2.5}}^3$	${PM_{2.5}}^3$	${PM_{2.5}}^2 \times RH$

Table A.3: Most relevant parameters selected through sequential feature selection (SFS) for each $PM_{2.5}$ channel (CF1, ATM, ALT) from Bengaluru collocation. Parameters: relative humidity (RH), temperature (T), and dew point (D). As expected, the $PM_{2.5}$ was selected as the most relevant for the ALT channel, followed by RH features. The other channels still select $PM_{2.5}$ but in combination with other features - likely an artifact of correlations between sensor performance, and diurnal temperature patterns. This is less noticeable in Hamirpur and Delhi where the temperature range is more seasonally dynamic.

Ranking	CF1	ATM	ALT
1	$PM_{2.5} \times T$	$PM_{2.5}^2 \times T$	$PM_{2.5}$
2	$PM_{2.5} \times T \times D$	$PM_{2.5}^3$	$PM_{2.5} \times RH^2$
3	$PM_{2.5}^2 \times T$	$PM_{2.5}^2$	$PM_{2.5}^2 \times T$
4	$PM_{2.5} \times RH^2$	$PM_{2.5} \times RH^2$	RH3
5	$PM_{2.5}$	T^3	$PM_{2.5} \times T^2$
6	D	$T^2 \times D$	$PM_{2.5} \times T$
7	$PM_{2.5}^2$	$PM_{2.5} \times T^2$	T^3
8	$RH \times T^2$	$PM_{2.5}$	$PM_{2.5}^2$
9	T	$PM_{2.5} \times T$	T^2
10	$RH \times T$	T	$PM_{2.5}^2 \times RH$
11	$PM_{2.5}^2 \times RH$	T^2	T
12	RH	$PM_{2.5} \times RH \times D$	$T^2 \times D$
13	$RH^2 \times T$	$PM_{2.5} \times RH$	$PM_{2.5} \times RH \times D$
14	D^3	$PM_{2.5} \times RH \times T$	$T \times D^2$
15	RH3	$PM_{2.5} \times D^2$	$RH^2 \times D$
16	$RH \times D^2$	$PM_{2.5} \times D$	$RH \times D^2$
17	$RH^2 \times D$	$PM_{2.5} \times T \times D$	$PM_{2.5} \times D^2$
18	$RH \times D$	D	$PM_{2.5} \times T \times D$
19	RH^2	D^2	$PM_{2.5}^2 \times D$
20	$RH \times T \times D$	$T \times D^2$	$RH \times T^2$
21	D^2	$RH \times T^2$	$PM_{2.5} \times RH \times T$
22	$T \times D$	D^3	D
23	$T \times D^2$	$T \times D$	$PM_{2.5} \times D$
24	T^2	$RH^2 \times D$	$PM_{2.5} \times RH$
25	T^3	RH	$T \times D$
26	$T^2 \times D$	$RH \times D$	D^2
27	$PM_{2.5} \times D^2$	RH3	RH
28	$PM_{2.5}^2 \times D$	$RH \times T \times D$	$RH \times D$
29	$PM_{2.5} \times T^2$	$RH \times D^2$	$RH^2 \times T$
30	$PM_{2.5} \times RH \times D$	RH^2	$RH \times T$
31	$PM_{2.5} \times RH \times T$	$RH^2 \times T$	D^3
32	$PM_{2.5} \times RH$	$RH \times T$	$RH \times T \times D$
33	$PM_{2.5} \times D$	$PM_{2.5}^2 \times RH$	$PM_{2.5}^3$
34	$PM_{2.5}^3$	$PM_{2.5}^2 \times D$	RH^2

Table A.4: Fitted coefficients from the hygroscopic growth model for each site and data channel. The broad variability in the β coefficient is indicative of the variable hygroscopic properties across India, and even among the two the Indo-Gangetic Plain sites, given the wide disparity between Delhi and Hamirpur fitted values.

		Delhi	Hamirpur	Bengaluru
ATM	α	1.01	0.887	0.907
	β	0.424	0.157	0.082
CF1	α	0.671	0.602	0.714
	β	0.379	0.126	0.107
ALT	α	4.82	3.84	3.598
	β	0.202	0.132	0.056

Table A.5: NRMSE comparison of best-performing CF1 models (see tables A.1-A.3 for parameters) for each site (Delhi, Hamirpur, and Bengaluru) from the SFS procedure compared with the Barkjohn, Gantt, and Clements [11] model commonly used by the US EPA for PurpleAir calibration Although the Barkjohn, Gantt, and Clements [11] model does improve performance, it still underperforms site-specific 2-parameter equations by about 5%.

	Delhi	Hamirpur	Bengaluru
Raw	90.5	123	75.3
1-parameter	33.4	25.8	21.6
2-parameter	31.7	21.3	19.5
3-parameter	31.4	21.3	19.5
Theory-driven	35.0	26.2	23.1
Barkjohn, Gantt, and Clements [11]	36.8	25.6	27.5

Table A.6: Mean Bias Error ($\mu g/m^3$) comparison of best-performing CF1 models (see tables A.1-A.3 for parameters) for each site (Delhi, Hamirpur, and Bengaluru) from the SFS procedure compared with the Barkjohn, Gantt, and Clements [11] model commonly used by the US EPA for PurpleAir calibration. Although the Barkjohn, Gantt, and Clements [11] model does improve performance, it systemically suppresses mass concentrations and results in more biased results than using a local model.

	Delhi	Hamirpur	Bengaluru
Raw	-56.3	-30.0	-12.9
1-parameter	-0.620	0.080	-0.220
2-parameter	-0.740	-0.040	-0.250
3-parameter	-0.360	-0.010	-0.220
Theory-driven	5.92	2.65	1.55
Barkjohn et al. 2021	21.1	5.04	5.98

A.3 Supporting Figures

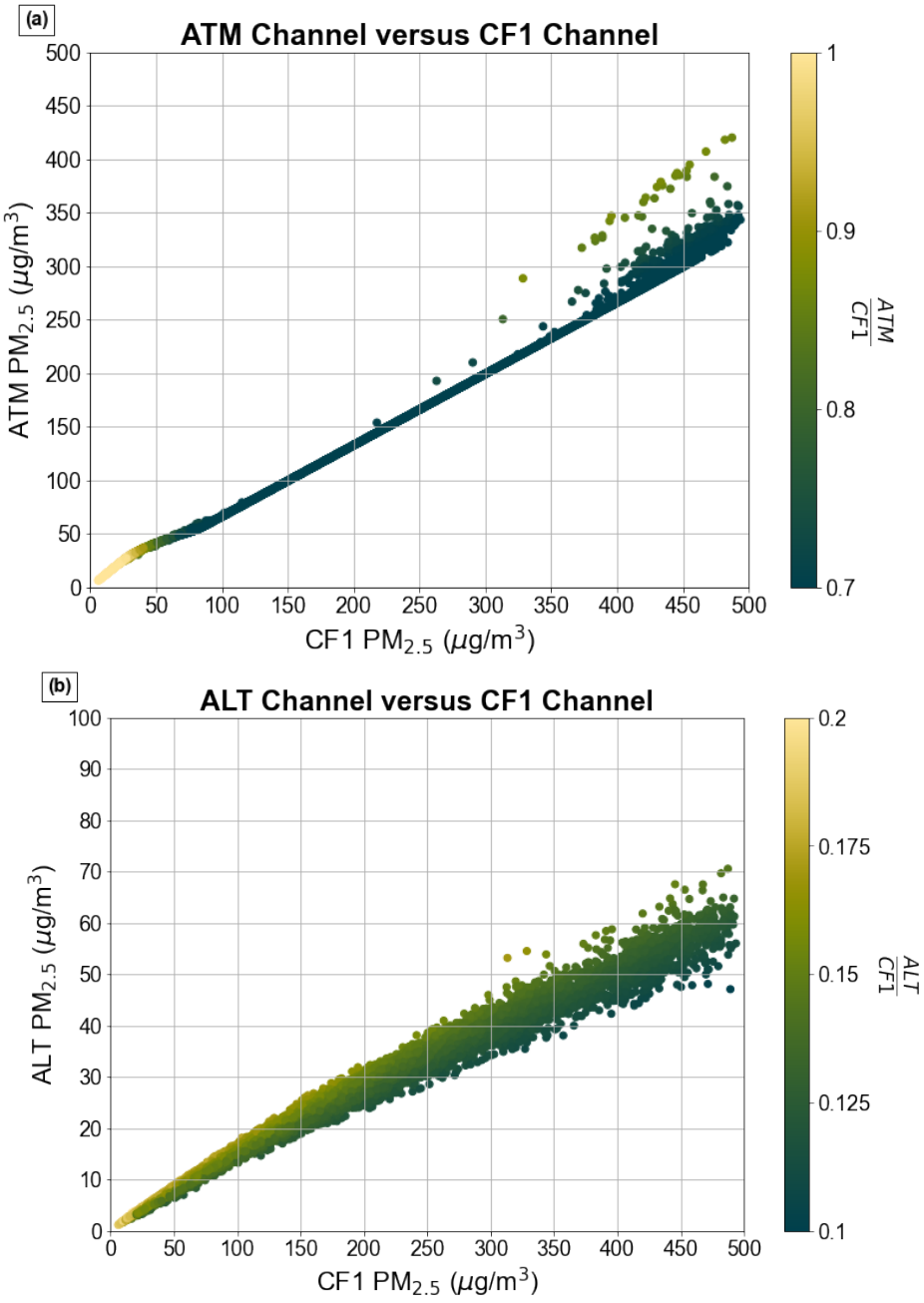


Figure A.1: Panel (a) shows correlation between PurpleAir ATM channel and CF1 channel. Values are 1:1 correlated until about 25 μg/m^3 where the ratio gradually transitions to 0.7:1 at around 40 μg/m^3 (CF1). Panel(b) shows correlation between PurpleAir ALT channel and CF1 channel. Since ALT does not include any density assumptions, and contains some noise from the particle distribution model, the ratio follows a distribution centered at around 0.15:1.

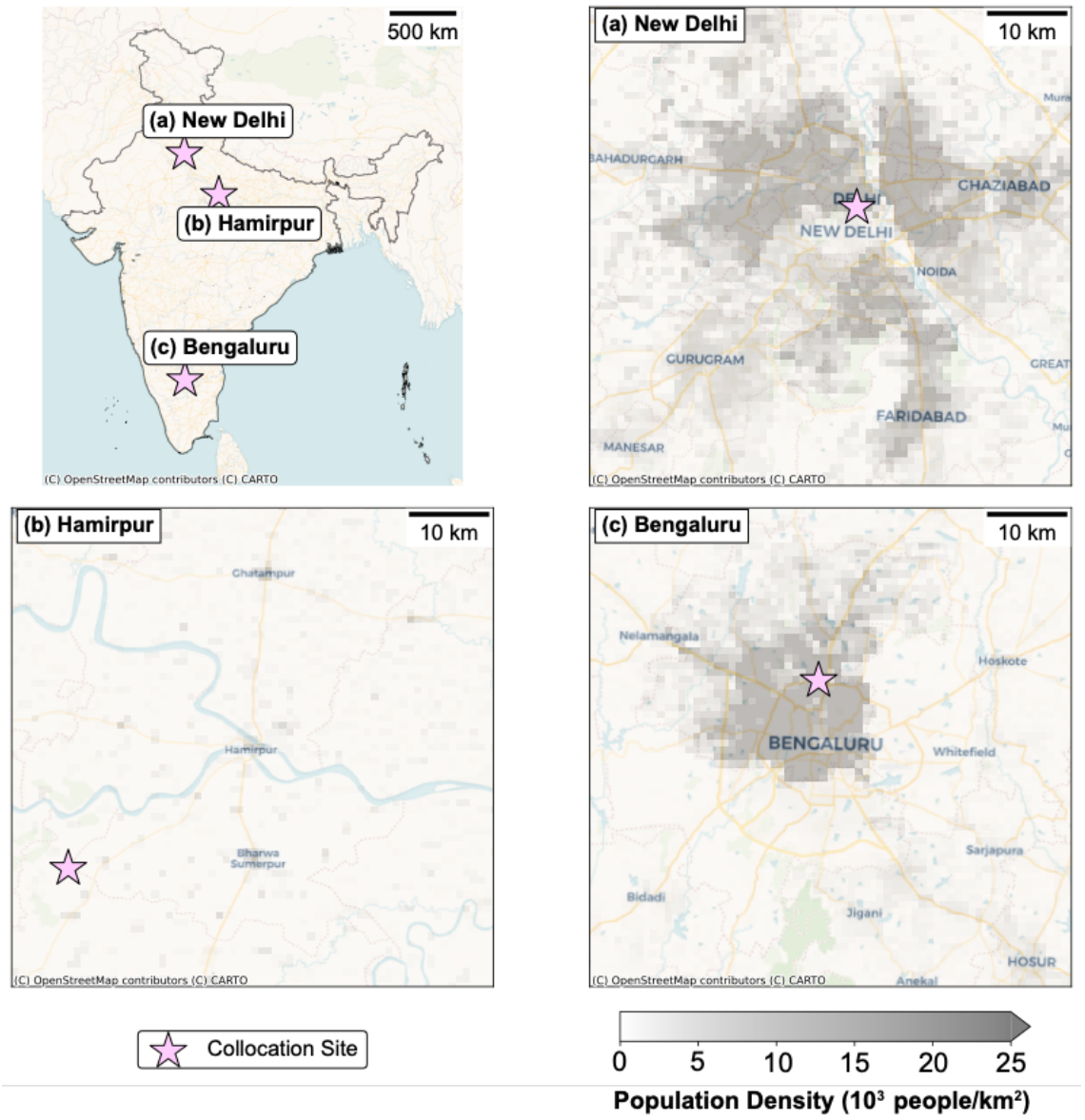


Figure A.2: Illustration of collocation sites (PurpleAir-Reference pairs) across India. The top left panel depicts the overall map of the country, with New Delhi and Hamirpur in the northern Indo-Gangetic Plain region, and Bengaluru in the south. Panels (a – c) highlight the locations of the collocation sites within a given settlement, with shading representing the population density from the Global Human Settlement Layer [114]. Panel (a) shows the central location of the US Embassy collocation site within the dense urban center of New Delhi. Panel (b) shows the extremely sparse IGP-CARE collocation site on the outskirts of Hamirpur. Panel (c) shows the CSTEP collocation site within the dense urban core of Bengaluru.

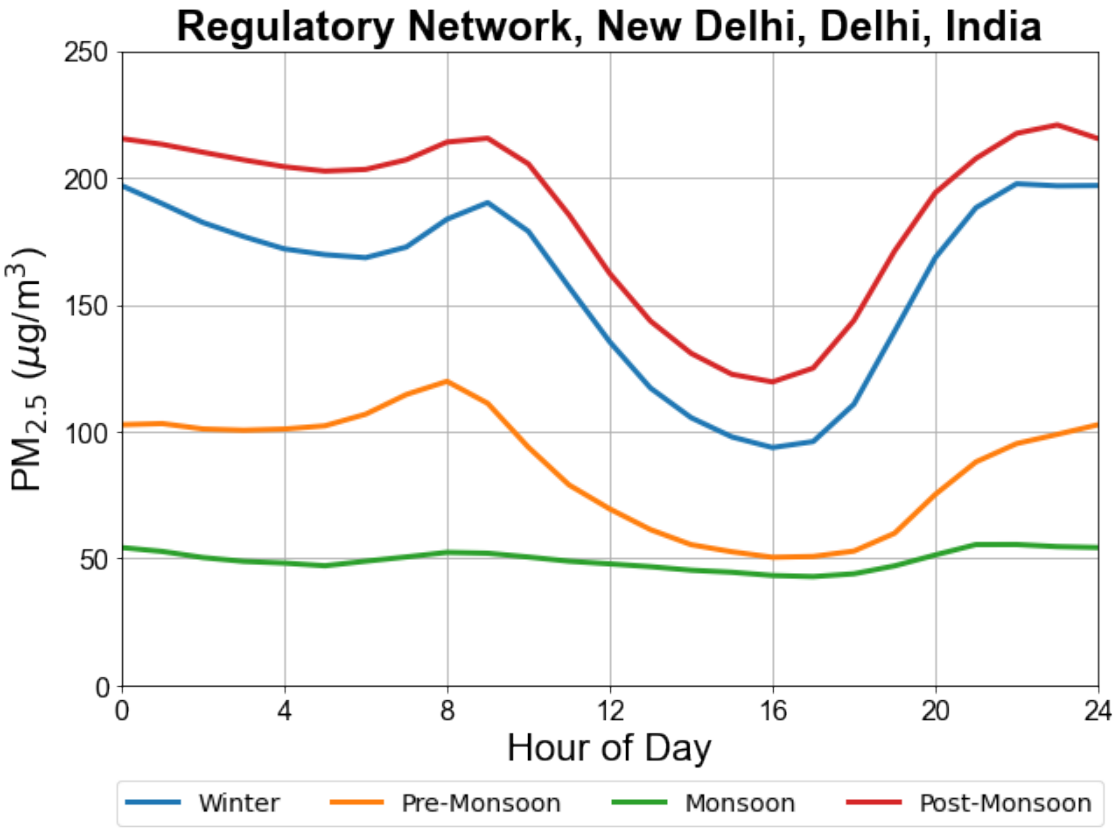


Figure A.3: Mean diurnal profiles of $PM_{2.5}$ by season averaged across all reference sites in Delhi. Mean concentrations are highest in the post-monsoon and winter seasons, with strong morning and evening peaks. The monsoon period features the lowest mass concentrations (albeit still above World Health Organization guidelines), as well as much less dynamic range due to the rains and ventilation conditions during the monsoon season.

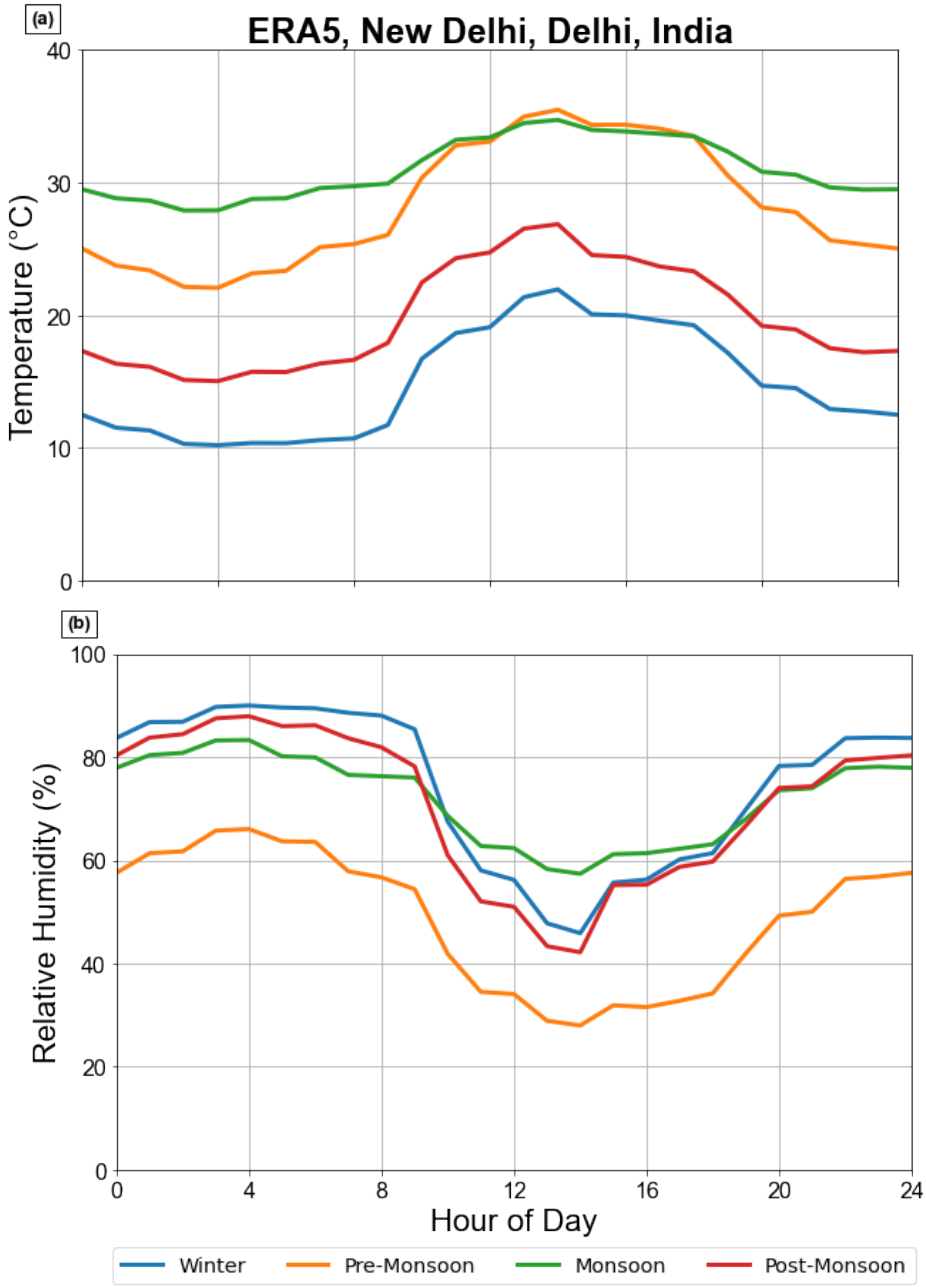


Figure A.4: Panel (a) shows mean diurnal profiles of relative humidity by season with the ERA5 pixel containing the Delhi collocation site. Panel (b) shows mean diurnal profiles of temperature by season with the ERA5 pixel containing the Delhi collocation site.

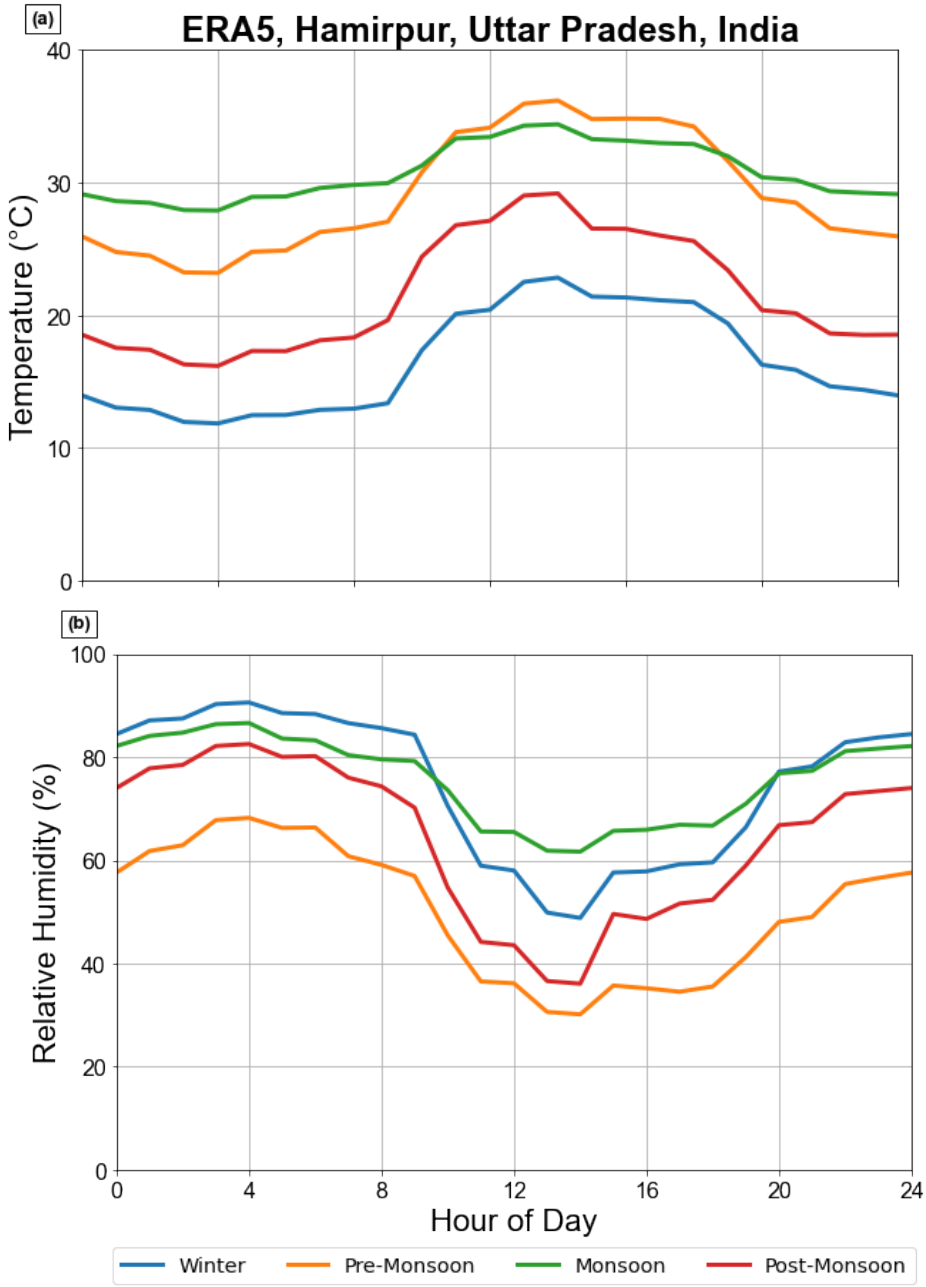


Figure A.5: Panel (a) shows mean diurnal profiles of relative humidity by season with the ERA5 pixel containing the Hamirpur collocation site. Panel (b) shows mean diurnal profiles of temperature by season with the ERA5 pixel containing the Hamirpur collocation site.

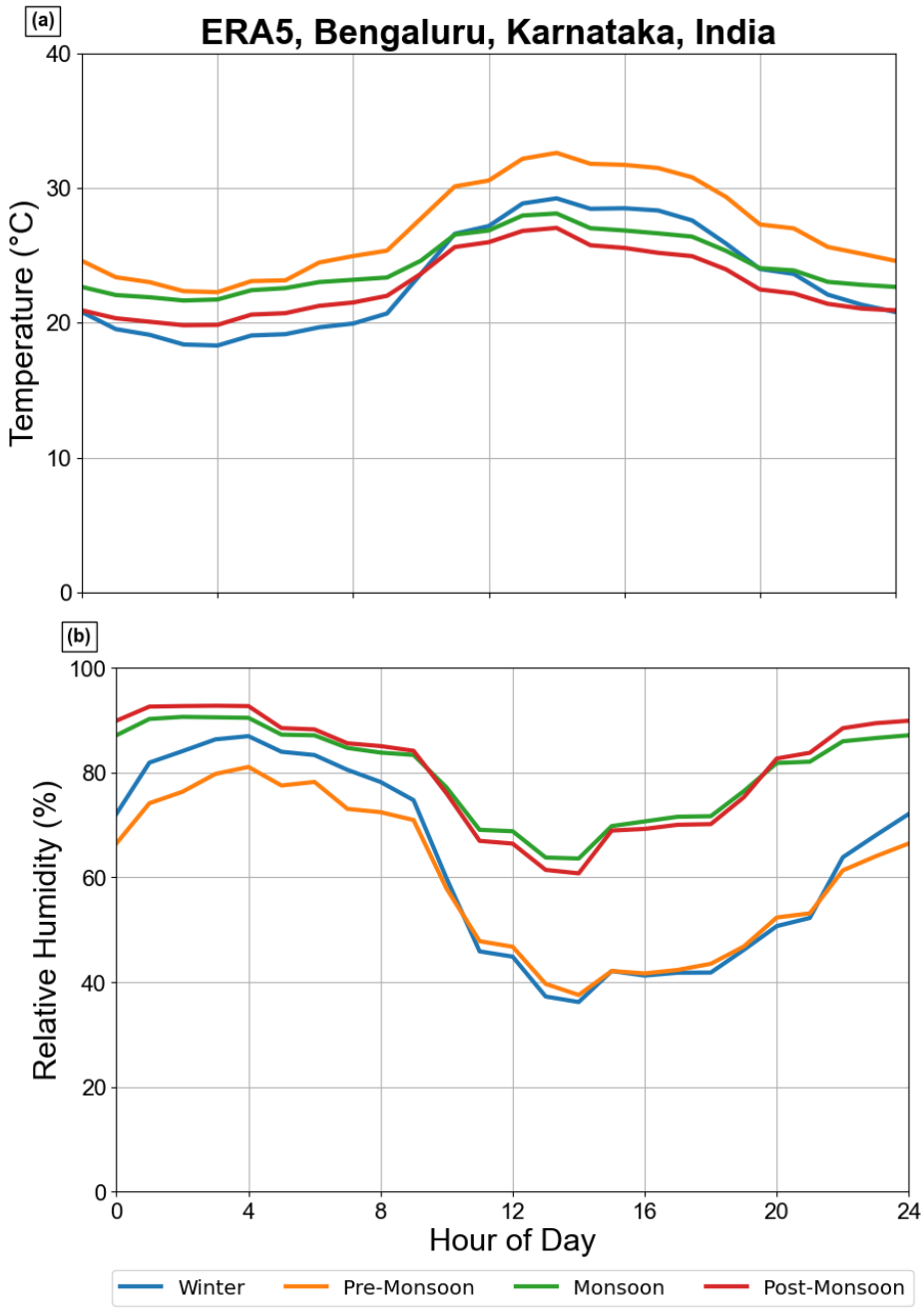


Figure A.6: Panel (a) shows mean diurnal profiles of relative humidity by season with the ERA5 pixel containing the Bengaluru collocation site. Panel (b) shows mean diurnal profiles of temperature by season with the ERA5 pixel containing the Bengaluru collocation site.

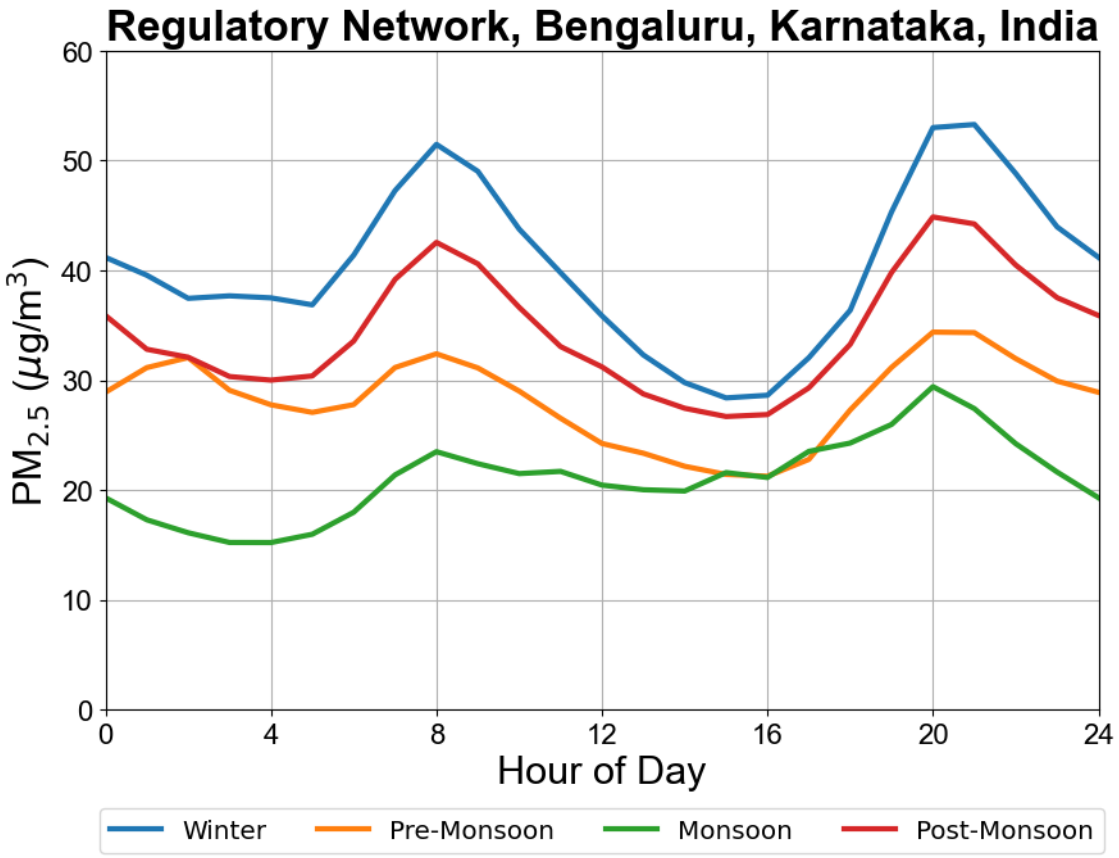


Figure A.7: Mean diurnal profiles of $PM_{2.5}$ by season averaged across all reference sites in Bengaluru. Mean concentrations are highest in the post-monsoon and winter, with strong morning and evening peaks. The monsoon period features the lowest mass as well as much less dynamic range due to the rains and ventilation conditions during the monsoon season.

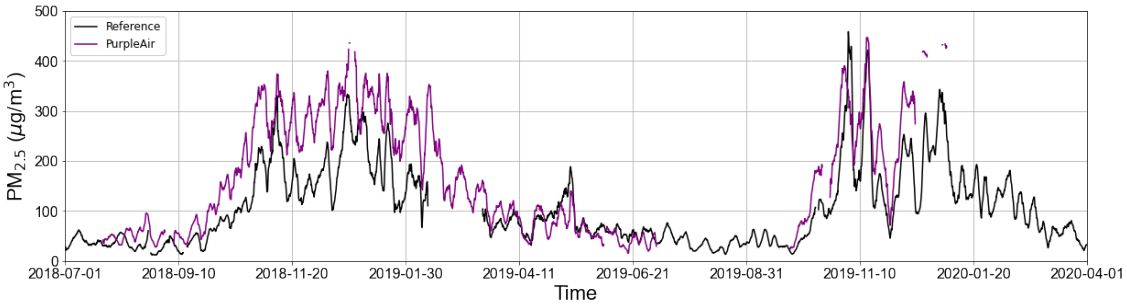


Figure A.8: Time series of Delhi PurpleAir (CF1) and reference (BAM-1020) signal throughout the 21-month collocation period with 72-hour rolling mean smoothing. Gaps indicate insufficient data.

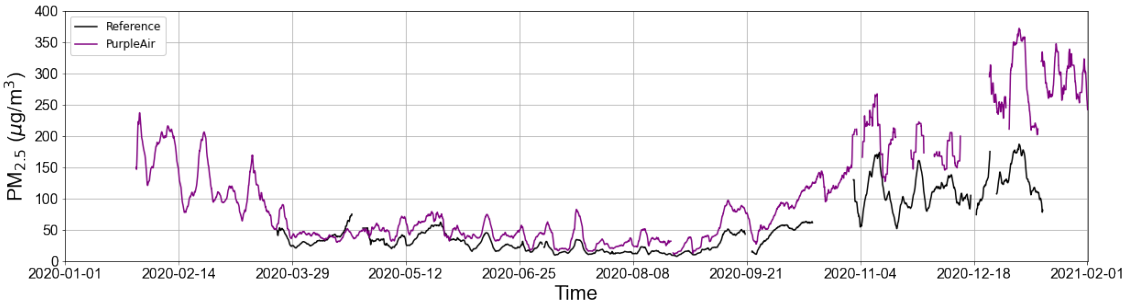


Figure A.9: Time series of Hamirpur PurpleAir (CF1) and reference (BAM-1022) signal throughout the collocation period with 72-hour rolling mean smoothing. Gaps indicate insufficient data.

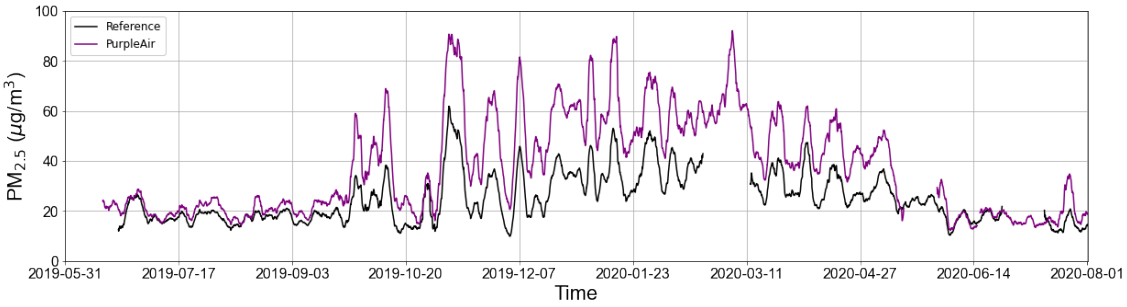


Figure A.10: Time series of Bengaluru PurpleAir (CF1) and reference (BAM-1022) signal throughout the collocation period with 72-hour rolling mean smoothing. Gaps indicate insufficient data.

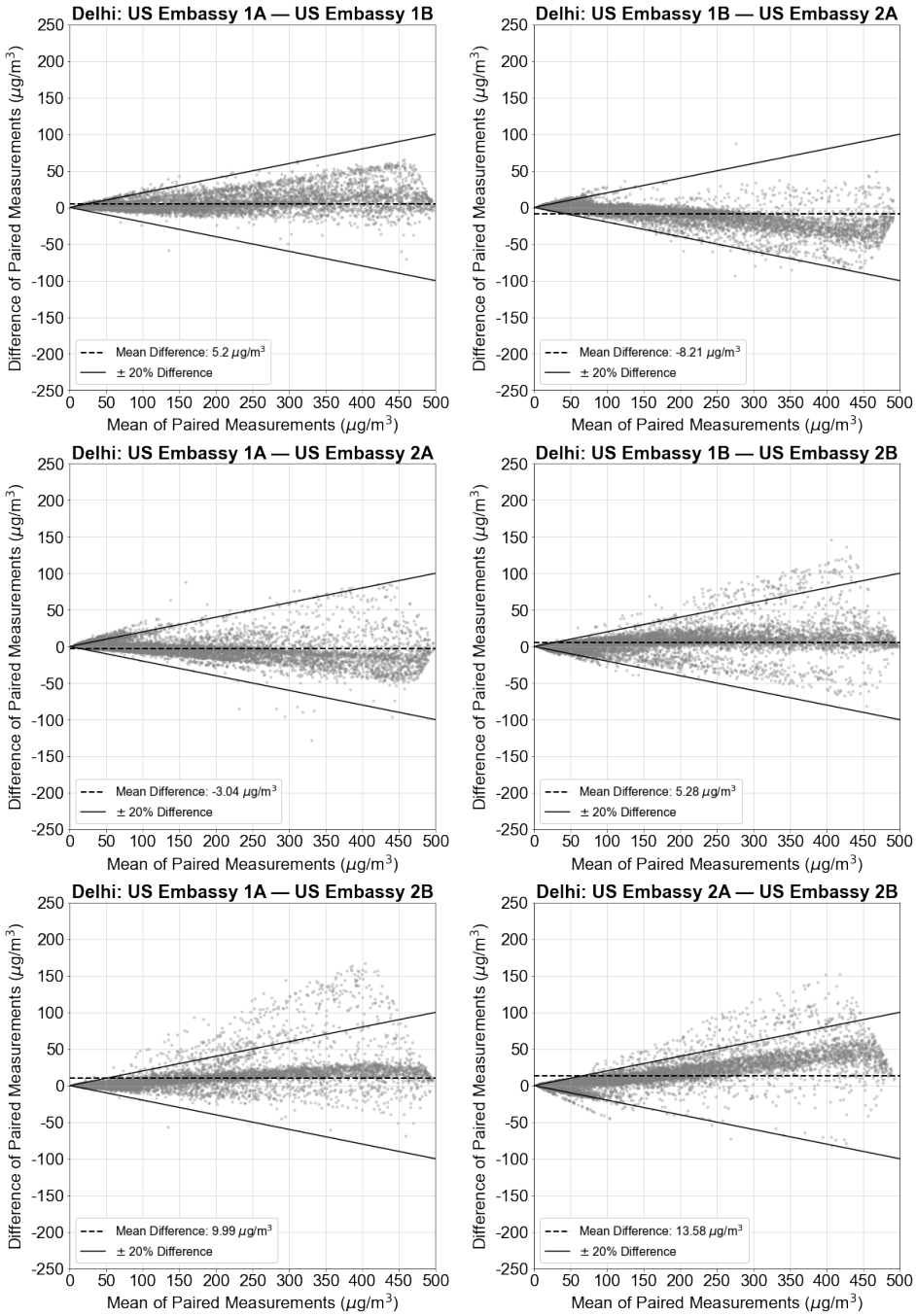


Figure A.11: Bland-Altman plots for PA at the Delhi collocation site, the US Embassy, indicating the structure of pairwise differences in four individual Plantower channels from two PurpleAir sensors as function of concentration. The bulk of hourly scatter points are within 20% difference.

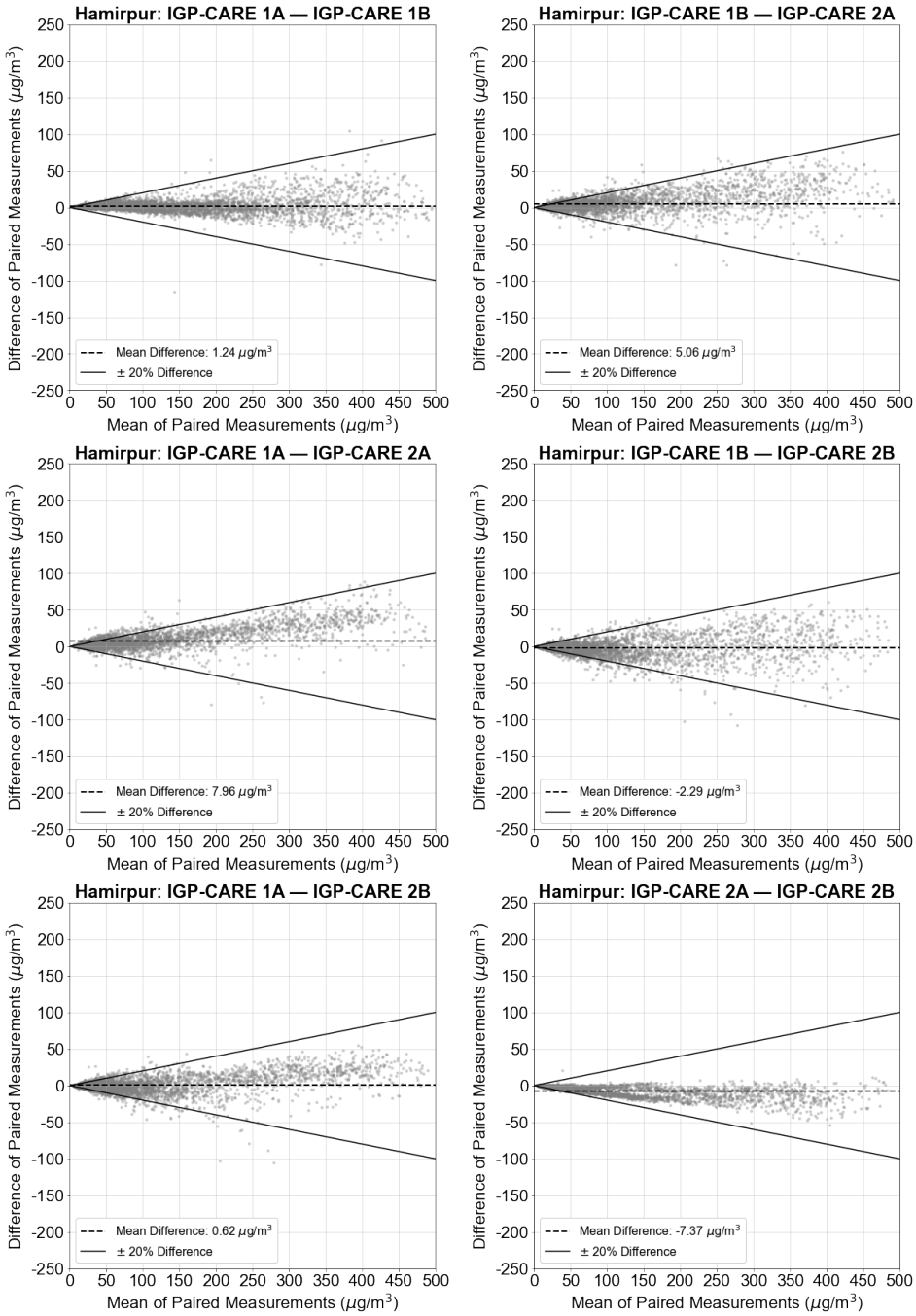


Figure A.12: Bland-Altman plots for PA at the Hamirpur collocation site, IGP-CARE, indicating the structure of pairwise differences in four individual Plantower channels from two PurpleAir sensors as function of concentration. The bulk of hourly scatter points are within 20% difference.

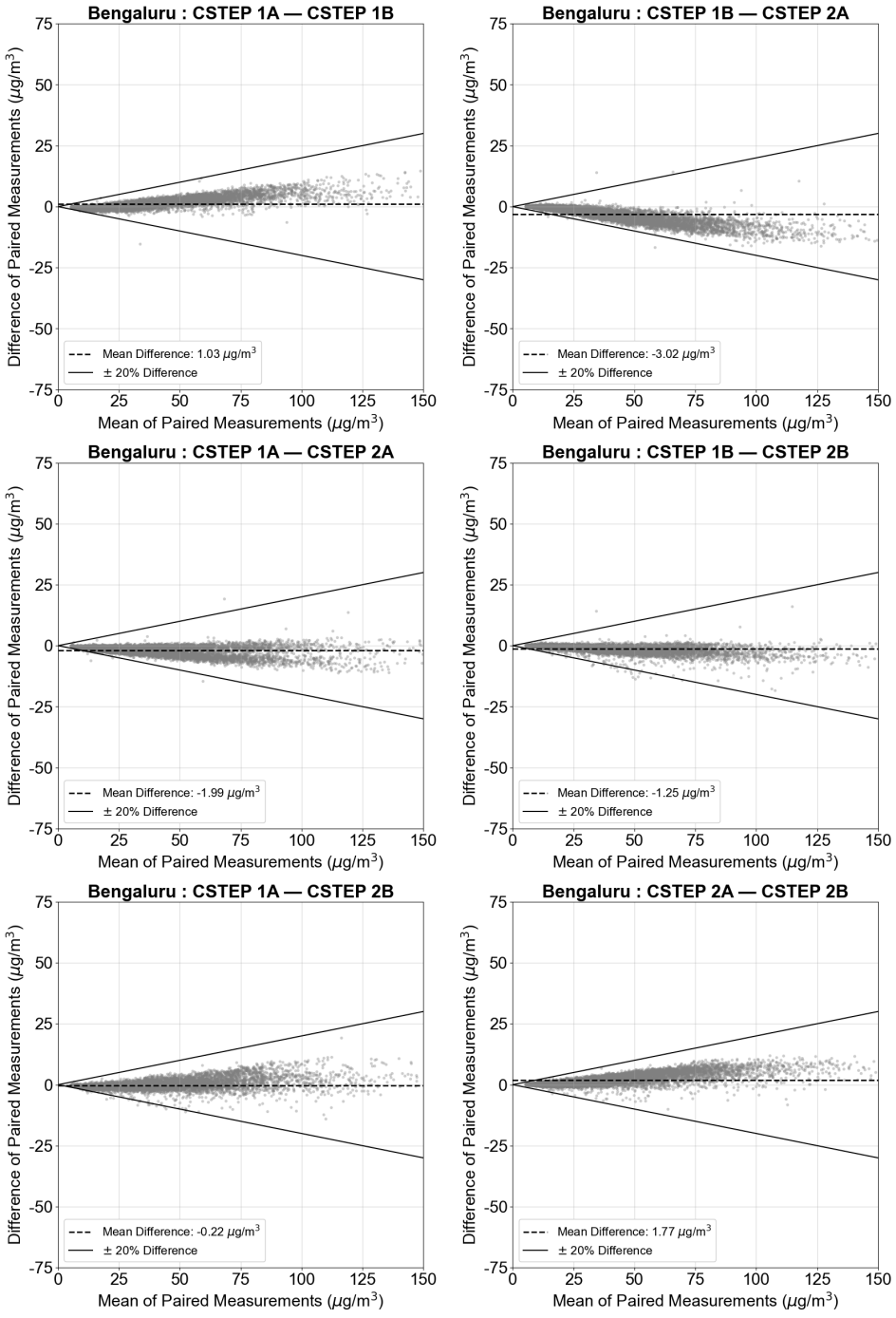


Figure A.13: Bland-Altman plots for PA at the Bengaluru collocation site, CSTEP, indicating the structure of pairwise differences in four individual Plantower channels from two PurpleAir sensors as function of concentration. The bulk of hourly scatter points are within 20% difference.

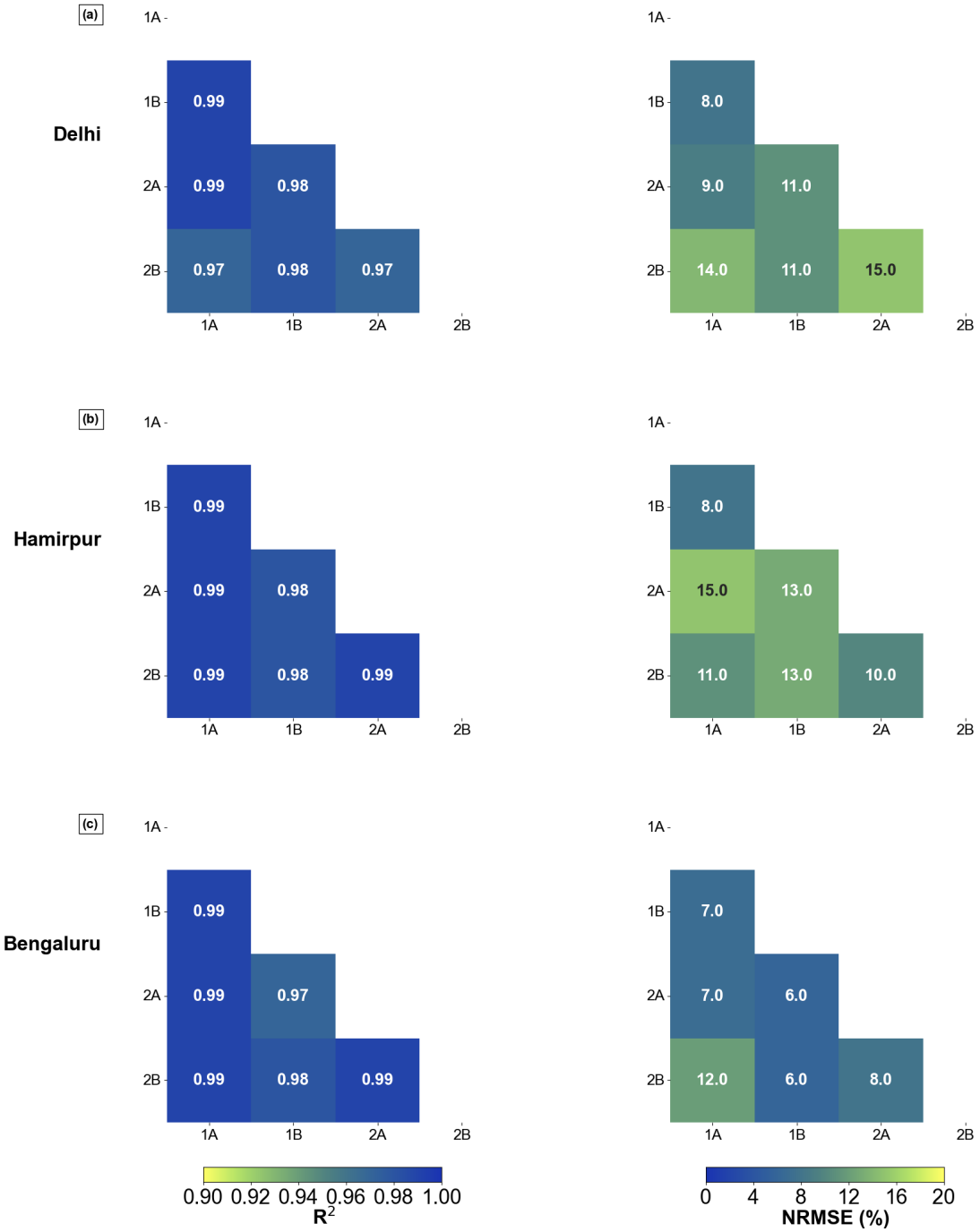


Figure A.14: Intra-Plantower R2 (left) and NRMSE (right) for the two collocated PurpleAir units in Delhi (panel[a]), Hamirpur (panel [b]), and Bengaluru (panel [c]). All units demonstrate high precision.

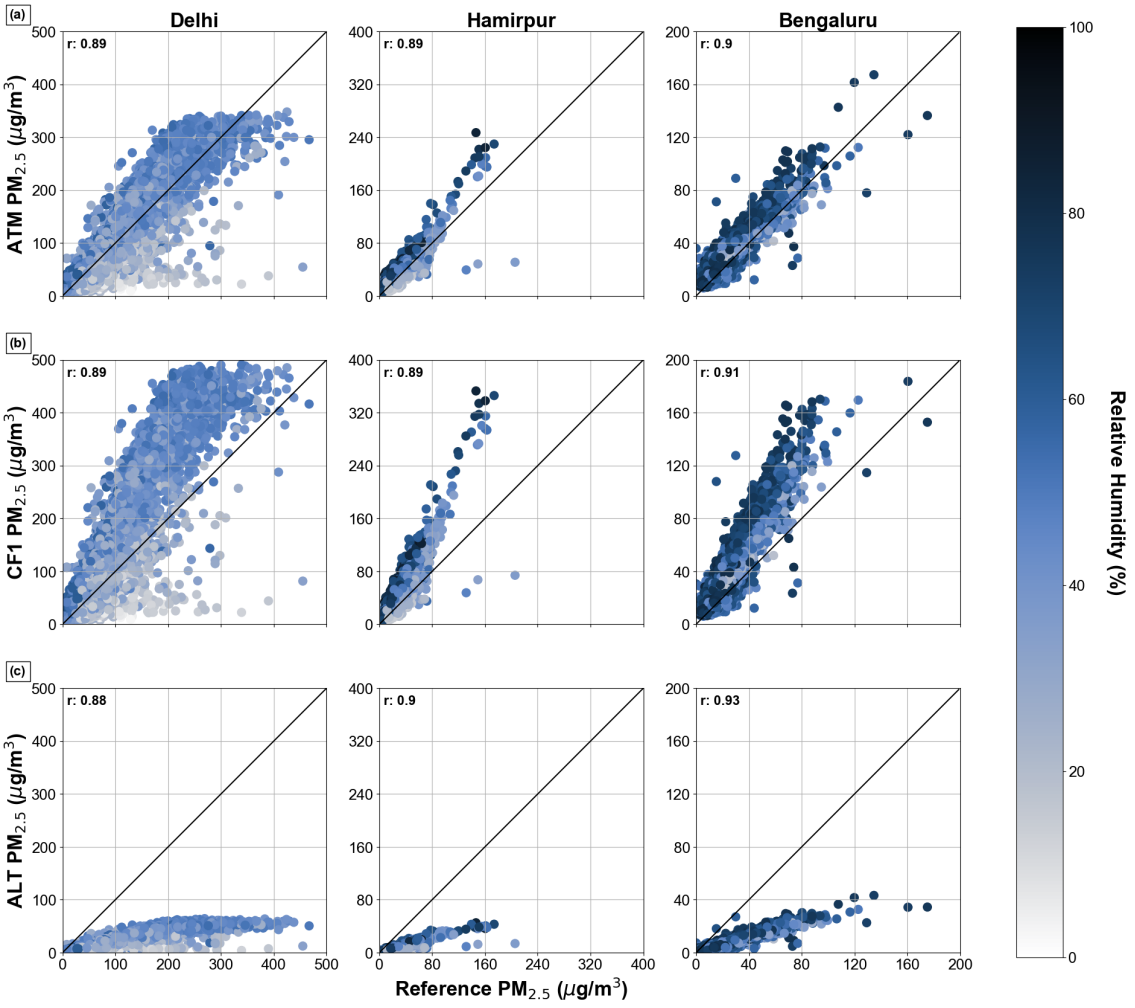


Figure A.15: Scatter plots of PurpleAir raw performance versus collocated reference signal for each hourly block average colored by PurpleAir RH and segregated by site and the three PurpleAir $PM_{2.5}$ channels ATM (panel [a]), CF1 (panel [b]), and ALT (panel [c]). Correlation coefficient (Pearson's r [r]) is presented on the top left of each subplot. Solid lines represent the 1:1 line in each subplot.

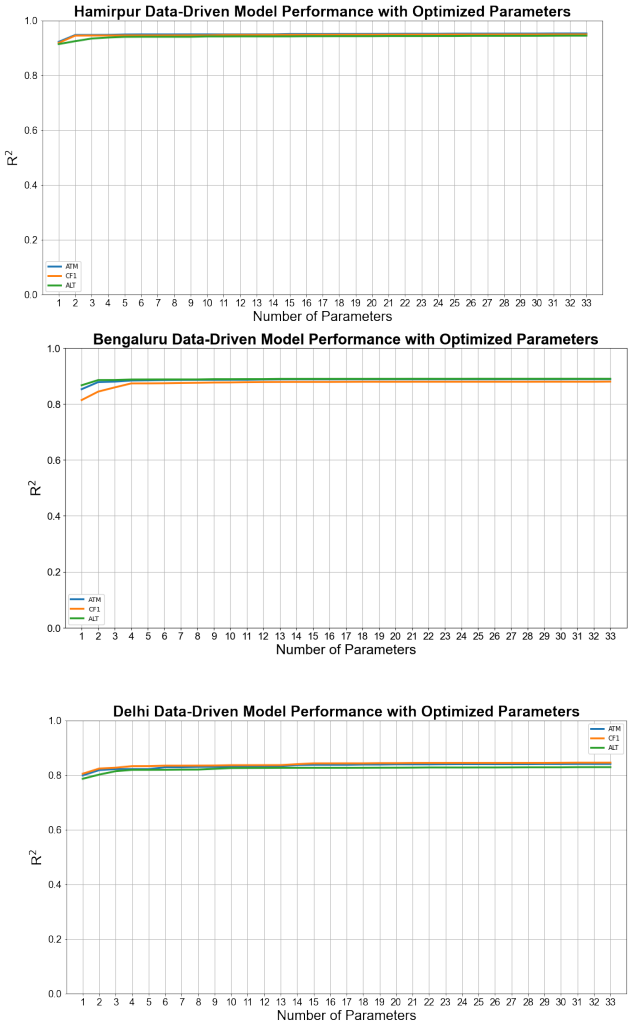


Figure A.16: Adjusted Coefficient of Determination (R2) for data-driven models for Delhi (panel [a]), Hamirpur (panel [b]), and Bengaluru (panel [c]) datasets. The number of parameters on the x-axis follows the ordering in the Tables A.1-A.3 which were chosen through the SFS procedure. Each line depicts the results using the ATM, CF1, or ALT data. For nearly all cases, more than 2 parameters results in only marginal improvement ($\Delta R^2 \approx 0.01$).

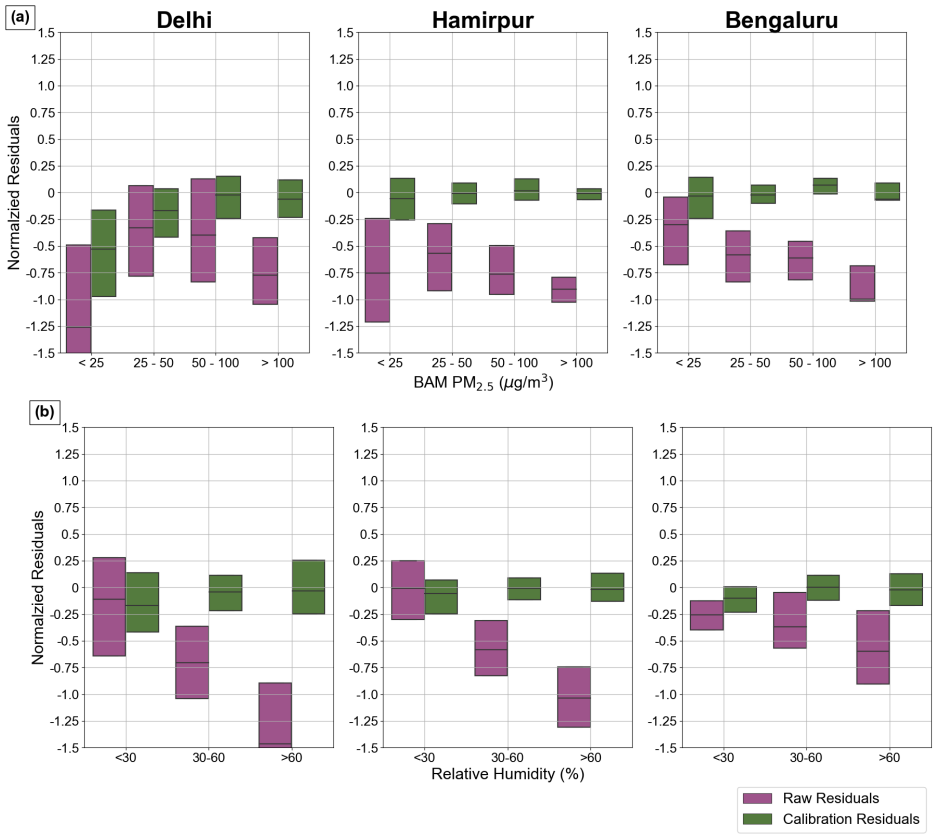


Figure A.17: Normalized Residual distributions for the raw PurpleAir data (CF1) and the calibration Models for each site. The panel (a) bins by reference $PM_{2.5}$ and panel (b) bins by PurpleAir relative humidity. The calibrated data effectively reduces bias correlated with all factors.

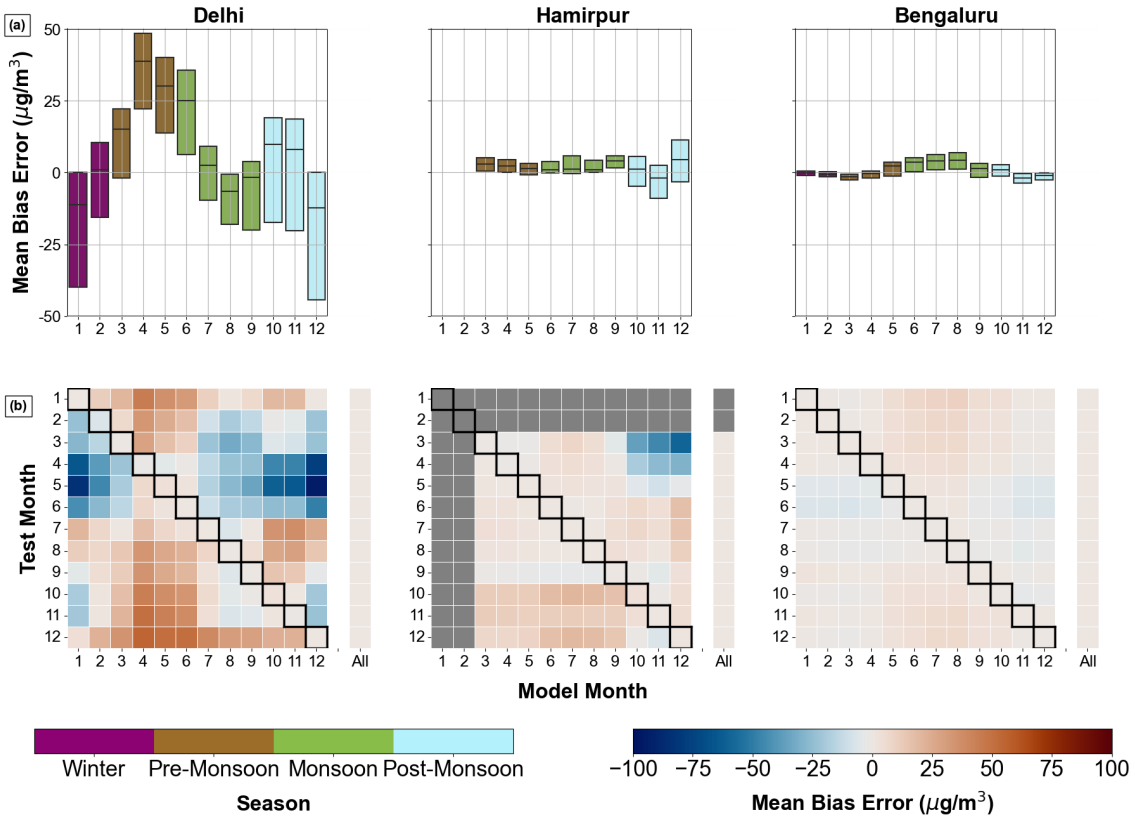


Figure A.18: Panel (a) depicts box plots of the distribution of mean bias for a given model starting month of a 4-week rolling ordinary least squares (ROLS) model on all other windows. The results of testing each window on equations 2 – 5 is denoted by "All." The bottom, solid line and top of the boxes represent the 25^{th}, 50^{th}, and 75^{th} percentiles respectively. Panel (b) presents the median mean bias of a 4-week ROLS model trained starting in the month (colored by season) on the x-axis and evaluated on all other windows as binned by starting month on the y-axis. The results of testing each window on equations 2 – 4 is denoted by "All." Gray boxes represent months without sufficient data. Models trained in the pre-monsoon (April, May) underpredicted in other seasons, contrary to the typical pattern of overprediction – with an especially strong effect in Delhi due to the higher mass concentrations relative to Bengaluru. Finally, as a point of comparison, we present the performance of our long-term calibration in individual months at each site in the column in (b) titled "All." Consistent with our observation that 4-week models trained in a single month generally do not perform as well in other months, we also note that in general, monthly models perform somewhat better for a given month than the long-term model does.

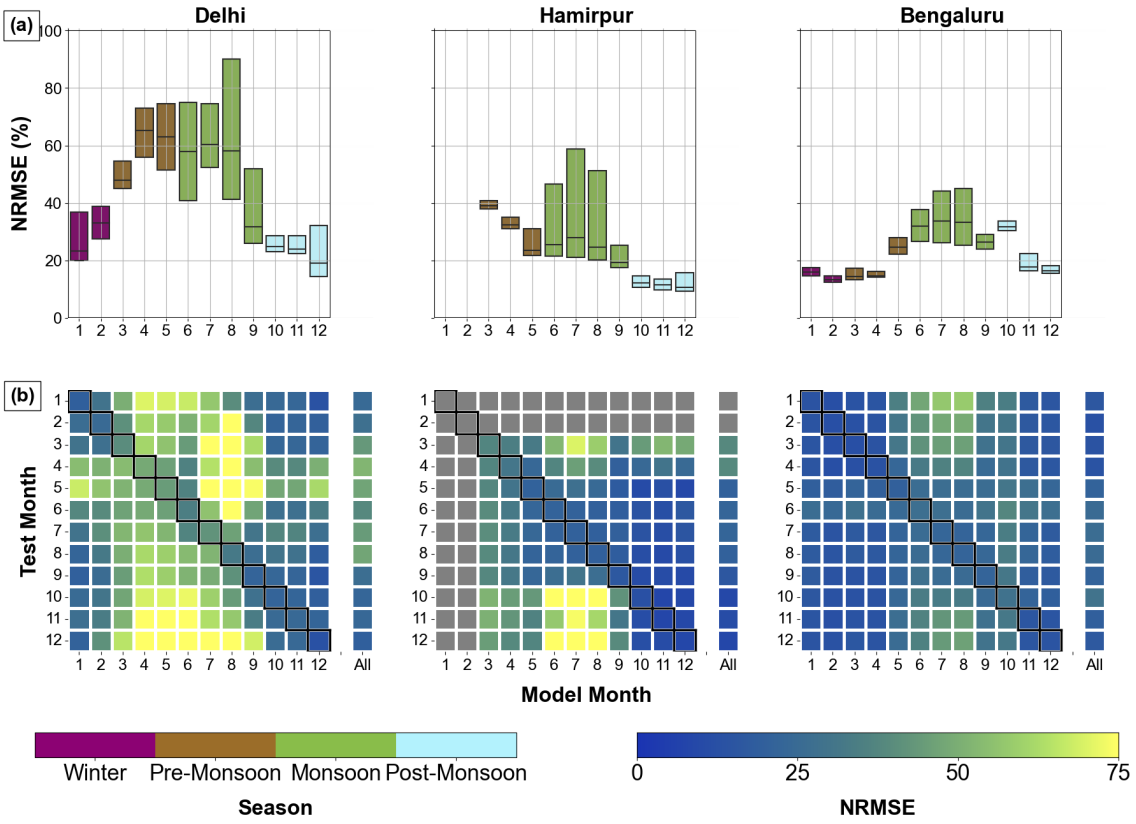


Figure A.19: Panel (a) depicts box plots of the distribution of NRMSE for a given model starting month of a 4- week ROLS model on all other windows. The bottom, solid line and top of the boxes represent the 25^{th}, 50^{th}, and 75^{th} percentiles respectively. Panel (b) presents the median NRMSE of a 4-week rolling ordinary least squares (ROLS) model trained starting in the month (colored by season) on the x-axis and evaluated on all other windows as binned by starting month on the y-axis. Gray boxes represent months without sufficient data. The strongest performance is always within the training month (i.e., the boxed diagonal cells), followed by months within the same training season. Models perform worst within the Pre-Monsoon (April, May) and early Monsoon (June, July), regardless of training month. Finally, as a point of comparison, we present the performance of our long-term calibration in individual months at each site in the column in (b) titled "All." Consistent with our observation that 4-week models trained in a single month generally do not perform as well in other months, we also note that in general, monthly models perform somewhat better for a given month than the long-term model does.

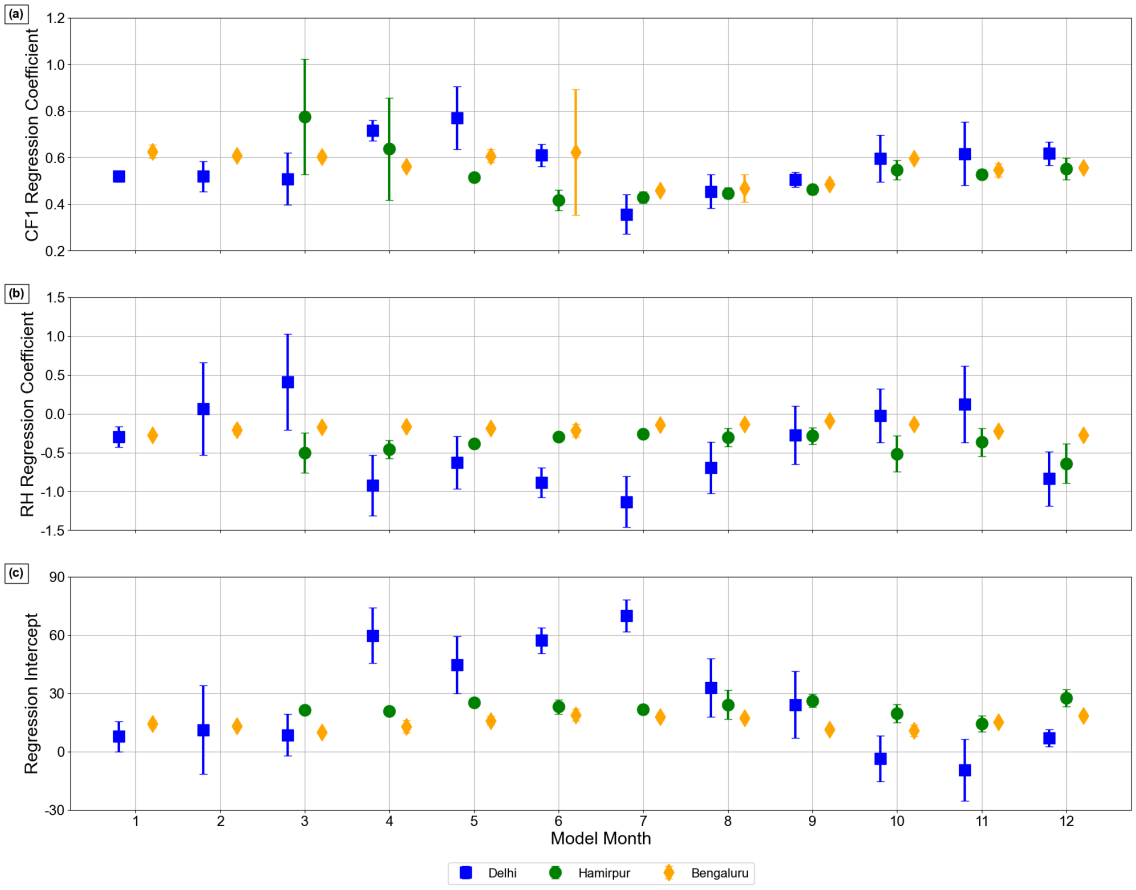


Figure A.20: Model results from 4-week rolling ordinary least squares (ROLS) exercise, with model start month on the x-axis and coefficient results on the y-axis. Panel (a), panel (b), and panel (c) show CF1 regression coefficient, RH regression coefficient, regression intercept respectively. Scatter points represent medians with upper and lower bounds defined by the interquartile range (75^{th} percentile minus 25^{th} percentile). All sites demonstrate seasonality, with lower magnitude CF1 coefficients, higher magnitude RH coefficients, and higher magnitude intercept terms during the monsoon (June-Sept). Monthly swings are especially pronounced in Delhi, where the diversity of sources, and dynamic particle size distribution leads to relatively erratic model formulation compared to the more stable Hamirpur and Bengaluru coefficient values.

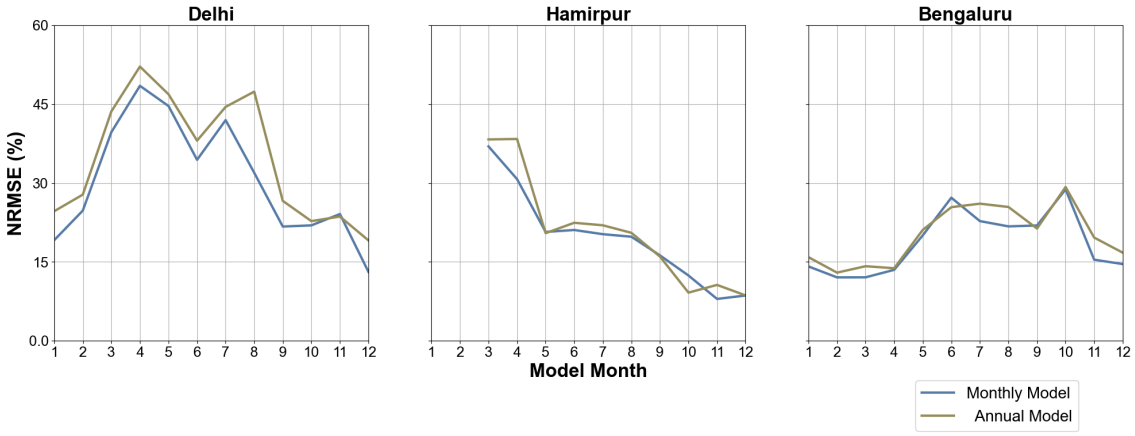


Figure A.21: Comparison of calibration model performance (NRMSE) in each month for two calibration approaches: the long-term annual model applied to a given month, as compared to a 4-week rolling ordinary least-squares (ROLS) evaluated in the month for which it is developed. The ROLS models generally have lower NRMSE annual models in any month since they are solely trained in the given month. However, annual model performance is generally within 5% of the ROLS model performance.

Appendix B

Supplementary Information: Mapping Air Pollution in Polluted Data-Sparse Environments: Resolving Spatial-Temporal $PM_{2.5}$ Trends with Low-cost Sensors in North India

B.1 Supporting Tables

Season	Intercept	PA	RH
Post-Monsoon	23.7	0.562	0.069
Winter	42.3	0.472	-0.782
Pre-Monsoon	38.7	0.764	-0.775
Monsoon	45.1	0.491	-0.570

Table B.1: Seasonal calibration coefficients derived from pooling all calibration sites and performing a regression fit. Coefficients vary from season to season, indicating the influence of shifting aerosol regimes.

Collocation Site	Intercept	PA	RH
IGPCARE	36.1	0.485	-0.487
IITD	23.7	0.722	-0.340
Mandir Marg, New Delhi - DPCC	45.9	0.756	-0.820
Najafgarh, Delhi - DPCC	23.8	0.813	-0.565
Patparganj, Delhi - DPCC	31.1	0.814	-0.539
R K Puram, Delhi - DPCC	85.6	0.785	-1.21
Sri Aurobindo Marg, Delhi - DPCC	30.2	0.606	-0.388
Vivek Vihar, Delhi - DPCC	38.1	0.783	-0.760
Wazirpur, Delhi - DPCC	25.3	0.879	-0.410
US Embassy	47.1	0.555	-0.878
Lodhi Road	49.8	0.424	-0.768

Table B.2: Site-wise calibration coefficients derived from pooling all seasons and performing a naïve Ordinary-Least Squares regression fit. Coefficients vary from site to site, but since sample size and collocation timelines do not align, the influence of seasonality is not possible to disentangle from the land-use category.

B.2 Supporting Figures

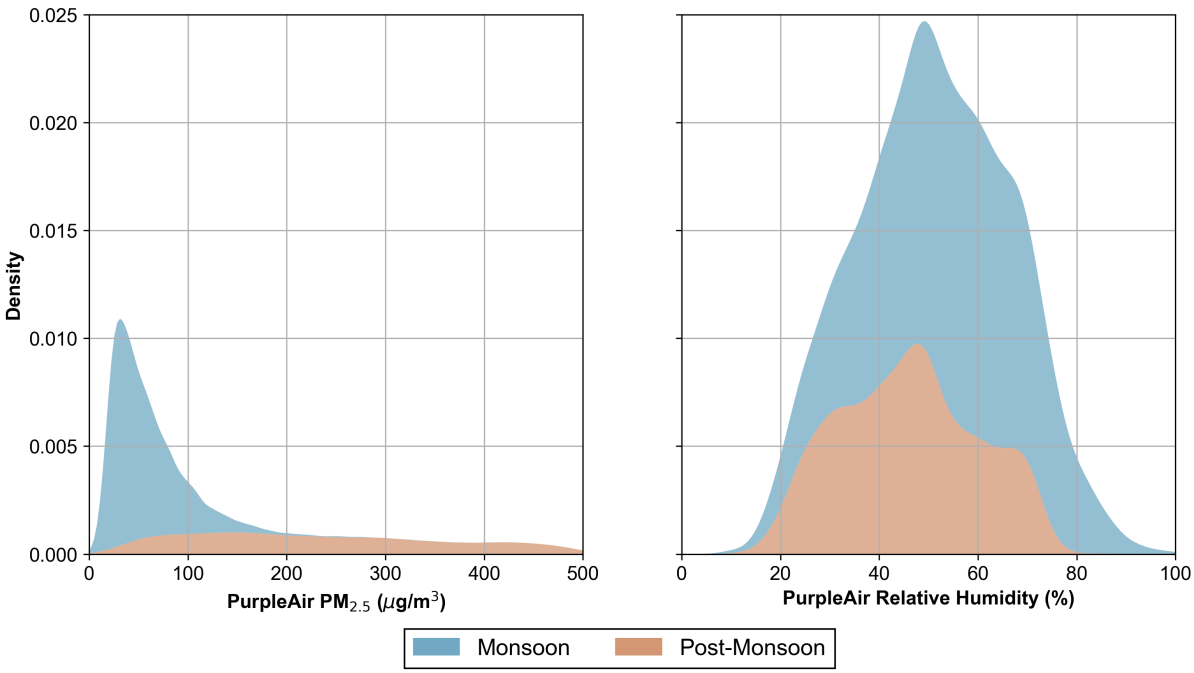


Figure B.1: Distributions of $PM_{2.5}$ (left) and RH (right) measured by LCS, and stratified by monsoon and post-monsoon. Although the seasons have very different mean conditions, the overlap in the distributions is useful for weighted domain adaptation techniques.

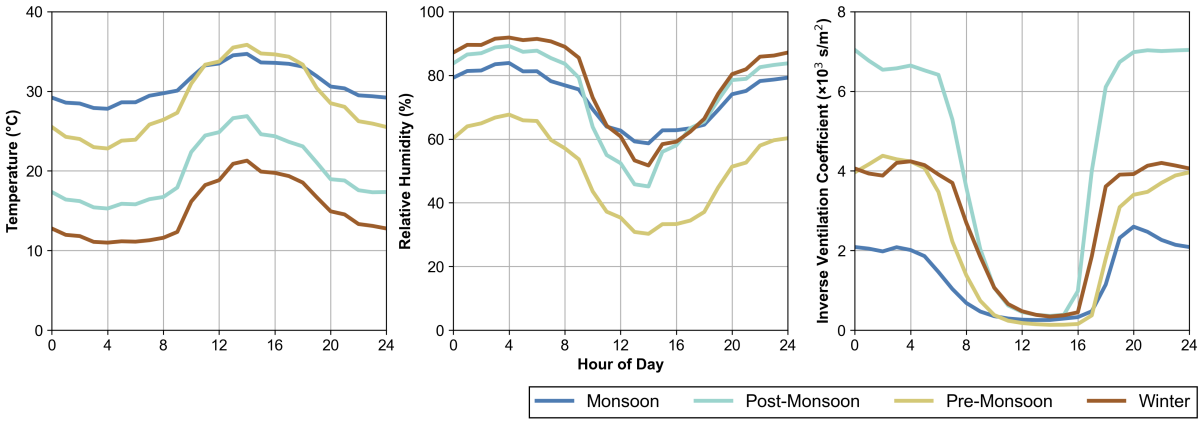


Figure B.2: Seasonal diurnal trends for temperature (left), relative humidity (center), and inverse ventilation coefficient (right; the product of boundary layer height and wind speed) in the ERA5 pixel containing the IITD collocation site.

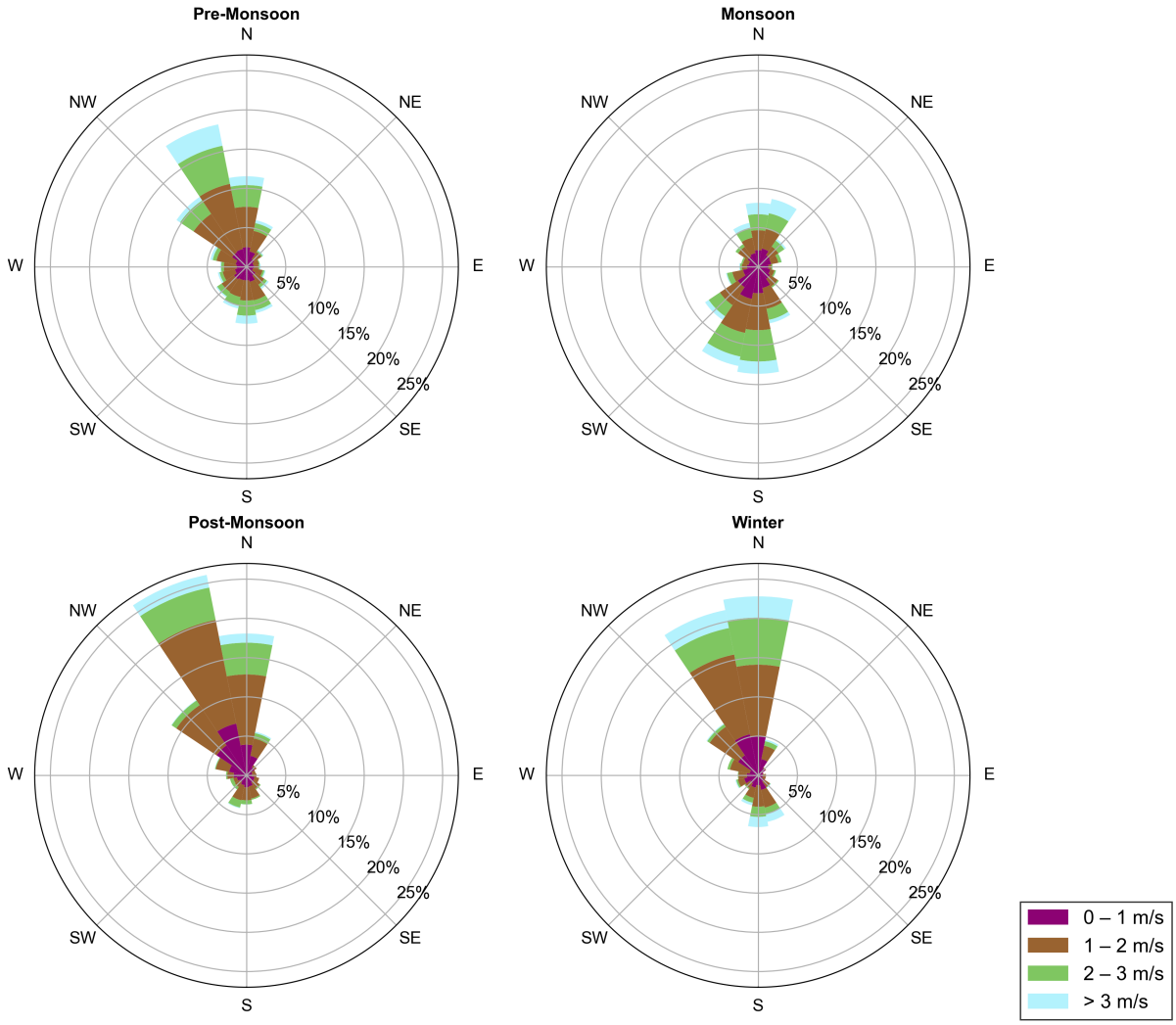


Figure B.3: Seasonal wind roses (top left: Pre-Monsoon, top right: Monsoon, bottom left: Post-Monsoon, bottom right: Winter) in the ERA5 pixel containing the IITD collocation site

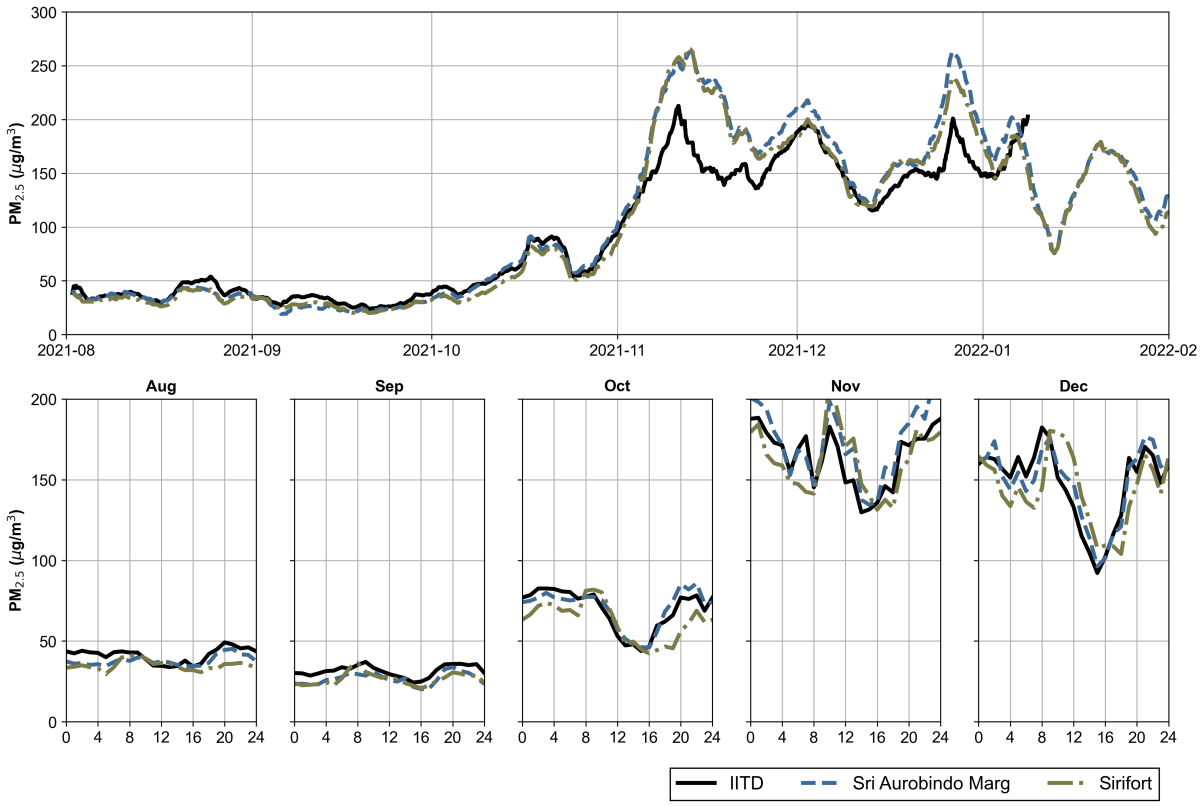


Figure B.4: Top plot shows the IITD reference instrument compared to two nearby reference monitors (Sirifort and Sri Aurobindo Marg) with 72-hour rolling mean smoothing. Gaps indicate insufficient data. Generally, the IITD reference signal is well-correlated with the nearby reference sensors, indicating robust performance. Bottom plot shows diurnal plots of IITD reference monitor and the two nearby reference monitors (Sirifort and Sri Aurobindo Marg) during the overlap period from 2021 August through 2021 December. Generally, all reference signals align, reporting both relative and absolute diurnal peaks and troughs similarly throughout the measurement period.

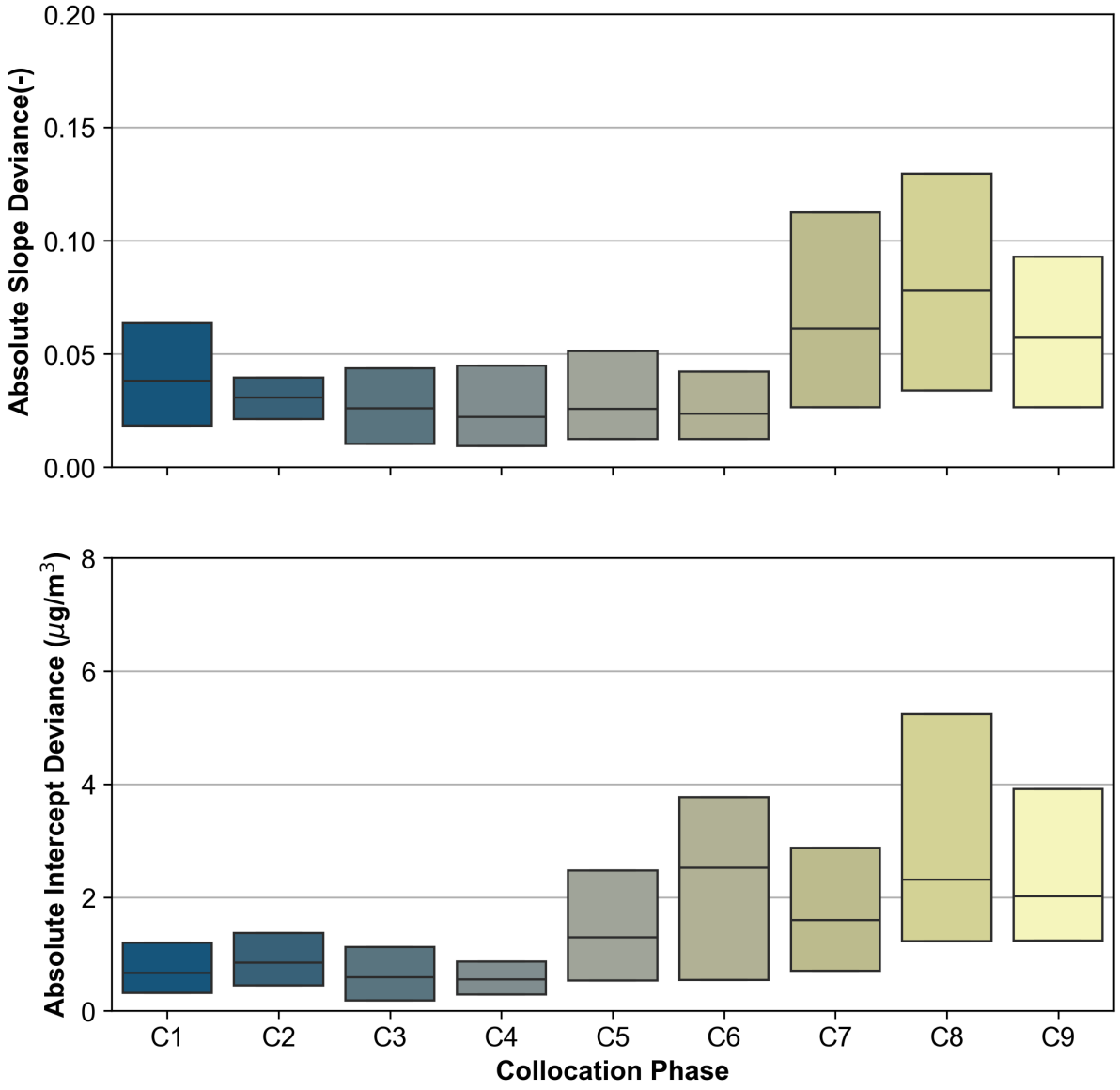


Figure B.5: Orthogonal Distance Regression (ODR) derived slope and intercept deviance values for each collocated PA-II relative to the fleet performance within a given collocation phase. Largely, slope and intercept deviance is low in the first four phases, but heterogeneity substantially increases following phase C4.

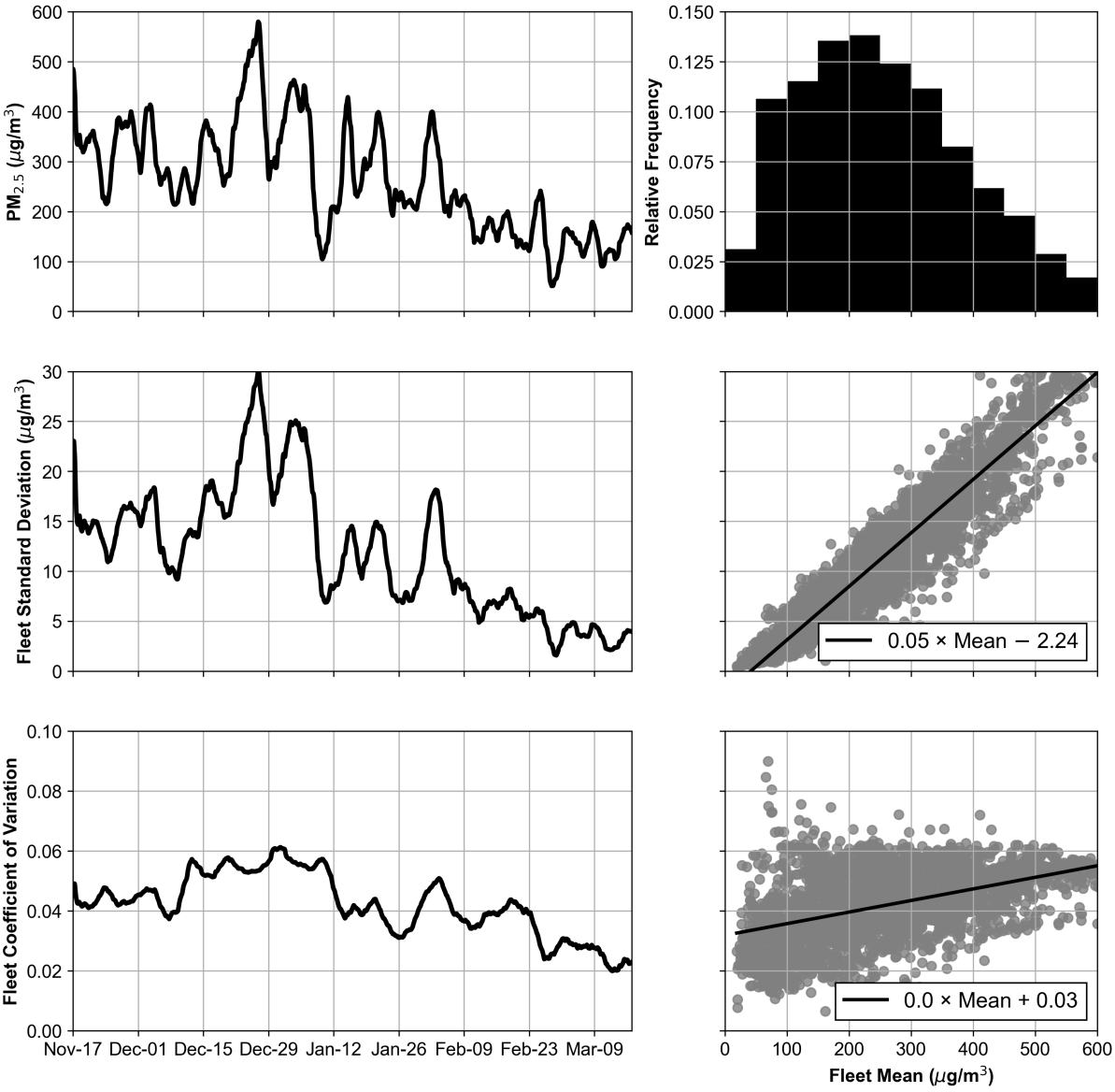


Figure B.6: Top panel shows the 168-hour rolling average time series (left) of the C1 IITD dataset aggregated fleet mean used for precision analysis, and histogram on the right. Middle panel shows the 168-hour rolling average time series (left) of the fleet standard deviation, with scatter plot of the long-term evaluation sensor hourly standard deviation versus hourly mean (right). Bottom panel shows the 168-hour rolling average time series (left) of the fleet coefficient of variation, with scatter plot of the long-term evaluation sensor hourly coefficient of variation versus hourly mean (right). The standard deviation as a measure of absolute precision shows a clear dependence on mass concentration.

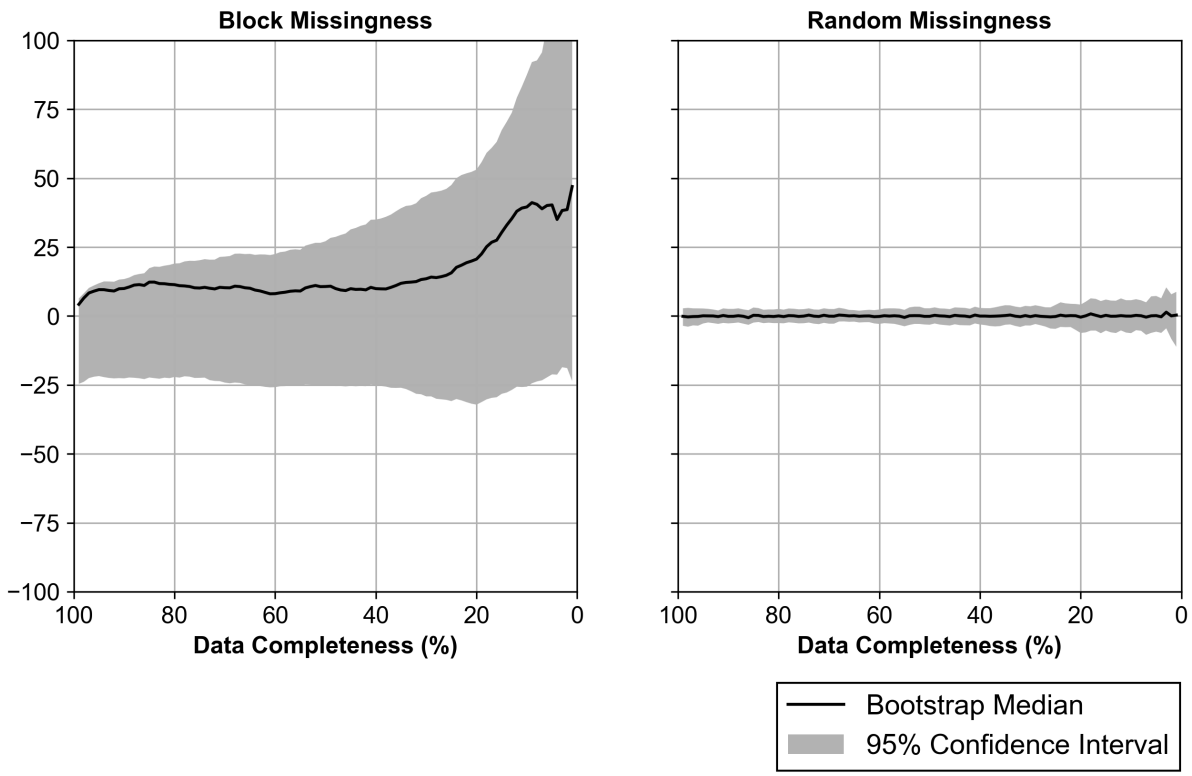


Figure B.7: Block (left) and random (right) data missingness experiments for the distribution p_{50} in the C1 phase subset. Random missingness follows expectations from the Central Limit Theorem, while block missingness lacks clear structure.

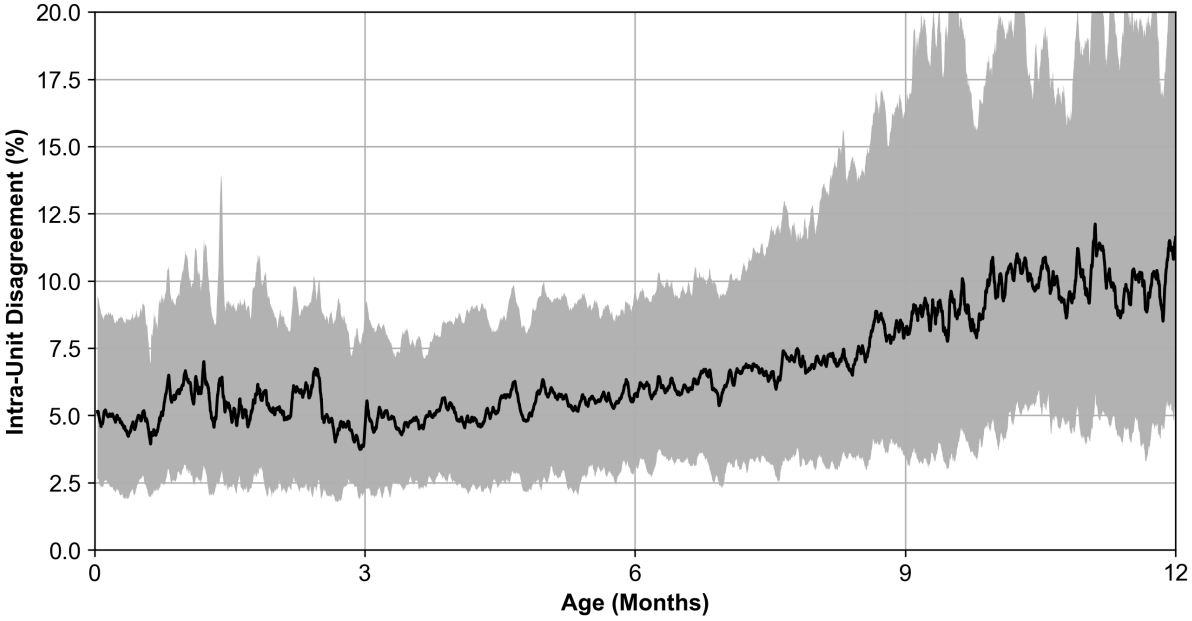


Figure B.8: Median and inter-quartile range of PA-II intra-unit disagreement as a function of sensor age across all deployed sensors (n=80 PA-II sensor packages). At the beginning of sampling, sensors feature low disagreement and increase slowly for the nine months, after which there is an abrupt increase in disagreement across the network.

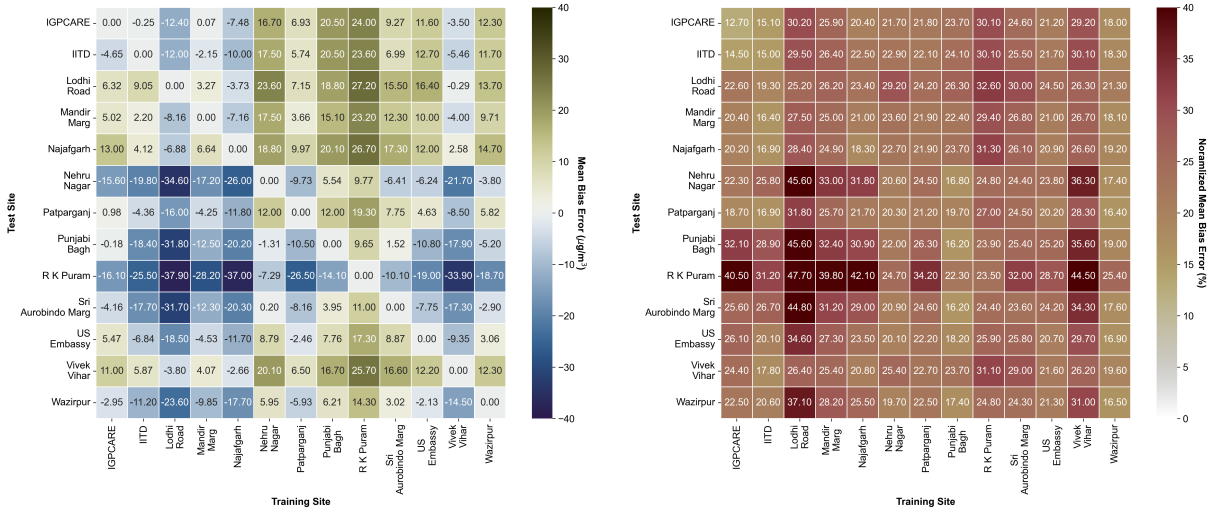


Figure B.9: Inter-site mean bias error (left) and normalized mean bias error (right) as a comparison between training a calibration regression on the site on the x-axis and applying to data on the y-axis. While within site performance is robust, few sites seem to share calibration information, with bias as high as 50%. However, deployment timelines rarely overlap exactly, so site-wise bias is likely over-represented.

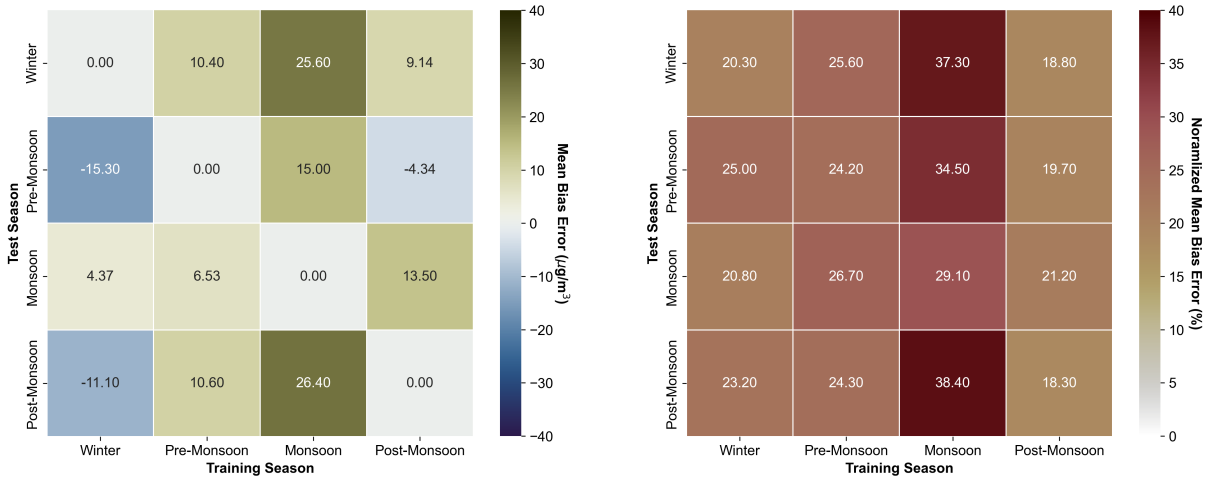


Figure B.10: Inter-season mean bias error (left) and normalized mean bias error (right) as a comparison between training a calibration regression in the season on the x-axis and applying to data on the y-axis. While within-season performance is robust, strong bias is introduced when testing on a season with differing aerosol regimes (i.e., applying a Winter model on Pre-Monsoon data. However, similar seasons cluster together, suggesting an ideal calibration would include some parameter sharing between seasons.

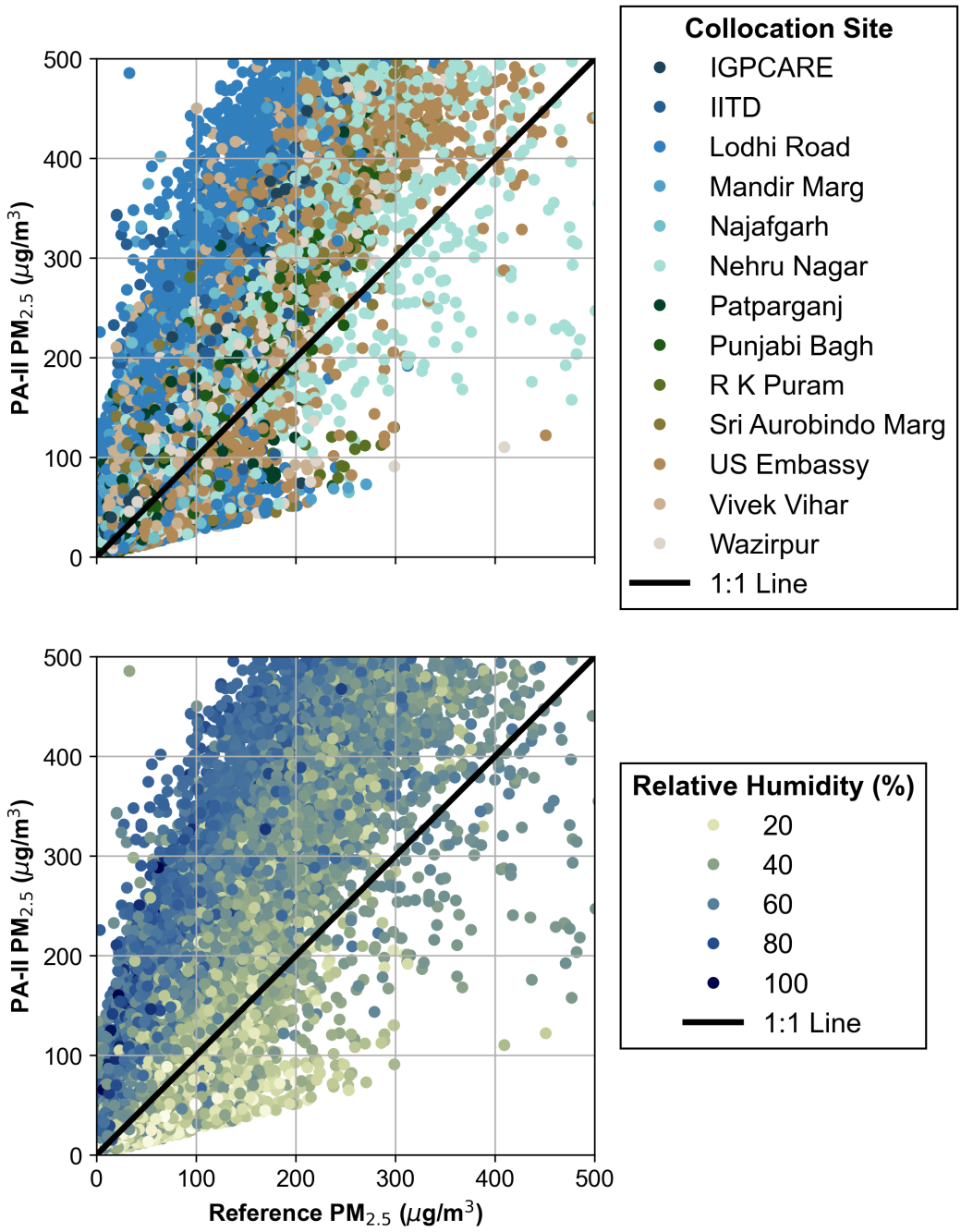


Figure B.11: Scatter plots of aggregate hourly PA-II data at each collocation site versus the reference $PM_{2.5}$ at the site binned by site (top), and RH (bottom). Clear RH dependence is shown as high humidity clusters above the 1:1 line. Generally, sites are well mixed - with short-term deployment sites clustering depending on season.

Appendix C

Supplementary Information: Rural Air Pollution Management Urgently Needed in North India

C.1 Supporting Tables

Table C.1: 10^{th}, 25^{th}, 50^{th}, 75^{th}, and 90^{th} percentiles of the 2022 annual $PM_{2.5}$ concentrations for monitored and unmonitored districts in the Indo-Gangetic Plains States using satellite-derived $PM_{2.5}$.

	p_{10} ($\mu g/m^3$)	p_{25} ($\mu g/m^3$)	p_{50} ($\mu g/m^3$)	p_{75} ($\mu g/m^3$)	p_{90} ($\mu g/m^3$)
Monitored Indo-Gangetic Plains Districts	46.7	61.3	73.1	82.8	91.3
Unmonitored Indo-Gangetic Plains Districts	44.6	52.6	71.8	82.9	87.8

Table C.2: 10^{th}, 25^{th}, 50^{th}, 75^{th}, and 90^{th} percentiles of the 2022 annual $PM_{2.5}$ concentrations for monitored and unmonitored districts in the Indo-Gangetic Plains States using satellite-derived $PM_{2.5}$, stratified by state.

Monitored	Monitored Districts						Unmonitored Districts					
	Punjab	Haryana	Delhi	Uttar Pradesh	Bihar	West Bengal	Punjab	Haryana	Delhi	Uttar Pradesh	Bihar	West Bengal
p_{10}	61.8	61.1	87.5	68.4	50.9	38.4	52.3	74.2	98.5	55.3	48.9	35.6
p_{25}	66.3	66.7	91.8	73.6	61.5	42.2	60.0	75.2	99.7	71.7	53.7	42.3
p_{50}	69.1	69.8	95.6	81.6	74.3	46.0	67.8	76.9	101.0	81.5	68.6	45.8
p_{75}	72.5	72.6	98.5	87.8	78.4	48.7	69.6	81.5	102.0	86.2	76.1	50.9
p_{90}	73.5	81.4	101.0	91.7	82.0	50.9	72.6	85.4	102.0	88.9	83.9	59.0

Table C.3: Settlement descriptions including number of LCS sites, campaign mean calibrated LCS $PM_{2.5}$, number of hourly data points, and settlement population. Note that campaign timeline is not identical for all sites.

Settlement Category	Settlement	Number of Sites	Average $PM_{2.5}$ ($\mu g/m^3$)	Number of Samples (Hours)	Population
Megacity	Kanpur	11	109.0	15767	4968745
	Lucknow	11	118.0	16073	5581546
	Varanasi	7	103.0	14968	2902577
City	Akbarpur	1	131.0	4623	56256
	Bahraich	4	98.9	15632	556963
	Hardoi	1	104.0	7647	229389
	Jaunpur	4	106.0	14354	640071
	Unnao	1	102.0	12450	440494
Non-urban	Bachhrawan	4	91.7	13701	31142
	Chandanpur	2	105.0	13139	12866
	Choubepur	1	106.0	13756	16837
	Gausganj	4	97.9	15344	1257
	Hamirpur	1	68.0	8994	2667
	Kachona Dehat	1	103.0	12865	29927
	Kerakat	3	133.0	12824	65550
	Khana Patti	3	128.0	14410	3455
	Laukahi	1	84.2	12435	7251
	Mai	4	98.6	14975	6185
	Moosanagar	6	101.0	15496	7399
	Munshiganj	2	159.0	5806	3897
	Radai	1	142.0	8922	1713
	Railway Settlement Roza Nagar	6	109.0	15636	932
	Semariya	4	97.7	14908	4373

Table C.4: Non-urban settlement type site-wise data summary, including number of samples, campaign mean LCS $PM_{2.5}$, and site land-use. Note that campaign timeline is not identical for all sites.

Settlement	Site ID	Number of Samples (Hours)	Average $PM_{2.5}$ ($\mu g/m^3$)	Land-Use Category
Bachhrawan	UP-BCN-1	15760	65.0	Residential / Transport
	UP-BCN-2	10413	65.9	Transport
	UP-BCN-3	12852	73.3	Residential / Transport
	UP-BCN-4	6502	76.5	Commercial / Residential
Chandanpur	UP-BRK-CHAN-1	14215	70.6	Open land / Residential
	UP-BRK-CHAN-2	5121	89.3	Open land / Residential
Choubepur	UP-KNP-CHO-1	15745	77.4	Residential / Transport
Gausganj	UP-KNP-GAU-1	12688	77.9	Open land / Residential
	UP-KNP-GAU-2	10812	80.3	Open land / Residential
	UP-KNP-GAU-3	12275	69.0	Residential
	UP-KNP-GAU-4	6936	65.6	Open land / Residential
Hamirpur	UP-HAMIRPUR-1	13291	61.1	Institutional / Open land
Kachona Dehat	UP-HRI-KD-1	13572	74.9	Commercial / Open land / Residential
Kerakat	UP-KCT-1	6537	104.0	Residential / Transport
	UP-KCT-2	7051	97.3	Residential
	UP-KCT-3	12197	72.2	Commercial / Residential
Khana Patti	UP-JAUN-KHANA-1	3769	103.0	Open land / Residential
	UP-JAUN-KHANA-2	14086	80.0	Open land / Residential
	UP-JAUN-KHANA-3	11931	75.1	Open land
Laukahi	UP-BRK-LAU-1	11951	68.6	Open land
Mai	UP-MAI-1	15062	75.1	Open land / Residential
	UP-MAI-2	13908	77.0	Open land / Residential / Transport
	UP-MAI-3	13111	79.0	Open land / Residential
	UP-MAI-4	13702	74.2	Open land / Residential
Moosanagar	UP-MOOSA-1	15069	53.3	Open land / Residential
	UP-MOOSA-2	10917	85.8	Open land / Residential
	UP-MOOSA-3	7847	66.7	Open land / Residential
	UP-MOOSA-4	9934	76.1	Open land / Residential
	UP-MOOSA-5	3366	68.6	Open land / Residential
	UP-MOOSA-6	4445	90.0	Open land / Residential
Munshiganj	UP-SITAPUR-MUNS-1	3441	119.0	Commercial / Residential
	UP-SITAPUR-MUNS-2	6405	83.2	Commercial / Open land / Residential
Radai	UP-RADAI-1	10472	97.8	Open land
Railway Settlement Roza Nagar	UP-ROZA-1	8570	80.4	Commercial / Residential
	UP-ROZA-2	8335	69.1	Commercial / Residential
	UP-ROZA-3	6910	87.0	Commercial / Residential
	UP-ROZA-4	11920	75.5	Industrial / Residential
	UP-ROZA-5	12705	89.3	Open land / Residential
	UP-ROZA-6	3511	77.9	Commercial / Residential
Semariya	UP-BRK-SE-1	12623	71.1	Open land / Residential
	UP-BRK-SE-2	11179	73.2	Open land / Residential
	UP-BRK-SE-3	8541	95.6	Open land / Residential
	UP-BRK-SE-4	12482	60.7	Open land / Residential

Table C.5: City settlement type site-wise data summary, including number of samples, campaign mean LCS $PM_{2.5}$, and site land-use. Note that campaign timeline is not identical for all sites.

Settlement	Site ID	Number of Samples (Hours)	Average $PM_{2.5}$ ($\mu g/m^3$)	Land-Use Category
Akbarpur	UP-KNP-AK-1	4623	131.0	Residential / Transport
Bahraich	UP-BRK-1	12514	102.0	Commercial / Residential
	UP-BRK-2	12798	92.3	Commercial / Residential / Transport
	UP-BRK-3	9914	111.0	Commercial / Residential
	UP-BRK-4	12021	90.5	Commercial / Residential
Hardoi	UP-HRI-1	7647	104.0	Commercial / Residential
Jaunpur	UP-JAUN-1	11762	118.0	Residential / Transport
	UP-JAUN-2	10510	96.5	Residential / Transport
	UP-JAUN-3	7114	103.0	Commercial / Residential
	UP-JAUN-4	11717	104.0	Residential / Transport
Unnao	UP-UNNAO-1	12450	102.0	Residential / Transport

Table C.6: Megacity settlement type site-wise data summary, including number of samples, campaign mean LCS $PM_{2.5}$, and site land-use. Note that campaign timeline is not identical for all sites.

Settlement	Site ID	Number of Samples (Hours)	Average $PM_{2.5}$ ($\mu g/m^3$)	Land-Use Category
Kanpur	UP-KNP-1	14420	87.8	Commercial / Residential / Transport
	UP-KNP-10	8419	83.9	Residential / Transport
	UP-KNP-11	3829	76.1	Commercial / Residential / Transport
	UP-KNP-2	14999	95.0	Residential / Transport
	UP-KNP-3	15086	88.8	Institutional / Transport
	UP-KNP-4	3316	181.0	Commercial / Residential / Transport
	UP-KNP-5	2155	189.0	Commercial / Residential / Transit point / Transport
	UP-KNP-6	3885	147.0	Industrial / Residential
	UP-KNP-7	5198	122.0	Commercial / Residential / Transit point / Transport
	UP-KNP-8	3939	54.4	Commercial / Residential / Transport
	UP-KNP-9	3709	69.0	Commercial / Residential
Lucknow	UP-LKO-1	15581	92.7	Commercial / Residential
	UP-LKO-10	3824	117.0	Residential / Transport
	UP-LKO-11	4812	67.9	Residential / Transport
	UP-LKO-12	2209	129.0	Commercial / Residential / Transport
	UP-LKO-2	2898	151.0	Residential / Transport
	UP-LKO-3	4703	130.0	Commercial / Residential / Transport
	UP-LKO-4	3123	169.0	Residential / Transport
	UP-LKO-5	14467	74.4	Industrial / Residential
	UP-LKO-6	4336	149.0	Commercial / Residential / Transport
	UP-LKO-7	7968	140.0	Commercial / Residential / Transport
	UP-LKO-9	11814	75.6	Residential
Varanasi	UP-VRI-1	13476	101.0	Commercial / Residential / Transport
	UP-VRI-2	13029	94.8	Residential / Transport
	UP-VRI-3	8161	99.3	Residential / Transport
	UP-VRI-4	13112	102.0	Residential / Transport
	UP-VRI-5	11735	108.0	Commercial / Residential / Transport
	UP-VRI-6	3625	115.0	Residential / Transport
	UP-VRI-7	12907	100.0	Commercial / Residential / Transport

C.2 Supporting Figures

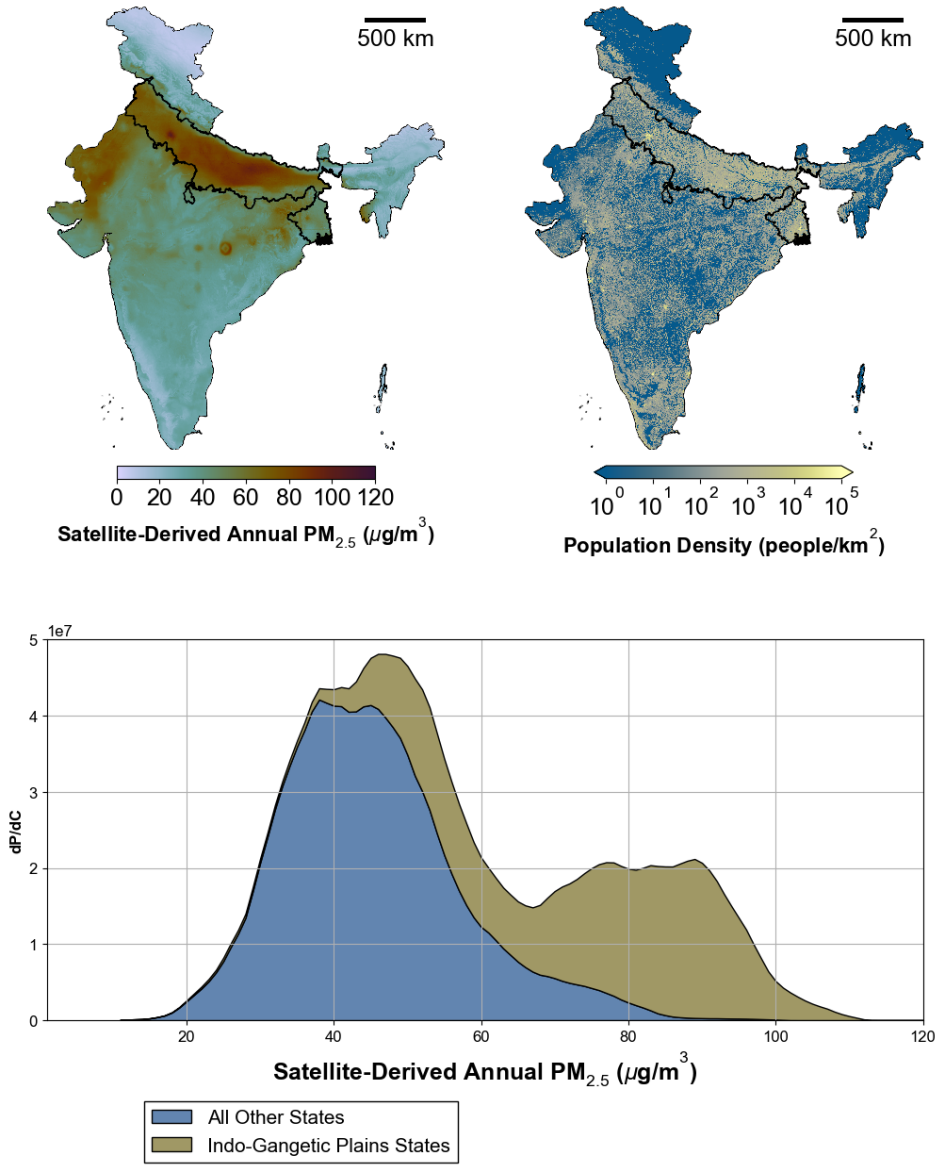


Figure C.1: Top panel shows the satellite-derived annual $PM_{2.5}$ in India for the year 2022 (right), and the population density from the Global Human Settlement Layer [114] with boundaries showing the Indo-Gangetic Plains states. The bottom panel shows the population normalized concentration for Non-Indo-Gangetic Plains and Indo-Gangetic Plains states. The extremely polluted and highly populous Indo-Gangetic Plains experience population-weighted annual exposure far higher than the rest of India.

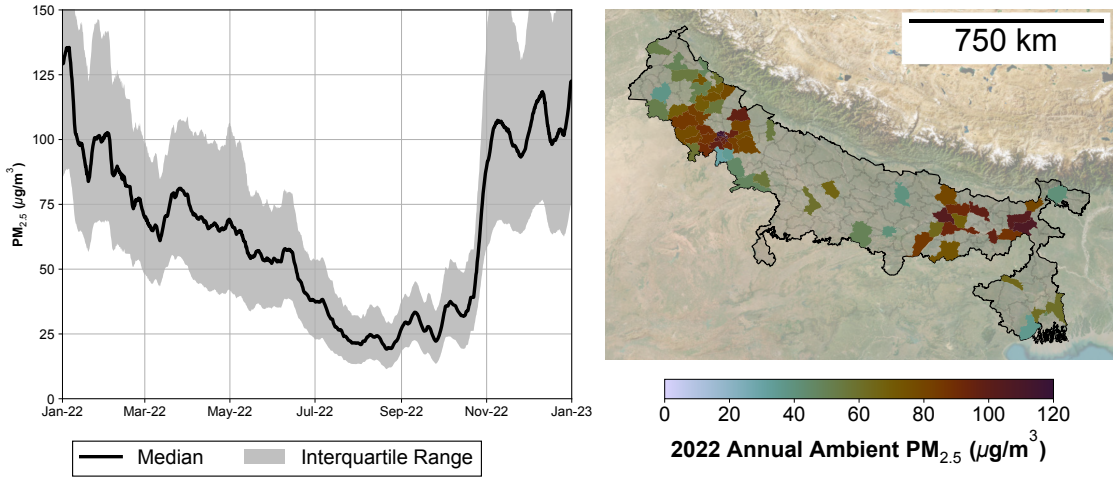


Figure C.2: Time-series (left) of aggregated $PM_{2.5}$ regulatory monitors in the Indo-Gangetic Plains states in North India. Map (right) of the annual average trend of the regulatory monitors in the time series plot aggregated by district. Uncolored districts are unmonitored. Most districts are unmonitored but monitored districts show extreme mass concentrations in the post-monsoon and winter.

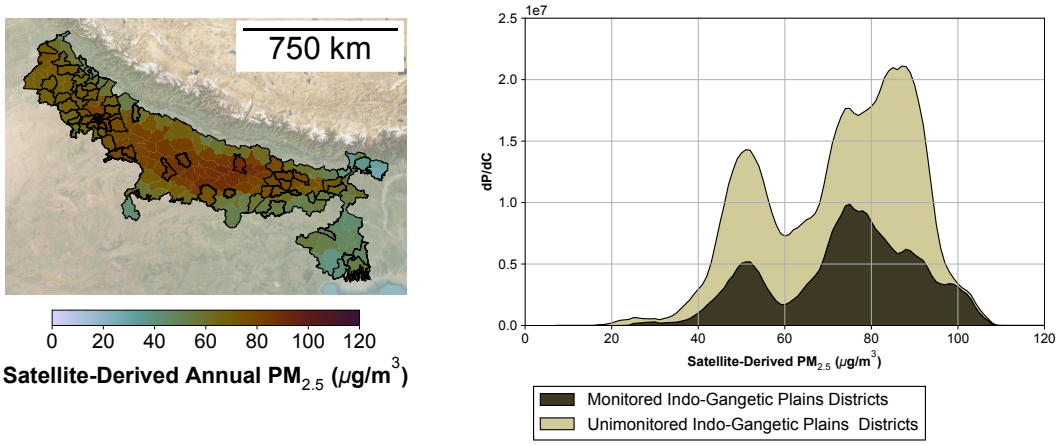


Figure C.3: Map (left) of both monitored (bold) and unmonitored district 2022 annual average $PM_{2.5}$ from satellite-derived products. Population normalized plot (right) of monitored and unmonitored districts in the Indo-Gangetic Plains states. Unmonitored districts have a higher population normalized concentration distribution than the monitored districts.

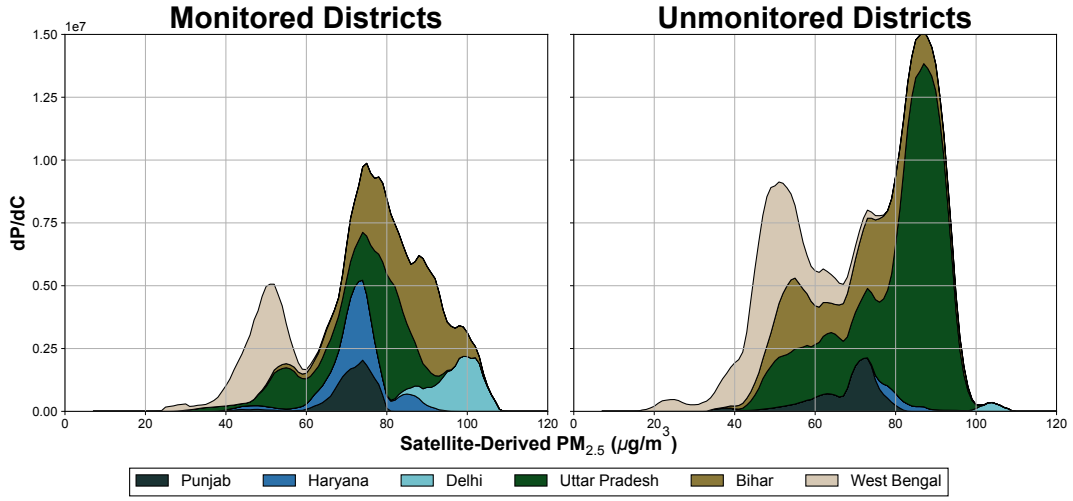


Figure C.4: Indo-Gangetic Plains states population normalized concentration distributions stratified by states, and monitored (left) and unmonitored (right) districts. Most of the population does not live in districts with reference monitors. Furthermore, the population-normalized concentration is larger in unmonitored districts, especially in Uttar Pradesh.

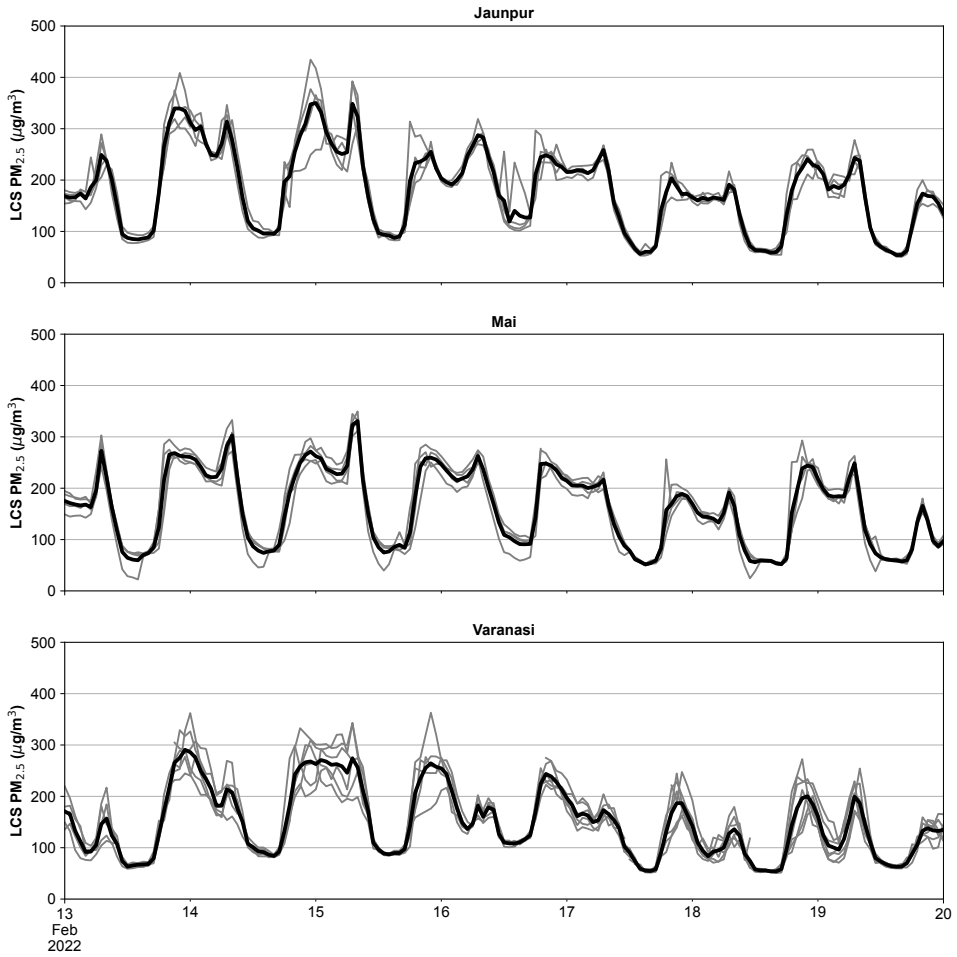


Figure C.5: Time series of the distribution of sensors in each of the settlements (Jaunpur [city], Mai [non-urban], and Varanasi [megacity]) used for the winter episodic analysis in Fig. 4.5. Individual sensors are shown in light gray, and the settlement average is shown in black. Generally, there is high correlation within each settlement, with more pronounced heterogeneity in the megacity, Varanasi.

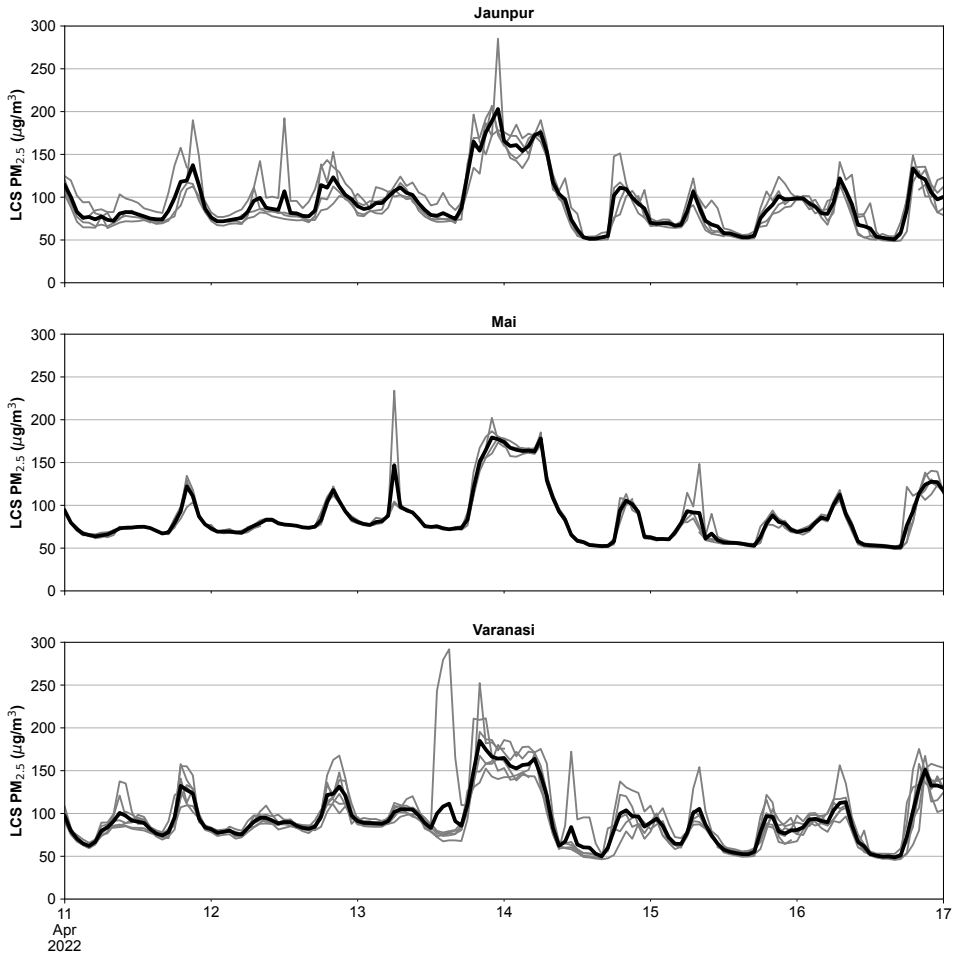


Figure C.6: Time series of the distribution of sensors in each of the settlements (Jaunpur [city], Mai [non-urban], and Varanasi [megacity]) used for the pre-monsoon episodic analysis in Fig. 4.5. Individual sensors are shown in light gray, and the settlement average is shown in black. Generally, there is high correlation within each settlement, with more pronounced heterogeneity in the megacity, Varanasi.

Bibliography

[1] Oriol Abril-Pla et al. "PyMC: a modern, and comprehensive probabilistic programming framework in Python". en. In: *PeerJ Computer Science* 9 (Sept. 2023). Publisher: PeerJ Inc., e1516. DOI: 10.7717/peerj-cs.1516.

[2] Faraz Enayati Ahangar, Frank R. Freedman, and Akula Venkatram. "Using Low-Cost Air Quality Sensor Networks to Improve the Spatial and Temporal Resolution of Concentration Maps". en. In: *International Journal of Environmental Research and Public Health* 16.7 (Jan. 2019). Number: 7 Publisher: Multidisciplinary Digital Publishing Institute, p. 1252. DOI: 10.3390/ijerph16071252.

[3] Joshua S. Apte and Pallavi Pant. "Toward cleaner air for a billion Indians". en. In: *Proceedings of the National Academy of Sciences* 116.22 (May 2019). Publisher: National Academy of Sciences Section: Commentary, pp. 10614–10616. DOI: 10.1073/pnas.1905458116.

[4] Joshua S. Apte et al. "Ambient PM2.5 Reduces Global and Regional Life Expectancy". In: *Environmental Science & Technology Letters* 5.9 (Sept. 2018), pp. 546–551. DOI: 10.1021/acs.estlett.8b00360.

[5] Joshua S. Apte et al. "Concentrations of fine, ultrafine, and black carbon particles in auto-rickshaws in New Delhi, India". en. In: *Atmospheric Environment* 45.26 (Aug. 2011), pp. 4470–4480. DOI: 10.1016/j.atmosenv.2011.05.028.

[6] Joshua S. Apte et al. "High-Resolution Air Pollution Mapping with Google Street View Cars: Exploiting Big Data". In: *Environmental Science & Technology* 51.12 (June 2017). Publisher: American Chemical Society, pp. 6999–7008. DOI: 10.1021/acs.est.7b00891.

[7] Tiago Araújo, Lígia Silva, and Adriano Moreira. "Evaluation of Low-Cost Sensors for Weather and Carbon Dioxide Monitoring in Internet of Things Context". en. In: *IoT* 1.2 (Dec. 2020). Number: 2 Publisher: Multidisciplinary Digital Publishing Institute, pp. 286–308. DOI: 10.3390/iot1020017.

[8] Zainab Arub et al. "Air mass physiochemical characteristics over New Delhi: impacts on aerosol hygroscopicity and cloud condensation nuclei (CCN) formation". English. In: *Atmospheric Chemistry and Physics* 20.11 (June 2020). Publisher: Copernicus GmbH, pp. 6953–6971. DOI: 10.5194/acp-20-6953-2020.

[9] Marek Badura et al. “Evaluation of Low-Cost Sensors for Ambient PM2.5 Monitoring”. en. In: *Journal of Sensors* 2018 (Oct. 2018). Publisher: Hindawi, e5096540. DOI: 10.1155/2018/5096540.

[10] Lu Bai et al. “Long-term Field Evaluation of Low-cost Particulate Matter Sensors in Nanjing”. en. In: *Aerosol and Air Quality Research* 20.2 (2020). Publisher: Taiwan Association for Aerosol Research, pp. 242–253. DOI: 10.4209/aaqr.2018.11.0424.

[11] Karoline K. Barkjohn, Brett Gantt, and Andrea L. Clements. “Development and application of a United States-wide correction for $PM_{2.5}$ data collected with the PurpleAir sensor”. English. In: *Atmospheric Measurement Techniques* 14.6 (June 2021). Publisher: Copernicus GmbH, pp. 4617–4637. DOI: 10.5194/amt-14-4617-2021.

[12] Karoline K. Barkjohn et al. “Correction and Accuracy of PurpleAir PM2.5 Measurements for Extreme Wildfire Smoke”. en. In: *Sensors* 22.24 (Jan. 2022). Number: 24 Publisher: Multidisciplinary Digital Publishing Institute, p. 9669. DOI: 10.3390/s22249669.

[13] F. B. Bennitt et al. “Estimating disease burden attributable to household air pollution: new methods within the Global Burden of Disease Study”. English. In: *The Lancet Global Health* 9 (Mar. 2021). Publisher: Elsevier, S18. DOI: 10.1016/S2214-109X(21)00126-1.

[14] Sahil Bhandari et al. “Contributions of primary sources to submicron organic aerosols in Delhi, India”. English. In: *Atmospheric Chemistry and Physics* 22.20 (Oct. 2022). Publisher: Copernicus GmbH, pp. 13631–13657. DOI: 10.5194/acp-22-13631-2022.

[15] Jianzhao Bi et al. “Incorporating Low-Cost Sensor Measurements into High-Resolution PM2.5 Modeling at a Large Spatial Scale”. In: *Environmental Science & Technology* 54.4 (Feb. 2020). Publisher: American Chemical Society, pp. 2152–2162. DOI: 10.1021/acs.est.9b06046.

[16] Craig F. Bohren and Donald R. Huffman. *Absorption and Scattering of Light by Small Particles*. 1st ed. John Wiley & Sons, Ltd, 1998.

[17] Michael Brauer et al. “Examination of monitoring approaches for ambient air pollution: A case study for India”. en. In: *Atmospheric Environment* 216 (Nov. 2019), p. 116940. DOI: 10.1016/j.atmosenv.2019.116940.

[18] Mark Joseph Campmier et al. “Seasonally optimized calibrations improve low-cost sensor performance: long-term field evaluation of PurpleAir sensors in urban and rural India”. English. In: *Atmospheric Measurement Techniques* 16.19 (Oct. 2023). Publisher: Copernicus GmbH, pp. 4357–4374. DOI: 10.5194/amt-16-4357-2023.

[19] Bhabesh Chakrabarti et al. “Performance evaluation of the active-flow personal Data RAM PM2.5 mass monitor (Thermo Anderson pDR-1200) designed for continuous personal exposure measurements”. en. In: *Atmospheric Environment*. Findings from EPA’s Particulate Matter Supersites Program 38.20 (June 2004), pp. 3329–3340. DOI: 10.1016/j.atmosenv.2004.03.007.

[20] Sarah E. Chambliss et al. “Comparison of Mobile and Fixed-Site Black Carbon Measurements for High-Resolution Urban Pollution Mapping”. In: *Environmental Science & Technology* 54.13 (July 2020). Publisher: American Chemical Society, pp. 7848–7857. DOI: 10.1021/acs.est.0c01409.

[21] Sarah E. Chambliss et al. “Local- and regional-scale racial and ethnic disparities in air pollution determined by long-term mobile monitoring”. en. In: *Proceedings of the National Academy of Sciences* 118.37 (Sept. 2021). Publisher: National Academy of Sciences Section: Physical Sciences. DOI: 10.1073/pnas.2109249118.

[22] Deepangsu Chatterjee et al. “Source Contributions to Fine Particulate Matter and Attributable Mortality in India and the Surrounding Region”. In: *Environmental Science & Technology* 57.28 (July 2023). Publisher: American Chemical Society, pp. 10263–10275. DOI: 10.1021/acs.est.2c07641.

[23] Ying Chen et al. “Ammonium Chloride Associated Aerosol Liquid Water Enhances Haze in Delhi, India”. In: *Environmental Science & Technology* 56.11 (June 2022). Publisher: American Chemical Society, pp. 7163–7173. DOI: 10.1021/acs.est.2c00650.

[24] Judith C Chow et al. “Designing monitoring networks to represent outdoor human exposure”. en. In: *Chemosphere* 49.9 (Dec. 2002), pp. 961–978. DOI: 10.1016/S0045-6535(02)00239-4.

[25] Aaron J. Cohen et al. “Estimates and 25-year trends of the global burden of disease attributable to ambient air pollution: an analysis of data from the Global Burden of Diseases Study 2015”. English. In: *The Lancet* 389.10082 (May 2017), pp. 1907–1918. DOI: 10.1016/S0140-6736(17)30505-6.

[26] Eric S. Coker et al. “Association between PM2.5 and respiratory hospitalization in Rio Branco, Brazil: Demonstrating the potential of low-cost air quality sensor for epidemiologic research.” In: *Environmental Research* 214 (Nov. 2022), p. 113738. DOI: 10.1016/j.envres.2022.113738.

[27] Ben Crawford et al. “Mapping pollution exposure and chemistry during an extreme air quality event (the 2018 Kīlauea eruption) using a low-cost sensor network”. In: *Proceedings of the National Academy of Sciences* 118.27 (July 2021). Publisher: Proceedings of the National Academy of Sciences, e2025540118. DOI: 10.1073/pnas.2025540118.

[28] Leigh R. Crilley et al. “Effect of aerosol composition on the performance of low-cost optical particle counter correction factors”. en. In: *Atmospheric Measurement Techniques* (Mar. 2020). Num Pages: 13 Publisher: York, pp. 1181–1193.

[29] Leigh R. Crilley et al. “Evaluation of a low-cost optical particle counter (Alphasense OPC-N2) for ambient air monitoring”. English. In: *Atmospheric Measurement Techniques* 11.2 (Feb. 2018). Publisher: Copernicus GmbH, pp. 709–720. DOI: https://doi.org/10.5194/amt-11-709-2018.

[30] Lalit Dandona et al. “Nations within a nation: variations in epidemiological transition across the states of India, 1990–2016 in the Global Burden of Disease Study”. English. In: *The Lancet* 390.10111 (Dec. 2017). Publisher: Elsevier, pp. 2437–2460. DOI: 10.1016/S0140-6736(17)32804-0.

[31] Priyanka deSouza and Patrick L. Kinney. “On the distribution of low-cost PM 2.5 sensors in the US: demographic and air quality associations”. en. In: *Journal of Exposure Science & Environmental Epidemiology* 31.3 (May 2021). Bandiera_abtest: a Cg_type: Nature Research Journals Number: 3 Primary_atype: Research Publisher: Nature Publishing Group, pp. 514–524. DOI: 10.1038/s41370-021-00328-2.

[32] Priyanka deSouza et al. “An analysis of degradation in low-cost particulate matter sensors”. en. In: *Environmental Science: Atmospheres* 3.3 (2023). Publisher: Royal Society of Chemistry, pp. 521–536. DOI: 10.1039/D2EA00142J.

[33] Sagnik Dey et al. “A Satellite-Based High-Resolution (1-km) Ambient PM2.5 Database for India over Two Decades (2000–2019): Applications for Air Quality Management”. en. In: *Remote Sensing* 12.23 (Jan. 2020). Number: 23 Publisher: Multidisciplinary Digital Publishing Institute, p. 3872. DOI: 10.3390/rs12233872.

[34] Vishal R. Dharaiya et al. “Evaluating the Performance of Low-cost PM Sensors over Multiple COALESCE Network Sites”. en. In: *Aerosol and Air Quality Research* 23.5 (2023). Publisher: Taiwan Association for Aerosol Research, p. 220390. DOI: 10.4209/aaqr.220390.

[35] Aaron van Donkelaar et al. “Monthly Global Estimates of Fine Particulate Matter and Their Uncertainty”. In: *Environmental Science & Technology* 55.22 (Nov. 2021). Publisher: American Chemical Society, pp. 15287–15300. DOI: 10.1021/acs.est.1c05309.

[36] Aditya Kumar Dubey et al. “Understanding the hot season dynamics and variability across India”. en. In: *Weather and Climate Extremes* 32 (June 2021), p. 100317. DOI: 10.1016/j.wace.2021.100317.

[37] U. C. Dumka et al. “Year-long variability of the fossil fuel and wood burning black carbon components at a rural site in southern Delhi outskirts”. en. In: *Atmospheric Research* 216 (Feb. 2019), pp. 11–25. DOI: 10.1016/j.atmosres.2018.09.016.

[38] F. J. Ferri et al. “Comparative study of techniques for large-scale feature selection* *This work was suported by a SERC grant GR/E 97549. The first author was also supported by a FPI grant from the Spanish MEC, PF92 73546684”. en. In: *Machine Intelligence and Pattern Recognition*. Ed. by Edzard S. Gelsema and Laveen S. Kanal. Vol. 16. Pattern Recognition in Practice IV. North-Holland, Jan. 1994, pp. 403–413. DOI: 10.1016/B978-0-444-81892-8.50040-7.

[39] Hans Fischer. *A History of the Central Limit Theorem: From Classical to Modern Probability Theory*. en. New York, NY: Springer New York, 2011. DOI: 10.1007/978-0-387-87857-7.

[40] Tanushree Ganguly, Kurinji L. Selvaraj, and Sarath K. Guttikunda. "National Clean Air Programme (NCAP) for Indian cities: Review and outlook of clean air action plans". en. In: *Atmospheric Environment: X* 8 (Dec. 2020), p. 100096. DOI: 10.1016/j.aeaoa.2020.100096.

[41] Shahzad Gani et al. "Particle number concentrations and size distribution in a polluted megacity: the Delhi Aerosol Supersite study". English. In: *Atmospheric Chemistry and Physics* 20.14 (July 2020). Publisher: Copernicus GmbH, pp. 8533–8549. DOI: 10.5194/acp-20-8533-2020.

[42] Shahzad Gani et al. "Submicron aerosol composition in the world's most polluted megacity: the Delhi Aerosol Supersite study". English. In: *Atmospheric Chemistry and Physics; Katlenburg-Lindau* 19.10 (2019), pp. 6843–6859. DOI: http://dx.doi.org.ezproxy.lib.utexas.edu/10.5194/acp-19-6843-2019.

[43] Shahzad Gani et al. "Systematizing the approach to air quality measurement and analysis in low and middle income countries". en. In: *Environmental Research Letters* 17.2 (Feb. 2022). Publisher: IOP Publishing, p. 021004. DOI: 10.1088/1748-9326/ac4a9e.

[44] Michael R. Giordano et al. "From low-cost sensors to high-quality data: A summary of challenges and best practices for effectively calibrating low-cost particulate matter mass sensors". In: *Journal of Aerosol Science* 158 (Nov. 2021), p. 105833. DOI: 10.1016/j.jaerosci.2021.105833.

[45] Frank T. Jr. Gucker et al. "A Photoelectronic Counter for Colloidal Particles1". In: *Journal of the American Chemical Society* 69.10 (Oct. 1947). Publisher: American Chemical Society, pp. 2422–2431. DOI: 10.1021/ja01202a053.

[46] Lovleen Gupta et al. "Assessment of PM10 and PM2.5 over Ghaziabad, an industrial city in the Indo-Gangetic Plain: spatio-temporal variability and associated health effects". en. In: *Environmental Monitoring and Assessment* 193.11 (Oct. 2021), p. 735. DOI: 10.1007/s10661-021-09411-5.

[47] Sarath Guttikunda et al. "Plugging the ambient air monitoring gaps in India's national clean air programme (NCAP) airsheds". In: *Atmospheric Environment* 301 (May 2023), p. 119712. DOI: 10.1016/j.atmosenv.2023.119712.

[48] Sarath K. Guttikunda and Bhola R. Gurjar. "Role of meteorology in seasonality of air pollution in megacity Delhi, India". en. In: *Environmental Monitoring and Assessment* 184.5 (May 2012), pp. 3199–3211. DOI: 10.1007/s10661-011-2182-8.

[49] Sarath K. Guttikunda et al. "Air quality, emissions, and source contributions analysis for the Greater Bengaluru region of India". en. In: *Atmospheric Pollution Research* 10.3 (May 2019), pp. 941–953. DOI: 10.1016/j.apr.2019.01.002.

[50] David H. Hagan and Eben S. Cross. "Introduction to the MODULAIR-PM". eng. In: (Sept. 2022). Publisher: Zenodo. DOI: 10.5281/zenodo.7062168.

[51] David H. Hagan and Jesse H. Kroll. "Assessing the accuracy of low-cost optical particle sensors using a physics-based approach". English. In: *Atmospheric Measurement Techniques* 13.11 (Nov. 2020). Publisher: Copernicus GmbH, pp. 6343–6355. DOI: https://doi.org/10.5194/amt-13-6343-2020.

[52] Gayle S. W. Hagler et al. "Air Quality Sensors and Data Adjustment Algorithms: When Is It No Longer a Measurement?" In: *Environmental Science & Technology* 52.10 (May 2018). Publisher: American Chemical Society, pp. 5530–5531. DOI: 10.1021/acs.est.8b01826.

[53] Eric Hall and Joseph Gilliam. *Reference and Equivalent Methods Used to Measure National Ambient Air Quality Standards (NAAQS) Criteria Air Pollutants - Volume I*. United States Environmental Protection Agency, June 2016. DOI: 10.13140/RG.2.1.2423.2563.

[54] Melanie S. Hammer et al. "Global Estimates and Long-Term Trends of Fine Particulate Matter Concentrations (1998–2018)". In: *Environmental Science & Technology* 54.13 (July 2020). Publisher: American Chemical Society, pp. 7879–7890. DOI: 10.1021/acs.est.0c01764.

[55] Tim Hanley. "Technical Note - PM2.5 Continuous Monitor Comparability Assessment". en. In: (2018).

[56] Meilu He, Nueraili Kuerbanjiang, and Suresh Dhaniyala. "Performance characteristics of the low-cost Plantower PMS optical sensor". In: *Aerosol Science and Technology* 54.2 (Feb. 2020), pp. 232–241. DOI: 10.1080/02786826.2019.1696015.

[57] Lucas R. F. Henneman et al. "Four Decades of United States Mobile Source Pollutants: Spatial–Temporal Trends Assessed by Ground-Based Monitors, Air Quality Models, and Satellites". In: *Environmental Science & Technology* (Jan. 2021). Publisher: American Chemical Society. DOI: 10.1021/acs.est.0c07128.

[58] Daniel A. Jaffe et al. "An evaluation of the U.S. EPA's correction equation for PurpleAir sensor data in smoke, dust, and wintertime urban pollution events". English. In: *Atmospheric Measurement Techniques* 16.5 (Mar. 2023). Publisher: Copernicus GmbH, pp. 1311–1322. DOI: 10.5194/amt-16-1311-2023.

[59] Sakshi Jain and Naomi Zimmerman. "Exploration of intra-city and inter-city PM2.5 regional calibration models to improve low-cost sensor performance". In: *Journal of Aerosol Science* 177 (Mar. 2024), p. 106335. DOI: 10.1016/j.jaerosci.2024.106335.

[60] Jaiprakash et al. "Chemical characterization of PM1.0 aerosol in Delhi and source apportionment using positive matrix factorization". en. In: *Environmental Science and Pollution Research* 24.1 (Jan. 2017), pp. 445–462. DOI: 10.1007/s11356-016-7708-8.

[61] Rohan Jayaratne et al. "The influence of humidity on the performance of a low-cost air particle mass sensor and the effect of atmospheric fog". English. In: *Atmospheric Measurement Techniques* 11.8 (Aug. 2018). Publisher: Copernicus GmbH, pp. 4883–4890. DOI: https://doi.org/10.5194/amt-11-4883-2018.

[62] Sonu Kumar Jha et al. "Domain Adaptation-Based Deep Calibration of Low-Cost PM. Sensors". In: *IEEE Sensors Journal* 21.22 (Nov. 2021). Conference Name: IEEE Sensors Journal, pp. 25941–25949. DOI: 10.1109/JSEN.2021.3118454.

[63] Karoline K. Johnson et al. "Field Test of Several Low-Cost Particulate Matter Sensors in High and Low Concentration Urban Environments". In: *Aerosol and air quality research* 18.3 (2018), pp. 565–578. DOI: 10.4209/aaqr.2017.10.0418.

[64] Alex A. Karner, Douglas S. Eisinger, and Deb A. Niemeier. "Near-Roadway Air Quality: Synthesizing the Findings from Real-World Data". In: *Environmental Science & Technology* 44.14 (July 2010). Publisher: American Chemical Society, pp. 5334–5344. DOI: 10.1021/es100008x.

[65] Varun Katoch et al. "Addressing Biases in Ambient PM2.5 Exposure and Associated Health Burden Estimates by Filling Satellite AOD Retrieval Gaps over India". In: *Environmental Science & Technology* 57.48 (Dec. 2023). Publisher: American Chemical Society, pp. 19190–19201. DOI: 10.1021/acs.est.3c03355.

[66] Kamaljeet Kaur and Kerry E. Kelly. "Laboratory evaluation of the Alphasense OPC-N3, and the Plantower PMS5003 and PMS6003 sensors". In: *Journal of Aerosol Science* 171 (June 2023), p. 106181. DOI: 10.1016/j.jaerosci.2023.106181.

[67] Kamaljeet Kaur and Kerry E. Kelly. "Performance evaluation of the Alphasense OPC-N3 and Plantower PMS5003 sensor in measuring dust events in the Salt Lake Valley, Utah". English. In: *Atmospheric Measurement Techniques* 16.10 (May 2023). Publisher: Copernicus GmbH, pp. 2455–2470. DOI: 10.5194/amt-16-2455-2023.

[68] K. E. Kelly et al. "Ambient and laboratory evaluation of a low-cost particulate matter sensor". In: *Environmental Pollution* 221 (Feb. 2017), pp. 491–500. DOI: 10.1016/j.envpol.2016.12.039.

[69] Bhargav Krishna et al. "Daily nonaccidental mortality associated with short-term PM2.5 exposures in Delhi, India". In: *Environmental Epidemiology* 5.4 (Aug. 2021), e167. DOI: 10.1097/EE9.0000000000000167.

[70] Vikas Kumar, Vasudev Malyan, and Manoranjan Sahu. "Significance of Meteorological Feature Selection and Seasonal Variation on Performance and Calibration of a Low-Cost Particle Sensor". en. In: *Atmosphere* 13.4 (Apr. 2022). Number: 4 Publisher: Multidisciplinary Digital Publishing Institute, p. 587. DOI: 10.3390/atmos13040587.

[71] Meenakshi Kushwaha et al. "Bias in PM2.5 measurements using collocated reference-grade and optical instruments". en. In: *Environmental Monitoring and Assessment* 194.9 (July 2022), p. 610. DOI: 10.1007/s10661-022-10293-4.

[72] Joel Kuula et al. “Laboratory evaluation of particle-size selectivity of optical low-cost particulate matter sensors”. English. In: *Atmospheric Measurement Techniques* 13.5 (May 2020). Publisher: Copernicus GmbH, pp. 2413–2423. DOI: https://doi.org/10.5194/amt-13-2413-2020.

[73] N. S. Laulainen. *Summary of conclusions and recommendations from a visibility science workshop*. English. Tech. rep. PNL-8606. Pacific Northwest National Lab. (PNNL), Richland, WA (United States), Apr. 1993. DOI: 10.2172/10149541.

[74] Johanna Lepeule et al. “Chronic Exposure to Fine Particles and Mortality: An Extended Follow-up of the Harvard Six Cities Study from 1974 to 2009”. In: *Environmental Health Perspectives* 120.7 (2012), pp. 965–970.

[75] Misti Levy Zamora et al. “Field and Laboratory Evaluations of the Low-Cost Plantower Particulate Matter Sensor”. In: *Environmental Science & Technology* 53.2 (Jan. 2019), pp. 838–849. DOI: 10.1021/acs.est.8b05174.

[76] Misti Levy Zamora et al. “Identifying optimal co-location calibration periods for low-cost sensors”. English. In: *Atmospheric Measurement Techniques* 16.1 (Jan. 2023). Publisher: Copernicus GmbH, pp. 169–179. DOI: 10.5194/amt-16-169-2023.

[77] Chi Li et al. “Reversal of trends in global fine particulate matter air pollution”. en. In: *Nature Communications* 14.1 (Sept. 2023). Publisher: Nature Publishing Group, p. 5349. DOI: 10.1038/s41467-023-41086-z.

[78] Yutong Liang et al. “Wildfire smoke impacts on indoor air quality assessed using crowdsourced data in California”. In: *Proceedings of the National Academy of Sciences* 118.36 (Sept. 2021). Publisher: Proceedings of the National Academy of Sciences, e2106478118. DOI: 10.1073/pnas.2106478118.

[79] Zongwei Ma et al. “A review of statistical methods used for developing large-scale and long-term PM2.5 models from satellite data”. en. In: *Remote Sensing of Environment* 269 (Feb. 2022), p. 112827. DOI: 10.1016/j.rse.2021.112827.

[80] Sandeep Madhwal et al. “Evaluation of PM2.5 spatio-temporal variability and hotspot formation using low-cost sensors across urban-rural landscape in lucknow, India”. In: *Atmospheric Environment* 319 (Feb. 2024), p. 120302. DOI: 10.1016/j.atmosenv.2023.120302.

[81] Brian I. Magi et al. “Evaluation of PM2.5 measured in an urban setting using a low-cost optical particle counter and a Federal Equivalent Method Beta Attenuation Monitor”. In: *Aerosol Science and Technology* 54.2 (Feb. 2020), pp. 147–159. DOI: 10.1080/02786826.2019.1619915.

[82] Carl Malings et al. “Fine particle mass monitoring with low-cost sensors: Corrections and long-term performance evaluation”. In: *Aerosol Science and Technology* 0.0 (May 2019), pp. 1–15. DOI: 10.1080/02786826.2019.1623863.

[83] Vasudev Malyan, Vikas Kumar, and Manoranjan Sahu. "Significance of sources and size distribution on calibration of low-cost particle sensors: Evidence from a field sampling campaign". en. In: *Journal of Aerosol Science* 168 (Feb. 2023), p. 106114. DOI: 10.1016/j.jaerosci.2022.106114.

[84] Max I. Manning et al. "Diurnal Patterns in Global Fine Particulate Matter Concentration". In: *Environmental Science & Technology Letters* 5.11 (Nov. 2018). Publisher: American Chemical Society, pp. 687–691. DOI: 10.1021/acs.estlett.8b00573.

[85] Randall V. Martin et al. "No one knows which city has the highest concentration of fine particulate matter". en. In: *Atmospheric Environment: X* 3 (July 2019), p. 100040. DOI: 10.1016/j.aeaoa.2019.100040.

[86] Celeste McFarlane et al. "Application of Gaussian Mixture Regression for the Correction of Low Cost PM2.5 Monitoring Data in Accra, Ghana". In: *ACS Earth and Space Chemistry* 5.9 (Sept. 2021). Publisher: American Chemical Society, pp. 2268–2279. DOI: 10.1021/acsearthspacechem.1c00217.

[87] Celeste McFarlane et al. "First Measurements of Ambient PM2.5 in Kinshasa, Democratic Republic of Congo and Brazzaville, Republic of Congo Using Field-calibrated Low-cost Sensors". en. In: *Aerosol and Air Quality Research* 21.7 (2021). Publisher: Taiwan Association for Aerosol Research, p. 200619. DOI: 10.4209/aaqr.200619.

[88] Ahmed Mehadi et al. "Laboratory and field evaluation of real-time and near real-time PM2.5 smoke monitors". In: *Journal of the Air & Waste Management Association* 70.2 (Feb. 2020), pp. 158–179. DOI: 10.1080/10962247.2019.1654036.

[89] Kyle P. Messier et al. "Mapping Air Pollution with Google Street View Cars: Efficient Approaches with Mobile Monitoring and Land Use Regression". en. In: *Environmental Science & Technology* 52.21 (Nov. 2018), pp. 12563–12572. DOI: 10.1021/acs.est.8b03395.

[90] David J. Miller et al. "Characterizing Elevated Urban Air Pollutant Spatial Patterns with Mobile Monitoring in Houston, Texas". In: *Environmental Science & Technology* 54.4 (Feb. 2020). Publisher: American Chemical Society, pp. 2133–2142. DOI: 10.1021/acs.est.9b05523.

[91] Emilio Molina Rueda et al. "Size-Resolved Field Performance of Low-Cost Sensors for Particulate Matter Air Pollution". In: *Environmental Science & Technology Letters* 10.3 (Mar. 2023). Publisher: American Chemical Society, pp. 247–253. DOI: 10.1021/acs.estlett.3c00030.

[92] Christopher J. L. Murray et al. "Global burden of 87 risk factors in 204 countries and territories, 1990–2019: a systematic analysis for the Global Burden of Disease Study 2019". English. In: *The Lancet* 396.10258 (Oct. 2020). Publisher: Elsevier, pp. 1223–1249. DOI: 10.1016/S0140-6736(20)30752-2.

[93] Audrey de Nazelle et al. "Improving estimates of air pollution exposure through ubiquitous sensing technologies". en. In: *Environmental Pollution* 176 (May 2013), pp. 92–99. DOI: 10.1016/j.envpol.2012.12.032.

[94] James Ouimette et al. "Fundamentals of low-cost aerosol sensor design and operation". In: *Aerosol Science and Technology* 58.1 (Jan. 2024). Publisher: Taylor & Francis _eprint: https://doi.org/10.1080/02786826.2023.2285935, pp. 1–15. DOI: 10.1080/02786826.2023.2285935.

[95] James R. Ouimette et al. "Evaluating the PurpleAir monitor as an aerosol light scattering instrument". English. In: *Atmospheric Measurement Techniques Discussions* (June 2021). Publisher: Copernicus GmbH, pp. 1–35. DOI: 10.5194/amt-2021-170.

[96] Christopher J. Paciorek and Yang Liu. "Limitations of Remotely Sensed Aerosol as a Spatial Proxy for Fine Particulate Matter". In: *Environmental Health Perspectives* 117.6 (June 2009). Publisher: Environmental Health Perspectives, pp. 904–909. DOI: 10.1289/ehp.0800360.

[97] Anamika Pandey et al. "Health and economic impact of air pollution in the states of India: the Global Burden of Disease Study 2019". en. In: *The Lancet Planetary Health* 5.1 (Jan. 2021), e25–e38. DOI: 10.1016/S2542-5196(20)30298-9.

[98] Pallavi Pant et al. "Monitoring particulate matter in India: recent trends and future outlook". en. In: *Air Quality, Atmosphere & Health* 12.1 (Jan. 2019), pp. 45–58. DOI: 10.1007/s11869-018-0629-6.

[99] Kanan Patel et al. "Persistence of Primary and Secondary Pollutants in Delhi: Concentrations and Composition from 2017 through the COVID Pandemic". In: *Environmental Science & Technology Letters* 8.7 (July 2021). Publisher: American Chemical Society, pp. 492–497. DOI: 10.1021/acs.estlett.1c00211.

[100] Kanan Patel et al. "Sources and Dynamics of Submicron Aerosol during the Autumn Onset of the Air Pollution Season in Delhi, India". In: *ACS Earth and Space Chemistry* 5.1 (Jan. 2021). Publisher: American Chemical Society, pp. 118–128. DOI: 10.1021/acsearthspacechem.0c00340.

[101] Hubert Sutton Patterson, R. Whytlaw Gray, and Nevil Vincent Sidgwick. "The scattering of light by the individual particles in smokes". In: *Proceedings of the Royal Society of London. Series A, Containing Papers of a Mathematical and Physical Character* 113.764 (Jan. 1926). Publisher: Royal Society, pp. 312–322. DOI: 10.1098/rspa.1926.0157.

[102] Daniel R. Peters et al. "Evaluating uncertainty in sensor networks for urban air pollution insights". English. In: *Atmospheric Measurement Techniques* 15.2 (Jan. 2022). Publisher: Copernicus GmbH, pp. 321–334. DOI: 10.5194/amt-15-321-2022.

[103] Brijal Prajapati et al. “Development of a physics-based method for calibration of low-cost particulate matter sensors and comparison with machine learning models”. In: *Journal of Aerosol Science* 175 (Jan. 2024), p. 106284. DOI: 10.1016/j.jaerosci.2023.106284.

[104] Jai Prakash et al. “Deployment of networked low-cost sensors and comparison to real-time stationary monitors in New Delhi”. In: *Journal of the Air & Waste Management Association* 71.11 (Nov. 2021), pp. 1347–1360. DOI: 10.1080/10962247.2021.1890276.

[105] Naveen Puttaswamy et al. “Indoor and Ambient Air Pollution in Chennai, India during COVID-19 Lockdown: An Affordable Sensors Study”. en. In: *Aerosol and Air Quality Research* 22.1 (2022). Publisher: Taiwan Association for Aerosol Research, p. 210170. DOI: 10.4209/aaqr.210170.

[106] Garima Raheja et al. “Low-Cost Sensor Performance Intercomparison, Correction Factor Development, and 2+ Years of Ambient PM2.5 Monitoring in Accra, Ghana”. In: *Environmental Science & Technology* 57.29 (July 2023). Publisher: American Chemical Society, pp. 10708–10720. DOI: 10.1021/acs.est.2c09264.

[107] T. V. Ramachandra et al. “Micro level analyses of environmentally disastrous urbanization in Bangalore”. en. In: *Environmental Monitoring and Assessment* 191.3 (Jan. 2020), p. 787. DOI: 10.1007/s10661-019-7693-8.

[108] Sebastian Raschka and Vahid Mirjalili. *Python Machine Learning: Machine Learning and Deep Learning with Python, scikit-learn, and TensorFlow*. en. 2nd ed. Google-Books-ID: sKXIDwAAQBAJ. Packt Publishing Ltd, Dec. 2019.

[109] A. R. Ravishankara et al. “Outdoor air pollution in India is not only an urban problem”. en. In: *Proceedings of the National Academy of Sciences* 117.46 (Nov. 2020). ISBN: 9782007236118 Publisher: National Academy of Sciences Section: Physical Sciences, pp. 28640–28644. DOI: 10.1073/pnas.2007236117.

[110] Brigitte Rooney et al. “Impacts of household sources on air pollution at village and regional scales in India”. English. In: *Atmospheric Chemistry and Physics* 19.11 (June 2019). Publisher: Copernicus GmbH, pp. 7719–7742. DOI: 10.5194/acp-19-7719-2019.

[111] Ravi Sahu et al. “Validation of Low-Cost Sensors in Measuring Real-Time PM10 Concentrations at Two Sites in Delhi National Capital Region”. en. In: *Sensors* 20.5 (Jan. 2020). Number: 5 Publisher: Multidisciplinary Digital Publishing Institute, p. 1347. DOI: 10.3390/s20051347.

[112] Federico M. San Martini, Christa A. Hasenkopf, and David C. Roberts. “Statistical analysis of PM2.5 observations from diplomatic facilities in China”. en. In: *Atmospheric Environment* 110 (June 2015), pp. 174–185. DOI: 10.1016/j.atmosenv.2015.03.060.

[113] T. Sayahi, A. Butterfield, and K. E. Kelly. "Long-term field evaluation of the Plantower PMS low-cost particulate matter sensors". en. In: *Environmental Pollution* 245 (Feb. 2019), pp. 932–940. DOI: 10.1016/j.envpol.2018.11.065.

[114] Marcello Schiavina et al. *GHSL Data Package 2022*. June 2022. DOI: 10.2760/19817.

[115] N. Searle, K. Kaur, and K. Kelly. "Technical note: Identifying a performance change in the Plantower PMS 5003 particulate matter sensor". In: *Journal of Aerosol Science* 174 (Nov. 2023), p. 106256. DOI: 10.1016/j.jaerosci.2023.106256.

[116] Anita V. Shankar et al. "Everybody stacks: Lessons from household energy case studies to inform design principles for clean energy transitions". In: *Energy Policy* 141 (June 2020), p. 111468. DOI: 10.1016/j.enpol.2020.111468.

[117] Siyuan Shen et al. "Enhancing Global Estimation of Fine Particulate Matter Concentrations by Including Geophysical a Priori Information in Deep Learning". In: *ACS ES&T Air* 1.5 (May 2024). Publisher: American Chemical Society, pp. 332–345. DOI: 10.1021/acsestair.3c00054.

[118] K. K. Shukla et al. "Evaluation of extreme dust storm over the northwest Indo-Gangetic plain using WRF-Chem model". en. In: *Natural Hazards* (Sept. 2021). DOI: 10.1007/s11069-021-05017-9.

[119] Heather Simon, Kirk R. Baker, and Sharon Phillips. "Compilation and interpretation of photochemical model performance statistics published between 2006 and 2012". en. In: *Atmospheric Environment* 61 (Dec. 2012), pp. 124–139. DOI: 10.1016/j.atmosenv.2012.07.012.

[120] Vikas Singh et al. "Diurnal and temporal changes in air pollution during COVID-19 strict lockdown over different regions of India". en. In: *Environmental Pollution* 266 (Nov. 2020), p. 115368. DOI: 10.1016/j.envpol.2020.115368.

[121] Maji Smaran and V. Vinoj. "Evaluation of Background Black Carbon Concentration in India". en. In: *Aerosol and Air Quality Research* 24.7 (2024). Publisher: Taiwan Association for Aerosol Research, p. 230300. DOI: 10.4209/aaqr.230300.

[122] Veronica A. Southerland et al. "Global urban temporal trends in fine particulate matter (PM2·5) and attributable health burdens: estimates from global datasets". English. In: *The Lancet Planetary Health* 6.2 (Feb. 2022). Publisher: Elsevier, e139–e146. DOI: 10.1016/S2542-5196(21)00350-8.

[123] L Spinelle et al. *Protocol of evaluation and calibration of low-cost gas sensors for the monitoring of air pollution.* en. OCLC: 870631567. Luxembourg: Publications Office, 2013.

[124] V. Sreekanth et al. "Impact of COVID-19 lockdown on the fine particulate matter concentration levels: Results from Bengaluru megacity, India". en. In: *Advances in Space Research* 67.7 (Apr. 2021), pp. 2140–2150. DOI: 10.1016/j.asr.2021.01.017.

[125] V. Sreekanth et al. "Inter- versus Intracity Variations in the Performance and Calibration of Low-Cost PM2.5 Sensors: A Multicity Assessment in India". In: *ACS Earth and Space Chemistry* 6.12 (Dec. 2022). Publisher: American Chemical Society, pp. 3007–3016. DOI: 10.1021/acsearthspacechem.2c00257.

[126] S Srishti et al. "Multiple PM Low-Cost Sensors, Multiple Seasons' Data, and Multiple Calibration Models". en. In: *Aerosol and Air Quality Research* 23.3 (2023). Publisher: Taiwan Association for Aerosol Research, p. 220428. DOI: 10.4209/aaqr.220428.

[127] *State of Global Air Report 2024 — State of Global Air*.

[128] Roland B. Stull, ed. *An Introduction to Boundary Layer Meteorology*. Dordrecht: Springer Netherlands, 1988. DOI: 10.1007/978-94-009-3027-8.

[129] Jessica Tryner et al. "Laboratory evaluation of low-cost PurpleAir PM monitors and in-field correction using co-located portable filter samplers". en. In: *Atmospheric Environment* 220 (Jan. 2020), p. 117067. DOI: 10.1016/j.atmosenv.2019.117067.

[130] David L Vaughn. *Standard Operating Procedure for the Continuous Measurement of Particulate Matter*. Aug. 2009.

[131] Chandra Venkataraman et al. "Source influence on emission pathways and ambient $PM_{2.5}$ pollution over India (2015–2050)". English. In: *Atmospheric Chemistry and Physics* 18.11 (June 2018). Publisher: Copernicus GmbH, pp. 8017–8039. DOI: 10.5194/acp-18-8017-2018.

[132] Theo Vos et al. "Global burden of 369 diseases and injuries in 204 countries and territories, 1990–2019: a systematic analysis for the Global Burden of Disease Study 2019". en. In: *The Lancet* 396.10258 (Oct. 2020), pp. 1204–1222. DOI: 10.1016/S0140-6736(20)30925-9.

[133] Lance Wallace and Wayne Ott. "Long-Term Indoor-Outdoor PM2.5 Measurements Using PurpleAir Sensors: An Improved Method of Calculating Indoor-Generated and Outdoor-Infiltrated Contributions to Potential Indoor Exposure". en. In: *Sensors* 23.3 (Jan. 2023). Number: 3 Publisher: Multidisciplinary Digital Publishing Institute, p. 1160. DOI: 10.3390/s23031160.

[134] Lance Wallace and Tongke Zhao. "Spatial Variation of PM2.5 Indoors and Outdoors: Results from 261 Regulatory Monitors Compared to 14,000 Low-Cost Monitors in Three Western States over 4.7 Years". en. In: *Sensors* 23.9 (Jan. 2023). Number: 9 Publisher: Multidisciplinary Digital Publishing Institute, p. 4387. DOI: 10.3390/s23094387.

[135] Lance Wallace et al. "Calibration of low-cost PurpleAir outdoor monitors using an improved method of calculating PM2.5". en. In: *Atmospheric Environment* 256 (July 2021), p. 118432. DOI: 10.1016/j.atmosenv.2021.118432.

[136] Lance Wallace et al. "Secondhand exposure from vaping marijuana: Concentrations, emissions, and exposures determined using both research-grade and low-cost monitors". en. In: *Atmospheric Environment: X* 8 (Dec. 2020), p. 100093. DOI: 10.1016/j.aeaoa.2020.100093.

[137] Jiandong Wang et al. "Historical Trends in PM2.5-Related Premature Mortality during 1990–2010 across the Northern Hemisphere". In: *Environmental Health Perspectives* 125.3 (Mar. 2017). Publisher: Environmental Health Perspectives, pp. 400–408. DOI: 10.1289/EHP298.

[138] John Watson et al. "Guidance for using continuous monitors in PM2.5 monitoring networks, U.S". In: (May 1998).

[139] Kalpit Yadav et al. "Few-Shot Calibration of Low-Cost Air Pollution ($PM_{2.5}$) Sensors Using Meta Learning". In: *IEEE Sensors Letters* 6.5 (May 2022). Conference Name: IEEE Sensors Letters, pp. 1–4. DOI: 10.1109/LSENS.2022.3168291.

[140] Katelyn A. Yu, Brian C. McDonald, and Robert A. Harley. "Evaluation of Nitrogen Oxide Emission Inventories and Trends for On-Road Gasoline and Diesel Vehicles". In: *Environmental Science & Technology* 55.10 (May 2021). Publisher: American Chemical Society, pp. 6655–6664. DOI: 10.1021/acs.est.1c00586.

[141] Tongshu Zheng et al. "Field evaluation of low-cost particulate matter sensors in high- and low-concentration environments". English. In: *Atmospheric Measurement Techniques* 11.8 (Aug. 2018). Publisher: Copernicus GmbH, pp. 4823–4846. DOI: https://doi.org/10.5194/amt-11-4823-2018.

[142] Tongshu Zheng et al. "Gaussian process regression model for dynamically calibrating and surveilling a wireless low-cost particulate matter sensor network in Delhi". English. In: *Atmospheric Measurement Techniques* 12.9 (Sept. 2019). Publisher: Copernicus GmbH, pp. 5161–5181. DOI: 10.5194/amt-12-5161-2019.

[143] Y Zhou and H Zheng. *PMS5003 Series Data Manual*. 2016.

[144] Naomi Zimmerman. "Tutorial: Guidelines for implementing low-cost sensor networks for aerosol monitoring". In: *Journal of Aerosol Science* 159 (Jan. 2022), p. 105872. DOI: 10.1016/j.jaerosci.2021.105872.

[145] Yangyang Zou, Jordan D. Clark, and Andrew A. May. "Laboratory evaluation of the effects of particle size and composition on the performance of integrated devices containing Plantower particle sensors". In: *Aerosol Science and Technology* 0.ja (Mar. 2021), pp. 1–13. DOI: 10.1080/02786826.2021.1905148.